CIRCADIAN CLOCK REGULATION OF THE ACTIVITY OF TRANSLATION INITIATION FACTOR EIF2α IN NEUROSPORA CRASSA

A Dissertation

by

ZHAOLAN DING

Submitted to the Office of Graduate and Professional Studies of
Texas A&M University
in partial fulfillment of the requirements for the degree of

DOCTOR OF PHILOSOPHY

Chair of Committee,	Deborah Bell-Pedersen
Committee Members,	Daniel Ebbole
	Paul Hardin
	Matthew Sachs
Head of Department,	Thomas McKnight

May 2021

Major Subject: Biology

ABSTRACT

At least half of proteins cycling in abundance under control of the circadian clock in eukaryotic cells are synthesized from non-cycling mRNAs. These data suggested that the clock controls posttranscriptional events, including mRNA translation; however, the mechanisms underlying this regulation were not known. We, and other labs, discovered that the circadian clock controls the phosphorylation and activity of eukaryotic translation initiation factor 2α (eIF2α). In *Neurospora crassa*, the peak in inhibitory eIF2α phosphorylation (P-eIF2α) levels occurs during the subjective day. The activity of the *N. crassa* eIF2α kinase, CPC-3, was shown to be necessary for rhythmic P-eIF2α accumulation. However, it was not known if CPC-3 activity is sufficient for rhythmic P-eIF2α, or if other factors are involved. In this study, I tested the hypothesis that rhythmic eIF2α activity also requires dephosphorylation of P-eIF2α at night by phosphatases. In support of this hypothesis, I demonstrated that mutation of *N. crassa* PPP1, a homolog of the yeast eIF2α phosphatase GLC7, leads to high and arrhythmic P-eIF2α levels, while maintaining core circadian oscillator function. Furthermore, PPP1 levels are clock-controlled, peaking at dusk, and rhythmic PPP1 levels were shown to be necessary for rhythmic P-eIF2α accumulation. I discovered that eIF2γ, a component of the eIF2 complex, functions to recruit PPP1 to dephosphorylate eIF2α. Thus, in addition to the activity of CPC-3 kinase, rhythmic P-eIF2α requires dephosphorylation by PPP1 phosphatase at night. To determine the impact of rhythmic eIF2α activity on mRNA translation, ribosome profiling, in parallel with RNA-seq, was carried out. In collaboration with Dr. Kathrina Castillo, I found that the *N. crassa* clock regulates the translation of 1328 mRNAs, of which 404 were translated arrhythmically in strains that lacked CPC-3 (Δ*cpc-3*) or had a constitutively active CPC-3 (*cpc-3*^{c}). These data revealed that rhythmic eIF2α activity regulates

translation of specific, rather than all, mRNAs. Experiments are in progress to investigate the mechanisms of rhythmic P-eIF2α regulation of these targeted mRNAs. Together, these data show how the circadian clock regulates protein production by controlling the activity of a central regulator of translation through the temporal coordination of phosphorylation and dephosphorylation events.

DEDICATION

I would like to dedicate my dissertation to my family, especially my parents, sister and fiancé, for their infinite love, encouragement and support.

ACKNOWLEDGEMENTS

I thank my professor, Dr. Deborah Bell-Pedersen for giving me the chance to do research in the lab under her supervision, and for her always being patient with me, helpful and supportive to me over the past few years. I am also thankful to my committee members, Dr. Paul Hardin, Dr. Matt Sachs, and Dr. Dan Ebbole, for their guidance and support throughout the course of this research. I also thank my current and previous colleagues in lab: Dr. Teresa M. Lamb, Dr. Kathrina Castillo, Johnny Fazzino, Jennifer Jung, Ebi Preh, Jana Gomez, Manuel Ramirez, Tamika Harford, Oneida Ibarra, Dr. Shanta Karki, Dr. Stephen Caster and undergrads Rachel Stroh, Ahmad Boukhris, Rachel Porter, Isiaah Samora, Emily Chapa and Travis Mosley. Thanks also go to my friends and the department faculty and staff for making my time at Texas A&M University a great experience. Finally, thanks to my mother, father and sister for their encouragement and to my fiancé for his support and love.

CONTRIBUTORS AND FUNDING SOURCES

Contributors

This work was supervised by a dissertation committee consisting of Dr. Deborah Bell-Pedersen, Dr. Paul Hardin, Dr. Matthew Sachs and Dr. Daniel Ebbole.

Dr. Kathrina Castillo contributed to Ribosome-sequencing library preparation and data analysis for Chapter IV.

Dr. Cheng Wu contributed to RNA-sequencing library preparations in Chapter IV.

All other work conducted for the dissertation was completed by the student independently.

Funding Sources

This work was funded by NIH R01 GM058529 and R35 GM126966 to DBP.

TABLE OF CONTENTS

Page

ABSTRACT ii

DEDICATION iv

ACKNOWLEDGEMENTS v

CONTRIBUTORS AND FUNDING SOURCES vi

TABLE OF CONTENTS vii

LIST OF FIGURES ix

LIST OF TABLES xi

CHAPTER I INTRODUCTION 1

- Circadian clock overview 1
- The circadian clock in the model organism *N. crassa* 2
- Output pathways of circadian clock 4
- Post-transcriptional control by the circadian clock 6
- Circadian clock regulation of eIF2α phosphorylation 6
- Objectives 11

CHAPTER II PPP1 PHOSPHATASE IS REQUIRED FOR CIRCADIAN CLOCK CONTROL OF TRANSLATION INITIATION FACTOR EIF2A ACTIVITY IN *NEUROSPORA CRASSA* 15

- Introduction 15
- Results 16
- Discussion 29
- Methods and Materials 33

CHAPTER III INVESTIGATION OF THE ROLES OF PPP1 REGULATION OF CPC-3 PHOSPHORYLATION 42

- Introduction 42
- Results 44
- Discussion 49
- Methods and Materials 52

CHAPTER IV CLOCK-CONTROLLED EIF2A ACTIVITY REGULATES RHYTHMIC TRANSLATION OF SPECIFIC MRNAS 59

Introduction 59
Results 61
Discussion 76
Methods and Materials 81

CHAPTER V SUMMARY AND FUTURE DIRECTIONS 90

Summary 90
Future directions 92

REFERENCES 98

APPENDIX A 112

LIST OF FIGURES

Page

Figure 1. Composition of eukaryotic circadian oscillators. 2

Figure 2. Model of canonical eukaryotic translation initiation. 7

Figure 3. PPP1 protein sequence is highly conserved. Multiple sequence alignment of the *N. crassa* PPP1 protein sequence to homologs in *M. musculus* and *S. cerevisiae*..... 16

Figure 4. PPP1 phosphatase reduces P-eIF2α levels.. 17

Figure 5. Anti-PPP1 antibody detects the *N. crassa* PPP1 protein.. 18

Figure 6. PPP1 phosphatase is critical for dephosphorylation of P-eIF2α *in vitro*..... 19

Figure 7. PPP1 is associated with ribosomes.. 20

Figure 8. PPP1 phosphatase is necessary for rhythmic P-eIF2α accumulation. 22

Figure 9. Deletion of the amino terminal 60 amino acids of *N. crassa* eIF2γ alters eIF2α phosphorylation levels..... 23

Figure 10. Deletion of the amino terminal 60 amino acids of *N. crassa* eIF2γ impacts the P-eIF2α *in vitro* dephosphorylation rate. 24

Figure 11. Deletion of the amino terminal 60 amino acids of *N. crassa* eIF2γ dampens eIF2α phosphorylation rhythmicity 25

Figure 12. The circadian clock controls PPP1 phosphatase levels, but not eIF2γ levels. 27

Figure 13. Clock control of PPP1 is necessary for rhythmic P-eIF2α levels..... 28

Figure 14. Model of the mechanisms of clock coordination of both the day-active eIF2α kinase CPC-3 and the night-active phosphatase PPP1 controlling rhythmic eIF2α activity and translation initiation. 30

Figure 15. Proposed model for PPP1 regulation of P-eIF2α rhythmicity through regulation of CPC-3 activity through dephosphorylation of inhibitory or activating phosphorylation residues of CPC-3 protein. 43

Figure 16. The phosphorylation levels of CPC-3 S876 and T879 are regulated by PPP1 protein levels. 45

Figure 17. T879 is required for CPC-3 activity. 47

Figure 18. S876 phosphorylation activates CPC-3, but is not required for rhythmic P-eIF2α levels..... 48

Figure 19. Potential pathways of PPP1 regulation of P-eIF2α rhythms 51

Figure 20. Sample preparation and library processing workflow for RNA-seq and ribo-seq of WT, Δ*frq*, Δ*cpc-3* and *cpc-3*^{C} strains. 62

Figure 21. Validation of FRQ and P-eIF2α rhythms in sequencing samples. 63

Figure 22. Ribosome profiling of *Neurospora* WT, Δ*frq*, Δ*cpc-3*, and *cpc-3*^{c} cells 66

Figure 23. Core clock genes and selected *ccgs* are rhythmic 67

Figure 24. A subset of mRNAs requires P-eIF2α for rhythmic translation 68

Figure 25. Proteins that depend on clock-controlled eIF2α activity for rhythmic translation arise from cycling and non-cycling transcripts. 70

Figure 26. Rhythmic translation of *idi-4* is regulated by rhythms in the levels of P-eIF2α. 73

Figure 27. Motifs in the 5' UTR of transcripts regulated by rhythmic P-eIF2α. 75

Figure 28. Read processing pipeline for the ribo-seq and RNA-seq datasets. 89

Figure 29. Model of the mechanisms of clock coordination of both the eIF2α kinase and the phosphatase to regulates day-night cycling of eIF2α activity and translation of specific mRNAs. 91

LIST OF TABLES

Page

Table 1. Primers used in Chapter II 40

Table 2. Primers used in Chapter III 56

Table 3. Correlation coefficients between ribo-seq replicates or RNA-seq replicates of WT, Δ*frq*, Δ*cpc-3*, and *cpc-3*^{c} cells across time points. 64

Table 4. Go analysis of the 234 class III cTICs. Categories shown were considered significantly enriched with $p < 0.5$. 71

Table 5. Primers used in Chapter IV 88

Table A1. Genes with rhythmic ribosome occupancies dependent on P-eIF2α rhythmicity…..112

Table A2. Genes of the 404 cTICs with predicted uORFs……..124

CHAPTER I

INTRODUCTION

Circadian clock overview

The capacity to adapt to a changing environment is critical for an organism's survival. The rotation of the Earth on its axis leads to predictable 24 h changes in light, temperature and humidity. As a consequence, an internal biological clock has evolved in diverse organisms to allow anticipation and coordination of an organism's physiology and behavior to daily environmental cycles [1-3]. This endogenous clock, called a circadian clock, is defined by several canonical properties. First, in the absence of environmental cues, the clock will free-run with a period close to 24 h. For example, in the fungus *Neurospora crassa* the free-running period is about 22.5 hours [4], and in humans it is around 24.2 h [5]. Second, the period of the free-running rhythm is temperature compensated such that the period stays fairly constant over a range of environmental temperatures. Lastly, the phase of the circadian clock can be reset by external signals, including light and temperature. Together, these defining features enable the circadian clock to maintain a relatively consistent period in different ambient temperatures, and to synchronize original processes to the right environmental time of day.

Broadly, the clock is composed of a molecular circadian oscillator that keeps time, input pathways that synchronize the oscillator to environmental cycles, and output pathways from the oscillator that control rhythms in the expression of target genes that ultimately lead to overt rhythms in physiology and behavior. In eukaryotes, the core oscillator is an auto-regulatory feedback loop composed of positive and negative elements (**Figure 1**) [6-11]. In the core circadian oscillator, positive elements activate the expression of the negative elements (called Clock Genes). The

negative elements feedback to repress the activity of the positive elements. Over the day, the negative elements are phosphorylated and degraded, which allows the positive elements to restart the cycle the next day.

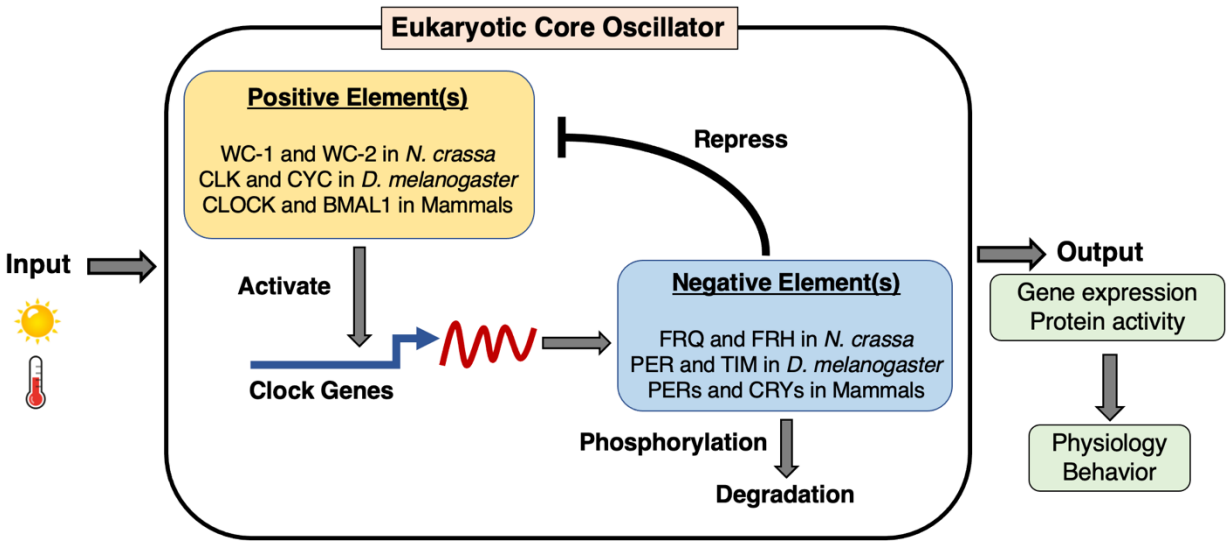

Figure 1. Composition of eukaryotic circadian oscillators. See the text for details of the figure. The names of core circadian positive and negative elements in *N. crassa*, *D. melanogaster* and mammals are indicated.

The circadian clock in the model organism *N. crassa*

The filamentous fungus *N. crassa* has a long and illustrious history as a genetic model organism. In 1958, the Nobel Prize in Physiology or Medicine was awarded to Edward Tatum and George Wells Beadle for their work in *N. crassa* that led to the "one gene, one enzyme" hypothesis [12]. *N. crassa* is a simple eukaryote, but has many pathways that are conserved with higher eukaryotes [13]. *N. crassa* is inexpensive and easy to grow and manipulate both genetically and biochemically, and has a haploid asexual cycle as well as a sexual cycle, making it an excellent model organism to study complex pathways, including the circadian clock system. The genome of *N. crassa* was sequenced [14], and the Fungal Genetics Stock Center (FGSC) maintains a collection of strains

containing deletions of almost all of its ~10,000 genes [15]. Essential genes can be sheltered in heterokaryons [16].

N. crassa is multicellular with tip-growing multinucleate vegetative hyphae that undergo regular branching. The nuclei within hyphae can have different genotypes, forming a heterokaryon [16]. Organelles are able to move between compartments within the tubular hyphae, since the hyphae have incomplete septa [17]. During development, specialized aerial hyphae are differentiated from vegetative hyphae in response to light or stress, including nutrient deprivation and desiccation. The aerial hyphae bud to give rise to chains of asexual spores (macroconidia) for dispersal [18]. In addition, uninucleate microconidia are differentiated from vegetative hypha through a specialized microconidiation process [18]. Limiting nitrogen induces hyphal aggregation and the generation of multicellular sexual organs called protoperithecia [19]. Ascogonia from the protoperithecia are fertilized after obtaining at least one nucleus of the other mating type (A or a) that is contributed by conidia, germ tubes or vegetative hyphae [20, 21]. Following fertilization, protoperithecia develop into fruiting bodies called perithecia, in which the fused diploid nuclei undergo meiosis and produce eight ordered haploid ascospores within each ascus [22].

In addition to induction of conidiation by acute environmental signals, *N. crassa* conidiation is regulated by the circadian clock, with a daily peak in conidia production near dawn. This overt developmental rhythm provides an easy way to monitor the period and phase of the circadian clock, and provides the ability to screen mutants that have a defective clock [3]. Study of these mutants led to the identification of core oscillator components that comprise the *N. crassa* clock and input pathways to the clock [23, 24]. The core circadian oscillator in *N. crassa* consists of the

positive elements WHITE COLLAR-1 (WC-1) and WC-2, which form the White-Collar Complex (WCC) (**Figure 1**). WC-1 can bind to DNA and activate transcription, and WC-2 stabilizes WC-1 protein [25]. The WCC is active in the morning and positively regulates transcription of the clock gene *frequency* (*frq*) [26], and directly controls the expression of more than 20 transcription factors in the output pathways [27]. FRQ protein interacts with FRQ-interacting RNA Helicase (FRH) to form the FRQ/FRH Complex (FFC) [28]. The FFC functions as the negative element by recruiting kinases to phosphorylate and thereby inhibit the activity of the WCC. This leads to a decrease in *frq* transcription in the subjective night [28, 29]. Over time, existing FRQ protein is phosphorylated, ubiquitinated, and degraded by the proteasome [30]. Phosphatases remove the inhibitory phosphates on the WCC [31], and together with newly synthesized WC proteins, the cycle of *frq* transcription restarts the next morning [3]. In constant growth conditions, such as constant darkness (DD), this endogenous feedback mechanism leads to circadian rhythms in gene expression and overt rhythmicity with a period of ~22.5 h.

In addition to the essential role in the circadian oscillator, WC-1 is also a photoreceptor and is activated by blue light [32, 33]. Upon blue light treatment, WC-1 binds flavin dinucleotide (FAD) at the LOV domain, leading to a conformational change in the protein that activates DNA binding [34]. WCC binding to the light-regulated elements (LREs) of the *frq* promoter is required for light activation of *frq* transcription, which resets the clock [25, 34, 35].

Output pathways of circadian clock

Circadian oscillators regulate the expression and activity of downstream clock-controlled genes (ccgs) through output pathways. These ccgs encode proteins that regulate physiology and behavior,

important for temporal order and health. For example, the circadian clock has a major impact on human mental and physical health, and living against the circadian clock, such as during shift work, has been associated with increased risk for cancer, heart disease, metabolic syndrome, and depression [36]. Furthermore, more than 50% of the top-selling drugs target proteins that are clock-controlled [37]. As a consequence, drugs are more toxic or more effective at different times of the day. For instance, acetaminophen overdose is the top cause of acute liver failure in the United States [38]. Acetaminophen, the main ingredient in Tylenol, is detoxified by glutathione [39], which is under control of the clock and peaks during the day. Tylenol taken at night, when glutathione levels are low, has increased toxicity [40]. Taken together, these data serve to emphasize the need to know how the circadian clock regulates rhythmic gene expression and protein activity.

Microarray, RNA-seq and/or ChIP-seq techniques have been used in the circadian field to determine the extent of clock control of transcription, and to learn more about what is controlled by the clock [10, 41-47]. Up to 50% of the eukaryotic genome was shown to be under control of the clock at the transcriptional level [10, 41-47]. The circadian clock regulates transcription initially through the direct regulation of gene expression by core clock components. For example, the WCC binds to the promoters of 5% of ~10,000 *N. crassa* genes, many of which are both light- and clock-regulated, and encode transcription factors that control rhythms in downstream target genes [27]. However, clock control of transcription is likely not the only mechanism controlling rhythmic gene expression. In support of this idea, post-transcriptional regulation by clock is known to play an important role in rhythmic gene expression [48-50].

Post-transcriptional control by the circadian clock

Several post-transcriptional steps are under clock control, including mRNA capping, splicing, polyadenylation, and de-adenylation [41, 51-54]. In addition, quantitative proteomic analysis of mouse liver samples harvested at different times of the day revealed that up to 50% of rhythmically accumulating proteins are expressed from non-cycling mRNAs [48-50]. Similarly, in *N. crassa*, up to 40% of the rhythmic proteome is expressed from arrhythmic transcripts [55]. These data indicated that protein accumulation rhythms are driven by circadian regulation of protein degradation and/or mRNA translation.

Consistent with the idea that clock controls mRNA translation, the expression (eIF1, eIF4A2, eF4G1, eIF5, eEF2, eEF1A) and/or phosphorylation levels (eIF4B, eIF4E, eIF4G, 4EBP1) of several translation factors are rhythmic in eukaryotic cells [48, 56]. Moreover, rhythms of several ribosomal proteins, including RPL5, RPL23, RPL32 and RPLP0 were observed, indicating potential rhythms in ribosome composition and function [57]. In *N. crassa*, the clock controls the activity of a conserved elongation factor, eEF2, through regulation of the activity of the eEF2 kinase, RCK-2. Rhythmic RCK-2 activity peaks during the day, leading to a daytime peak in the phosphorylation levels of eEF2 and a reduction in translation elongation rate. Rhythms in eEF2 activity are necessary for rhythmic translation of *luciferase* mRNA *in vitro*, and for rhythms in the accumulation of Glutathione S-transferase (GST-3) *in vivo* [58].

Circadian clock regulation of eIF2α phosphorylation

Translation initiation starts with the formation of the ternary complex, which contains initiation factor eIF2 (composed of α, β and γ subunits), Met-tRNA $_i^{Met}$, and GTP [59, 60] (**Figure 2**). This

active ternary complex binds to the 40s-ribosomal subunit that is associated with several initiation factors, including eIF1, eIF1A, eIF5 and the eIF3 complex, to form the 43S pre-initiation complex (PIC). With the assistance of eIF4F, which is composed of the cap-binding protein eIF4E, eIF4G and the RNA helicase eIF4A, the PIC binds to the mRNA cap to form the 48S PIC and begins scanning.

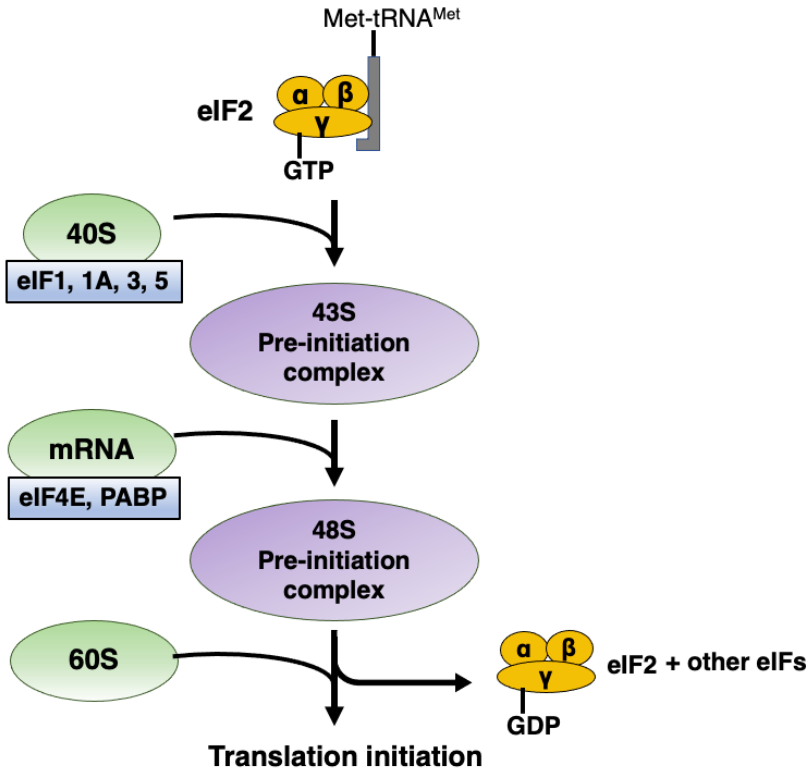

Figure 2. Model of canonical eukaryotic translation initiation. The pathway to initiation involves a series of discrete steps starting with the formation of the ternary complex. See the text for details.

When the 48S PIC with open conformation selects a start codon for protein synthesis [61, 62] a closed conformation forms resulting in eIF5-mediated hydrolysis of GTP bound to eIF2α, binding of the 60s subunit, and release of the initiation factors. To initiate another round of translation, the

guanine nucleotide exchange factor (GEF) eIF2B exchanges GDP-eIF2α for GTP [59]. This eIF2 recycling step is critical for controlling the translation initiation [59, 60]. Phosphorylation of eIF2α inhibits the exchange of GDP for GTP bound to eIF2α by competitively binding to eIF2B [60], leading to reduced translation initiation of many mRNAs [59, 60], while also promoting translation of mRNAs with special motifs, including upstream ORFs (uORFs) [63]. In mammals [64, 65] and *N. crassa* [66], the clock controls rhythmic phosphorylation of eIF2α, with the levels of phosphorylated eIF2α (P-eIF2α) peaking during the subjective day and requiring a conserved eIF2α kinase. The eIF2α kinase is called GCN2 in yeast and mammals, and CPC-3 in *N. crassa*.

In *S. cerevisiae*, GCN2 is activated by binding of uncharged tRNAs. The levels of uncharged tRNA depend on tRNA abundance, amino acid levels and/or the activity of aminoacyl tRNA synthetases (aaRSs) [67]. Binding of uncharged tRNA to the histidyl tRNA synthetase domain of GCN2 leads to autophosphorylation of Threonine 882 and 887 (T882, T887) in the kinase domain. This is followed by a conformational change and dimerization, which is critical for GCN2 kinase activity [68-73]. In addition, GCN1 is required for uncharged tRNA to activate GCN2. GCN1 binds to N-terminal RWD (RING finger-containing proteins, WD-repeat-containing proteins) domain of GCN2, and transfers uncharged tRNA from ribosomes to GCN2 [74-77]. Furthermore, GCN20, a member of the ATP-binding cassette (ABC) superfamily, binds ribosomes and GCN1 to stabilize interactions between GCN1 and ribosomes [74]. In *N. crassa*, application of 3-Amino-1,2,4-triazole (3-AT), a competitive inhibitor of imidazole glycerol phosphate dehydratase enzyme necessary for histidine production, leads to higher levels of phosphorylation of eIF2α [66]. Moreover, deletion of *gcn-1* abolishes phosphorylation of eIF2α, supporting that the mechanisms of uncharged tRNA activation of CPC-3 in *N. crassa* is conserved with *S. cerevisiae* [66].

In addition to uncharged tRNAs, GCN2 activity is also regulated by the Target of Rapamycin (TOR) pathway through regulation of the inhibitory phosphorylation of Serine 577 (S577), which inhibits the activity of GCN2 [78]. When TOR is active, the negative regulator TAP42 binds to the type 2A-related phosphatase SIT4 and inhibits its activity. Inhibition of SIT4 leads to increased levels of S577 phosphorylation, which in turn lowers GCN2 activity by reducing uncharged tRNA binding affinity and resulting in low levels of phosphorylated eIF2α [78]. Alternatively, when TOR is inhibited by amino acid starvation or rapamycin treatment, SIT4 phosphatase is active, leading to low levels of S577 phosphorylation and high GCN2 activity that results in high levels of phosphorylated eIF2α [79]. In *N. crassa*, rapamycin treatment leads to increased eIF2α phosphorylation [66], indicating that the regulation of GCN2/CPC-3 kinase by TOR pathway is conserved.

In *N. crassa*, CPC-3 protein levels are clock-controlled, however, rhythms in CPC-3 levels are not necessary for rhythmic P-eIF2α accumulation. Instead, the rhythmic activity of CPC-3 is essential for P-eIF2α rhythms, and the activity of CPC-3 is regulated by the rhythmic accumulation of uncharged tRNA though clock control of aaRSs [66]. Rhythmic phosphorylation of eIF2α leads to rhythms in translation initiation rates *in vitro* [66].

In addition to the activity of CPC-3 kinase controlling the phosphorylation of eIF2α during the day, I hypothesized that a phosphatase might also be required to remove the phosphate from eIF2α at night. A balance between kinases and phosphatases is crucial to maintain cell homeostasis. Based on substrate specificity, sequence homology and structural characteristics, phosphatases are classified into two primary families: protein tyrosine phosphatases and serine/threonine (S/T)

protein phosphatases [80, 81]. Generally, protein phosphatases execute dephosphorylation by nucleophilic attack on the phosphate ester moiety of the substrate [82, 83]. A metal-activated water molecule in the catalytic groove of S/T phosphatases initiates the nucleophilic attack, while protein tyrosine phosphatases utilize a catalytic cysteine residue as the nucleophile [84]. In both yeast and *N. crassa* cells, the number of protein kinases encoded in the genome far exceeds the number of protein phosphatases. Yeast cells encode more than 100 protein kinases, but only about 30 protein phosphatases [85, 86]. Similarly, in *N. crassa*, 107 S/T kinases [14, 87] and 30 protein phosphatase catalytic subunits are predicted to be encoded in the genome [88]. These data are consistent with the idea that phosphatases can act on more than one substrate.

Protein phosphatase 1 (PP1), a S/T phosphatase, dephosphorylates eIF2α in yeast [89] and mammalian [90] cells. This activity requires the catalytic subunit GLC7 in yeast [89], and PP1α, PP1β or PP1γ isoforms in mammalian cells [90]. PP1 activity also requires one or more noncatalytic regulatory subunits to associate and target it to different cellular compartments and to specify substrates [91]. In mammalian cells, GADD34 (PPP1R15A) and CReP (PPP1R15B) are the regulatory subunits that recruit PP1 to dephosphorylate Ser51 on eIF2α [92, 93]. GADD34 and/or CReP homologs are present in chickens, frogs, and zebrafish, and a degenerate ortholog was identified in Drosophila [94]. Alternatively, in yeast cells, an N-terminal extension of eIF2γ recruits GLC7 to dephosphorylate Ser51 of eIF2α [94]. *N. crassa* PPP1 (NCU00043) is the homolog of yeast GLC7, and is essential for growth. PPP1 was previously shown to dephosphorylate FRQ protein to regulate the pace of the circadian clock [95]. However, it was not known if PPP1 also functions to dephosphorylate eIF2α in *N. crassa*, and if this activity is required for rhythmic accumulation of P-eIF2α.

Objectives

Understanding how circadian clocks function is critical because of the important roles they play in many organisms' lives, including humans. The basic mechanisms of circadian oscillators are conserved in eukaryotes. Similarly, many of the same output pathways that are controlled by the clock are conserved, such as control of MAPK signaling pathways [96, 97], DNA repair mechanisms [98, 99], and mRNA translation [48, 55, 64-66]. Therefore, elucidating the detailed mechanisms of output pathways in a simple model, such as clock control of eIF2α activity in *N. crassa*, are critical to our deeper understanding of this regulation in more complex eukaryotic organisms.

In mammals [64, 65] and *N. crassa* [66], clock control of eIF2α activity requires the eIF2α kinase GCN2/CPC-3. However, the role of phosphatases in clock regulation of P-eIF2α rhythms and mRNA translation was not known. In this work, I test the hypothesis that the circadian clock regulates the expression of phosphatase PPP1, which rhythmically dephosphorylates P-eIF2α at night. This would be predicted to lead to increased eIF2α activity and increased translation of specific mRNAs at night. The following questions were studied to test this hypothesis:

1. Does the N-terminus of eIF2γ recruit PPP1 to dephosphorylate P-eIF2α?

I examined *N. crassa* P-eIF2α levels in *ppp1* and *eIF2γ* mutant cells. If PPP1 and eIF2γ are required for the dephosphorylation of P-eIF2α, I expected to see increased levels of P-eIF2α in the mutant strains. As expected, high levels of P-eIF2α accumulated in both *ppp1* and *eIF2γ* mutant cells compared to WT cells. In addition, I found that dephosphorylation of P-eIF2α is reduced in extracts

isolated from *ppp1* and *eIF2γ* mutant cells in an *in vitro* dephosphorylation assay. Together, these data support that eIF2γ recruits PPP1 to dephosphorylate P-eIF2α in *N. crassa*.

2. Is PPP1 critical for circadian clock regulation of P-eIF2α?

To determine if dephosphorylation of P-eIF2α is rhythmic, and if cycling PPP1 levels are necessary for rhythms in eIF2α activity, I examined P-eIF2α rhythms in both *ppp1* and *eIF2γ* mutant cells. I discovered that P-eIF2α rhythms were abolished in both mutant strains. These mutations did not abolish the rhythmic activity of the core FRQ/WCC circadian oscillator, supporting that PPP1 is necessary for P-eIF2α rhythms. To determine if dephosphorylation of P-eIF2α is clock controlled, I examined the levels of PPP1 in a circadian time course. I found that PPP1 levels are clock-controlled, with the peak in PPP1 levels occurring in the early evening corresponding to the trough of P-eIF2α levels. Alternatively, eIF2γ levels are not clock-controlled, supporting the idea that the night time peak in PPP1 levels drives rhythmic dephosphorylation of P-eIF2α. To test this idea, I examined if rhythmic accumulation of PPP1 is necessary for P-eIF2α rhythms. In cells with constitutive PPP1 levels, P-eIF2α levels were arrhythmic. These data support that the rhythms of PPP1 protein levels are necessary for P-eIF2α rhythms.

3. Does PPP1 regulate the phosphorylation levels and activity of CPC-3 protein?

Considering that both the kinase CPC-3 [66] and the phosphatase PPP1 are required for P-eIF2α rhythms, another possible pathway for PPP1 to regulate P-eIF2α rhythms is through the regulation of the phosphorylation and activity of CPC-3. To test this possibility, I examined the phosphorylation levels of CPC-3 in cells with low or high PPP1 expression levels using Post Translational Modification Mass Spectrometry (PTM-MS). The phosphorylation levels of CPC-3

Serine 876 (S876) and Threonine 879 (T879) were significantly lower when PPP1 levels were overexpressed, compared with cells with low PPP1 levels. To determine if S876 and/or T879 phosphorylation is important for CPC-3 activity and P-eIF2α rhythms, no phosphorylation (A) and phosphor-mimic (E) mutations of these two sites were generated. I discovered that the phosphorylation of S876 activates CPC-3, but that this is not required for the rhythmic activity of CPC-3. CPC-3 activity appeared to be abolished in T879 mutants as evidenced by no detectable P-eIF2α in the mutants. Although I was unable to directly test if phosphorylation of CPC-3 T879 is necessary for P-eIF2α rhythms, these data support a direct role for PPP1 dephosphorylation of P-eIF2α at night controlling P-eIF2α rhythmicity.

4. Do P-eIF2α rhythms regulate translation of specific mRNAs?

Previous studies suggested that about half of available eEF2 [58] and eIF2α [66] in *N. crassa* are phosphorylated under control of the clock. Consistent with these data, not all *N. crassa* proteins accumulate with a circadian rhythm [55]. Thus, some mRNAs appear to be more sensitive, and whereas others are more resistant, to increased levels of P-eEF2 and P-eIF2α levels. For example, FRQ protein abundance was rhythmic when P-eEF2 [58] or P-eIF2α rhythms [66] were abolished. I hypothesized that rhythmic P-eIF2α regulates the translation of a specific subset of mRNAs. To test this hypothesis, and to identify the mRNAs that are rhythmically translated under control of eIF2α activity rhythms, Dr. Kathrina Castillo and I performed ribosome profiling using circadian time course samples of WT cells, clock mutant Δ*frq* cells, Δ*cpc*-3 cells that lack any P-eIF2α, and constitutively active *cpc-3*^{c} cells that have high and arrhythmic P-eIF2α levels. Using ribo-seq, we identified actively translated mRNAs, and carried out parallel RNA-seq to determine mRNA abundance. We found that the clock regulates the translation of 1328 transcripts, and 404 of these

mRNAs have arrhythmic translation in strains with abolished P-eIF2α rhythms. Experiments are in progress to investigate potential *cis*-elements present in the transcripts that target them to be regulated by P-eIF2α.

The following chapters include the main results of my research. Chapter II has been submitted to PNAS for publication. Chapter III provides insights in regulation of CPC-3 activity, that will continue being studied in the lab. Chapter IV describes a collaborative project with Dr. Kathrina Castillo, that will be submitted for publication. In Chapter IV, I carried out ribo-seq for the constitutively active *cpc-3*^{c} cells, and helped with data analysis and manuscript preparation.

CHAPTER II

PPP1 PHOSPHATASE IS REQUIRED FOR CIRCADIAN CLOCK CONTROL OF TRANSLATION INITIATION FACTOR eIF2α ACTIVITY IN *NEUROSPORA CRASSA*

Introduction

Protein phosphatase 1 (PP1) dephosphorylates eIF2α in yeast [89] and mammalian [90] cells. This activity requires the catalytic subunit GLC7 in yeast, and PP1α, PP1β or PP1γ isoforms in mammalian cells, and also requires one or more non-catalytic regulatory subunits to target PP1 to P-eIF2α [91]. In mammalian cells, the RVxF motif present on GADD34 (PPP1R15A) and CReP (PPP1R15B) recruits PP1 to dephosphorylate Ser51 on eIF2α [92, 93]. GADD34 and/or CReP homologs are present in chickens, frogs, and zebrafish, and a degenerate ortholog was identified in Drosophila [94]. In yeast cells, however, there is no GADD34 or CReP homolog, but instead, an N-terminal extension of eIF2γ contains an RVxF motif that recruits GLC7 to dephosphorylate Ser51 of eIF2α [94]. *N. crassa* PPP1 (NCU00043) is the homolog of yeast GLC7 with 91% identity **(Figure 3)**, and is essential for survival [88]. PPP1 was previously shown to dephosphorylate FRQ protein to regulate the pace of the circadian clock [95]. However, it was not known if PPP1 also functions to dephosphorylate P-eIF2α and control rhythmic eIF2α activity in *N. crassa*. In this study we show that PPP1 dephosphorylates eIF2α *in vitro*, that PPP1 levels are clock-controlled with a peak during the subjective night, and that the rhythm in PPP1 accumulation is necessary for cycling P-eIF2α levels. Our study further reveals that the N-terminus of eIF2γ is required to recruit PPP1 to dephosphorylate eIF2α and maintain robust P-eIF2α rhythmicity, but is not required to maintain the pace of the circadian clock.

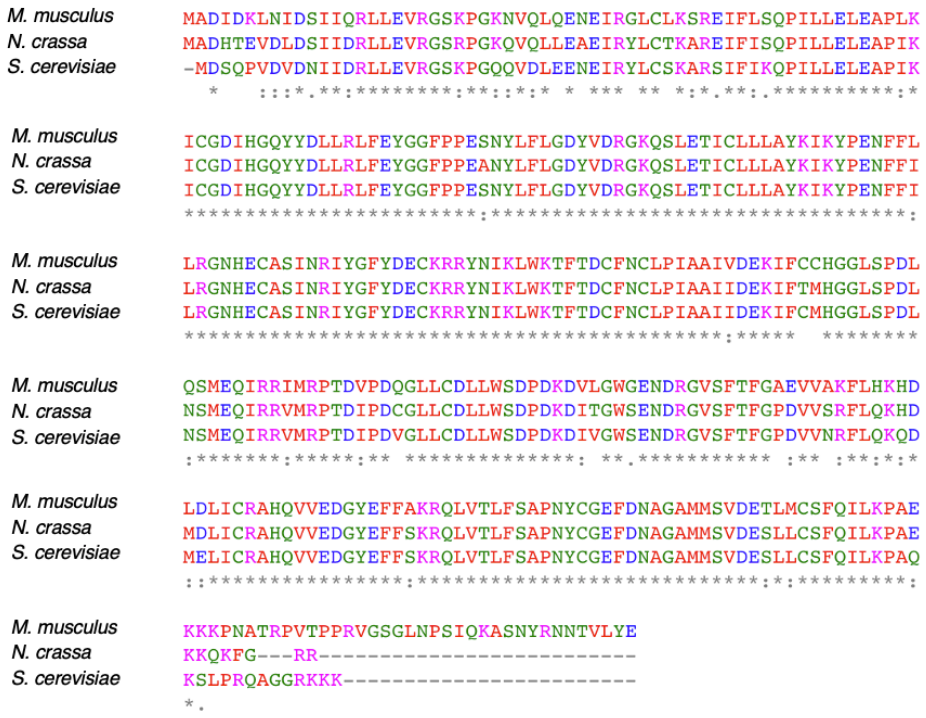

Figure 3. PPP1 protein sequence is highly conserved. Multiple sequence alignment of the *N. crassa* PPP1 protein sequence to homologs in *M. musculus* and *S. cerevisiae*.

Results

PPP1 phosphatase reduces P-eIF2α levels

To determine if phosphatase PPP1 regulates the levels of P-eIF2α in *N. crassa*, the levels and phosphorylation status of eIF2α were examined in *ppp1*^{RIP} mutant cells [95] from cultures grown in constant dark (DD) and harvested at 28h which represents the time when the levels of rhythmic P-eIF2α are low in WT cells [66] (**Figure 4B**). The *ppp1*^{RIP} mutant, with 4 amino acid mutation(**Figure 4A**), was previously shown to reduce PPP1 activity by ~70% [95]. P-eIF2α levels were ~2-fold higher in *ppp1*^{RIP} cells compared to WT cells, whereas the levels of total eIF2α were not altered (**Figure 4B**). Complementation of *ppp1*^{RIP} cells with a wild type copy of *ppp1* inserted into the *csr-1* locus (*ppp1*^{RIP}; *csr-1::ppp1)* reduced P-eIF2α levels to WT levels (**Figure 4B**). These data support a role for PPP1 in maintaining the low levels of P-eIF2α present at subjective night.

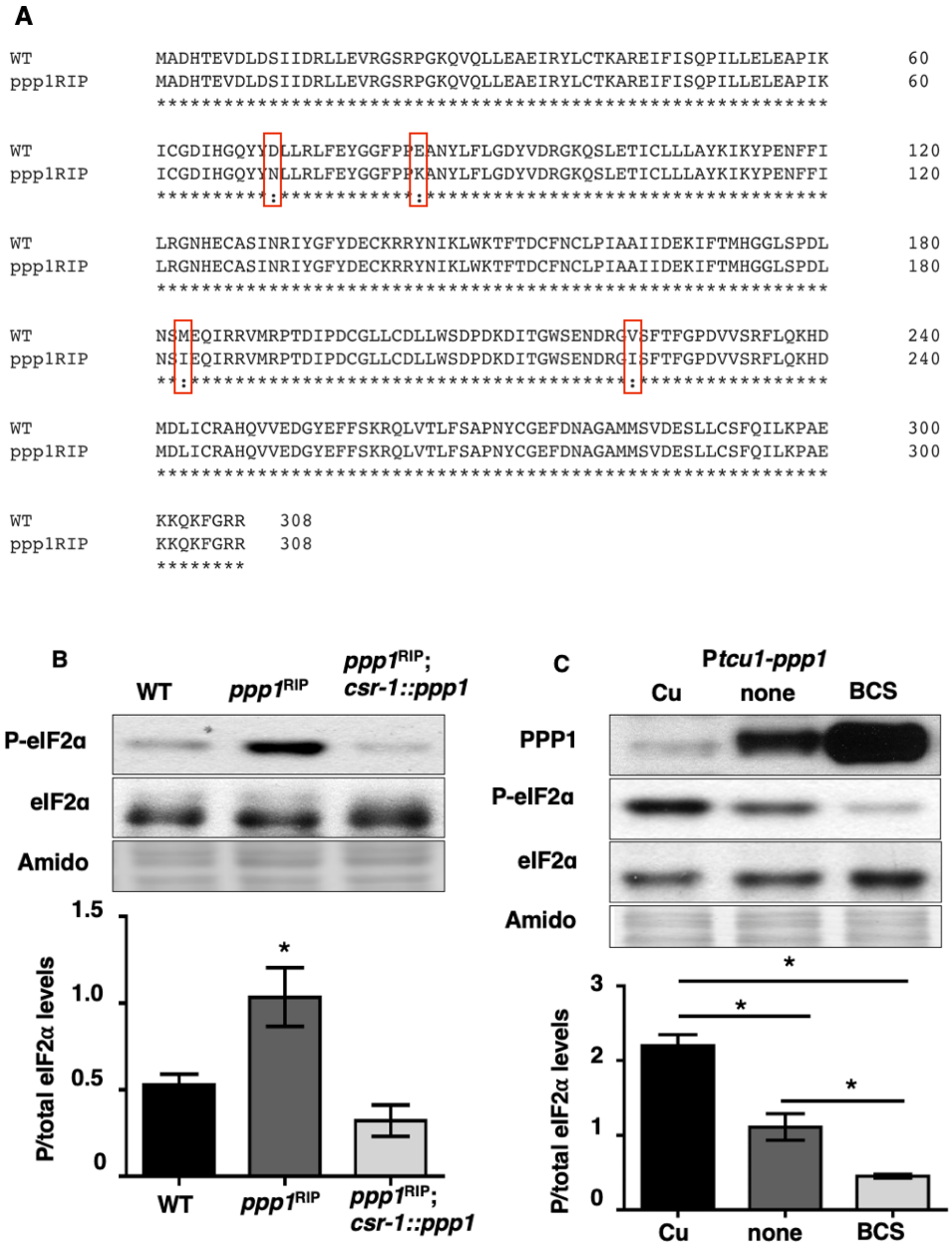

Figure 4. PPP1 phosphatase reduces P-eIF2α levels. (A) The *N. crassa* PPP1 protein sequence in the *ppp1*^{RIP} mutant is aligned with the WT sequence. Red boxes show the mutated amino acids. (B) Western blot of protein extracted from WT, *ppp1*^{RIP} mutant and *ppp1*^{RIP}; *csr1::ppp1* complemented strains during the subjective night (DD28) and probed with anti-P-eIF2α and total eIF2α antibodies. The P-eIF2α/total eIF2α signal is plotted below for each strain (mean ± SEM, n=3; *p< 0.05, student T-test). (C) Western blot of protein extracted from P*tcu1-ppp1* cells grown in the presence of copper sulfate (Cu), BCS, or control (none), harvested at DD28, and probed with anti-PPP1, anti-P-eIF2α, and anti-eIF2α antibodies. The graph below indicates the average signal of P-eIF2α/total eIF2α (mean ± SEM, n=3; *p< 0.05, student T-test).

To determine if changes in PPP1 protein abundance can control P-eIF2α levels, *ppp1* was put under control of the copper regulatable P*tcu-1* promoter [100], and PPP1 levels were detected using a PPP1-specific antibody **(Figure 5).** Consistent with the idea that PPP1 controls P-eIF2α levels *in vivo*, copper sulfate (Cu) repression of P*tcu-1*::*ppp1* led to low PPP1 protein expression and high P-eIF2α levels. Conversely, addition of the copper chelator bathocuproinedisulfonic acid (BCS), led to high PPP1 protein expression and low P-eIF2α levels compared to the control (none) (**Figure 4C**). No significant changes were observed in eIF2α levels in any of the conditions used. Together, these data support the idea that PPP1 either directly, and/or indirectly, reduces P-eIF2α levels in *N. crassa*.

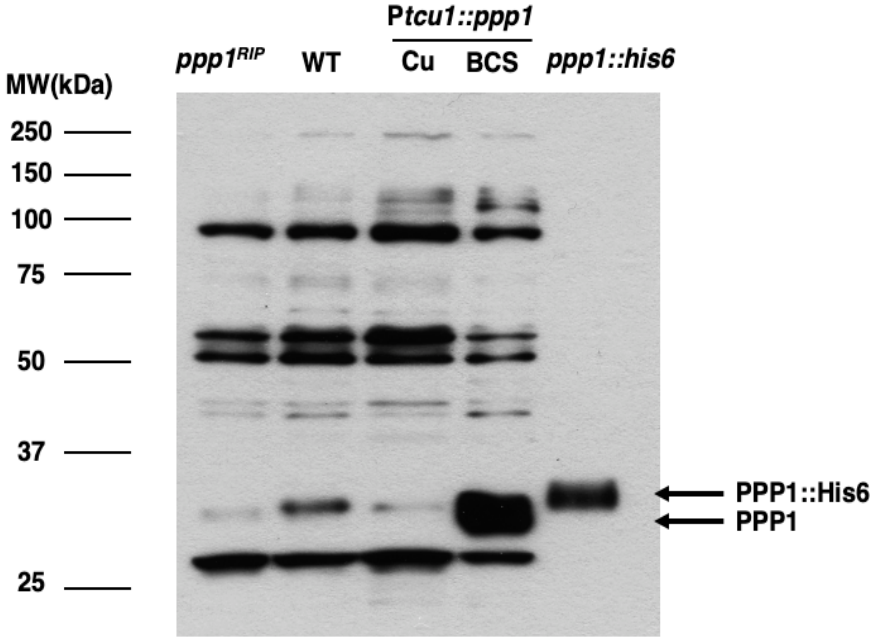

Figure 5. Anti-PPP1 antibody detects the *N. crassa* PPP1 protein. Protein extracted from indicated *Neurospora* cells (*ppp1*^{RIP}, WT, and *Ptcu1::ppp1*) and *E. coli* cells expressing PPP1::His6 were probed with PPP1 antibody.

To determine if PPP1 directly dephosphorylates P-eIF2α, the eIF2 complex was purified from *N. crassa* cells containing a C-terminal V5-tagged eIF2γ (*eIF2γ::v5*) by Co-IP with anti-V5 antibody **(Figure 6A & B).** The eIF2 complex containing P-eIF2α was incubated with total protein extracts (containing PPP1) from subjective evening (DD28) cells that are deficient in their ability to phosphorylate eIF2α (Δ*cpc-3*) to avoid re-phosphorylation of the eIF2α substrate (**Figure 6C**). Cell extracts deficient in PPP1 (*ppp1*^{RIP}; Δ*cpc-3*) served as a negative control (**Figure 6C**). Extracts from Δ*cpc-3* cells led to an ~50% reduction of P-eIF2α levels after 120 mins, while no significant dephosphorylation of eIF2α was detected using extracts from *ppp1*^{RIP}; Δ*cpc-3* cells.

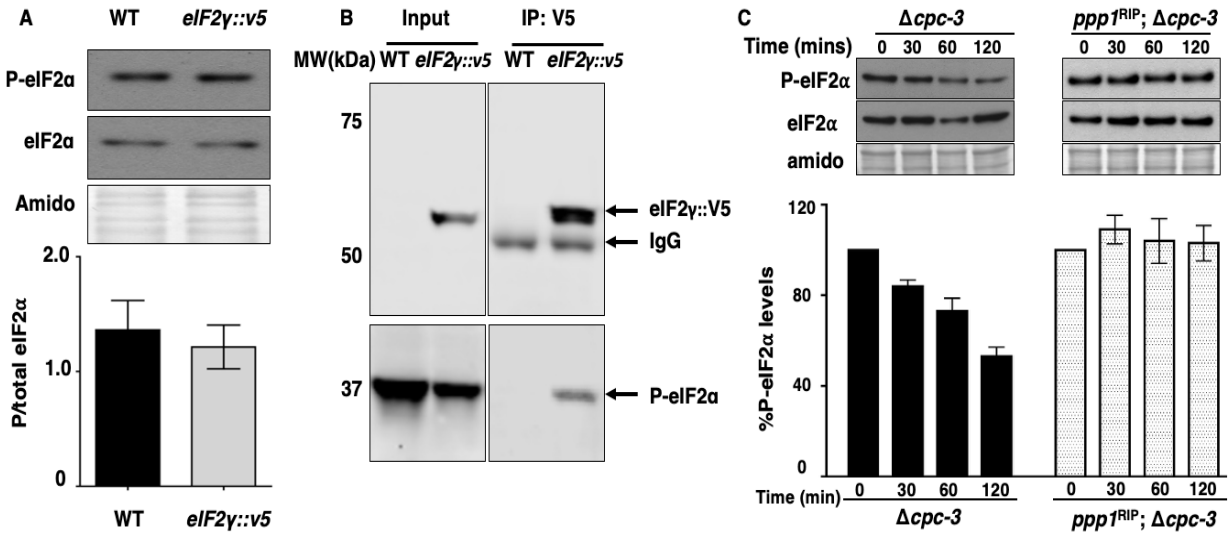

Figure 6. PPP1 phosphatase is critical for dephosphorylation of P-eIF2α *in vitro*. The eIF2γ-V5 tagged protein is functional in *N. crassa*. Western blot of protein extracted from the indicated strains harvested at DD28 were probed with anti-P-eIF2α and total eIF2α antibodies. P-eIF2α/total eIF2α signals are plotted below (mean ± SEM, n=3). No significant difference in the levels of P-eIF2α were detected between WT and eIF2γ::v5 strains (student t-test). (B) Coimmunoprecipitations (IP) with anti-V5 in eIF2γ::v5 cell is able to pull down P-eIF2α. V5 antibody was used to pull down protein from cell extracts of WT and eIF2γ::V5 strains. Western blots were performed using the indicated antibodies. (C) *In vitro* dephosphorylation assay using cell extracts from Δcpc-3 and *ppp1*^{RIP}; Δcpc-3 cells incubated with P-eIF2α from eIF2γ::v5 cells for 0, 30, 60 and 120 mins. P-eIF2α and total eIF2α levels were examined by western blot. The graph below shows the average signal of P-eIF2α normalized to total protein for each time point and normalized to the value at time 0 (mean ± SEM, n=4). In A and C, amido black-stained protein is shown as a protein loading control.

In *S. cerevisiae*, activation of the eIF2α kinase GCN2 *in vivo* requires its association with ribosomes [101]. Uncharged tRNAs are transferred from ribosomes to GCN2 by GCN1 to activate GCN2 [74-77]. We found that *N. crassa* PPP1 associates with ribosomes (**Figure 7**), suggesting the possibility that this interaction may facilitate direct access to its substrate P-eIF2α. Taken together, these results support the idea that PPP1 promotes P-eIF2α dephosphorylation, and are consistent with PPP1 directly dephosphorylating eIF2α.

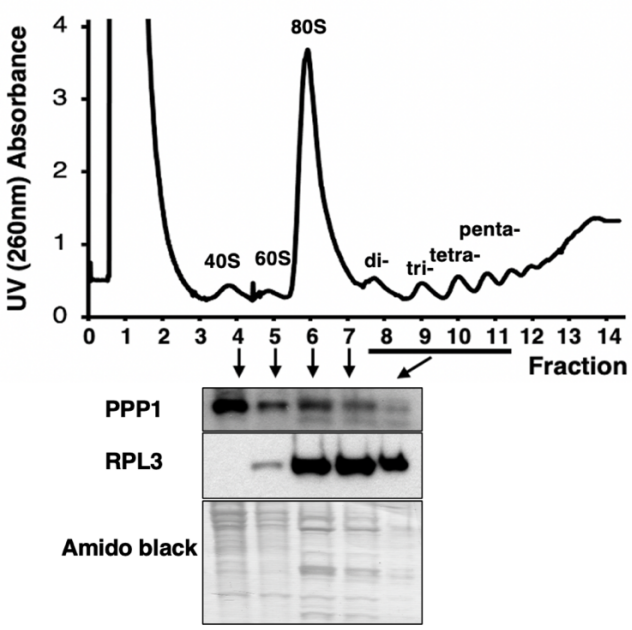

Figure 7. PPP1 is associated with ribosomes. Cell extracts from WT cells harvested at DD24 were separated using sucrose density gradient (10%-50%) centrifugation and fractionation. Western blots of the indicated fractions were probed with PPP1 and control RPL3 antibodies. Membranes were stained with amido black as a protein loading control.

PPP1 phosphatase is required for clock control of P-eIF2α levels

To determine if PPP1 phosphatase controls rhythmic P-eIF2α levels in *N. crassa*, the phosphorylation status of eIF2α was tested in WT and $ppp1^{RIP}$ cells grown in a circadian time course (**Figure 8**). In WT cells, P-eIF2α, but not total eIF2α levels, were rhythmic, with a peak in the subjective late morning (**Figure 8A & 8B**), consistent with our previous studies [66]. While P-

eIF2α and total eIF2α levels fluctuated in *ppp1*^{RIP} cells, P-eIF2α rhythms were abolished (**Figure 8C & 8D**). Because the circadian clock was previously shown to be functional in *ppp1*^{RIP} cells [95], it seemed unlikely that P-eIF2α rhythms were abolished due to a clock defect in these cells. However, to confirm clock function in the mutant, FRQ::LUC protein rhythms were examined in WT and *ppp1*^{RIP} cells. Consistent with published data [95], FRQ levels oscillated robustly in *ppp1*^{RIP} cells, but with ~2 h shorter period as compared to WT cells (**Figure 8E**). Taken together, these data support the idea that the loss of P-eIF2α rhythms in *ppp1*^{RIP} cells is not due to loss of rhythmicity of the core oscillator, but instead results from disruption of downstream circadian regulation of P-eIF2α levels.

Deletion of the N-terminus of eIF2γ alters eIF2α phosphorylation levels and dephosphorylation rate of eIF2α in vitro

The N-terminus of *N. crassa* eIF2γ (NCU02810) resembles the N-terminus of the *S. cerevisiae* eIF2γ in that it has an 80 amino acid extension compared to eIF2γ homologs in higher eukaryotes. In *S. cerevisiae* this region is required to recruit PPP1 to eIF2α [94] **(Figure 9A).** We predicted that if the N-terminus of *N. crassa* eIF2γ functions analogously, the levels of P-eIF2α would be high in strains that have an N-terminal eIF2γ deletion. To test this prediction, residues 2-62 of eIF2γ were deleted (hereafter referred as *eIF2γ*$^{\Delta 2\text{-}62}$) and P-eIF2α levels were examined in cultured germinated conidia samples harvested at DD28 (**Figure 9C**). As predicted, removal of this putative phosphatase-recruiting domain resulted in significantly higher P-eIF2α levels in *eIF2γ*$^{\Delta 2\text{-}62}$ compared to WT cells. Furthermore, P-eIF2α levels in *eIF2γ*$^{\Delta 2\text{-}62}$ cells were not significantly different than the high levels observed in *ppp1*^{RIP} cells. These results support a role for the N-terminal region of *N. crassa* eIF2γ in recruiting PPP1 phosphatase to P-eIF2α *in vivo*.

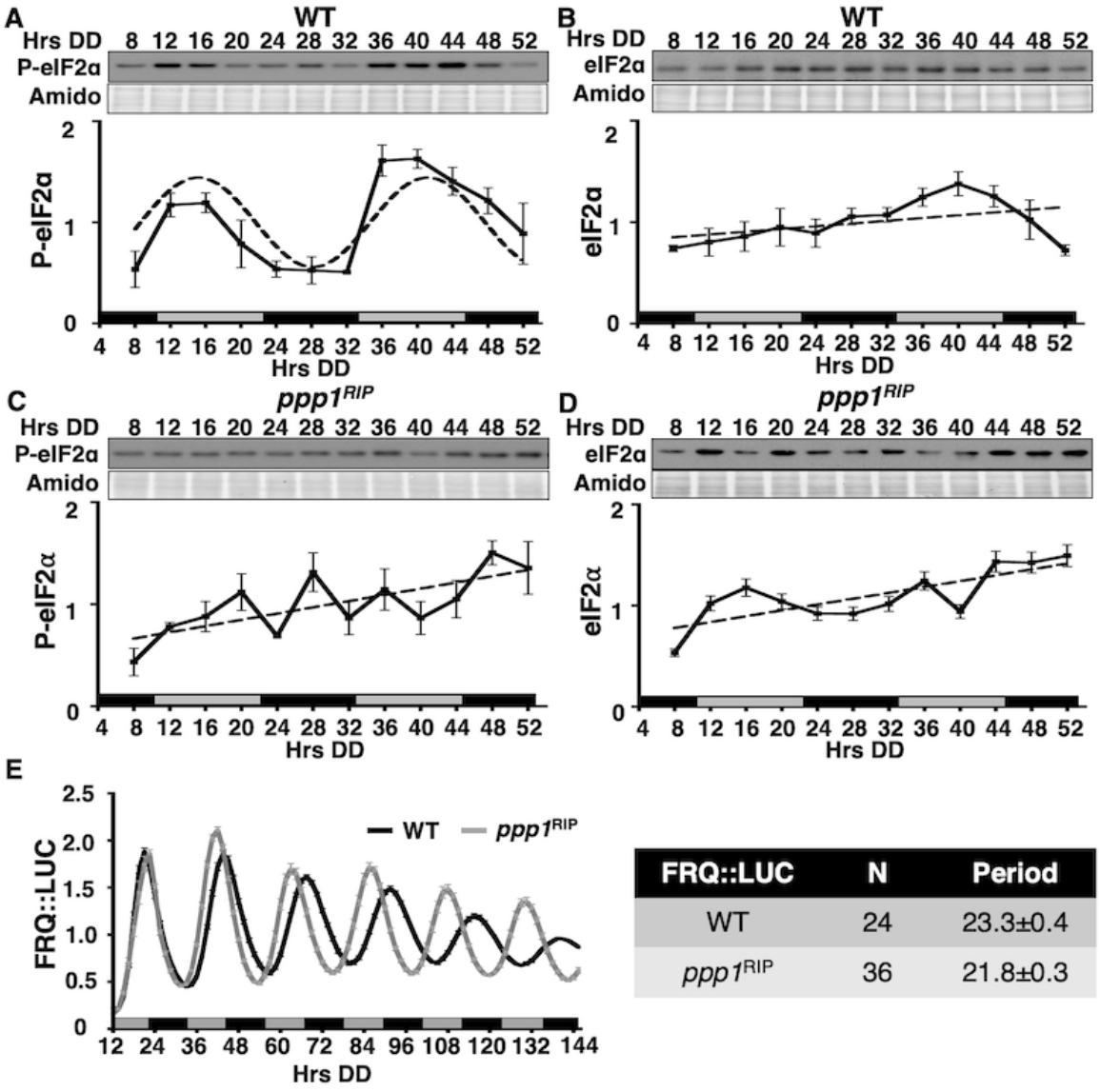

FRQ::LUC	N	Period
WT	24	23.3±0.4
ppp1^{RIP}	36	21.8±0.3

Figure 8. PPP1 phosphatase is necessary for rhythmic P-eIF2α accumulation. Representative western blots of protein extracted from WT (A, B) or *ppp1*^{RIP} (C, D) strains cultured in a circadian time course, harvested at the indicated times in the dark (Hrs DD), and probed with anti-P-eIF2α antibody (A, C) or total eIF2α antibody (B, D). Membranes were stained with amido black as a protein loading control. Plots of the data (mean ± SEM, n=3) below show the average P-eIF2α (A, C) or eIF2α (B, D) signal normalized to amino black signal (solid line). F-tests determined rhythmicity of P-eIF2α in WT cells (A) fit to a sine wave (dotted line, $p<0.001$), while P-eIF2α in *ppp1*^{RIP} cells (C) and eIF2α in WT (B) and *ppp1*^{RIP} cells (D) better fit to a line (dotted lines). The blots were probed separately, and therefore cannot be used to compare protein levels between the strains. (E) Luciferase activity from a FRQ::LUC translational fusion in WT (black line) and *ppp1*^{RIP} (grey line) cells cultured in DD and monitored every 90 min for 6 days (Hrs DD). The average bioluminescence signal is plotted (mean ± SEM). Period and phase (mean ± SEM) of the FRQ::LUC rhythm are shown on the right.

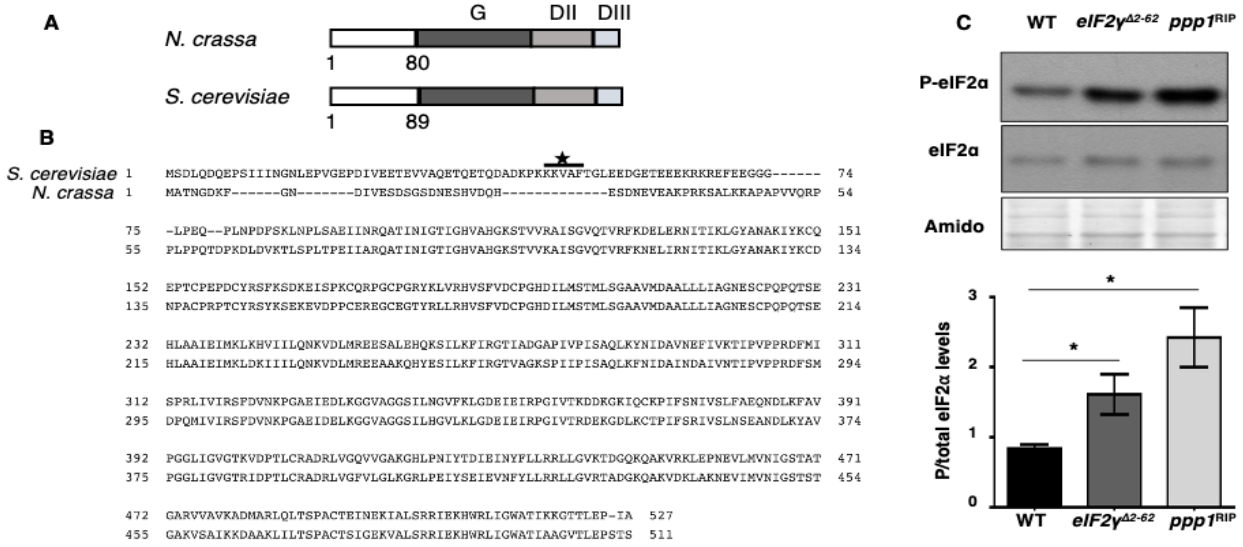

Figure 9. Deletion of the amino terminal 60 amino acids of *N. crassa* eIF2γ alters eIF2α phosphorylation levels. (A) Schematic diagram shows the location of the GTP-binding (G) domain and domains II (DII) and III (DIII) of eIF2γ in *N. crassa* and *S. cerevisiae* based on domain information from InterPro (https://www.ebi.ac.uk/interpro/). The numbers mark the amino acids that make up the N-terminal extension. (B) Alignment of eIF2γ protein sequence in *N. crassa* with *S. cerevisiae*. The sequence marked with a star indicates the binding motif KKVAF of eIF2γ in *S. cerevisiae.* (C) Western blot of protein extracted from the indicated strains harvested at DD28 were probed with anti-P-eIF2α or total eIF2α antibodies. P-eIF2α/total eIF2α signals are plotted below (mean ± SEM, n=3; *p< 0.05, student T-test).

To determine if the N terminus of eIF2γ impacts dephosphorylation of eIF2α by PPP1 *in vitro*, the eIF2 complex was purified from *N. crassa eIF2γ::v5* and *eIF2γ*$^{\Delta 2\text{-}62}$*::v5* cells by Co-IP with anti-V5 antibody **(Figure 10A).** The eIF2 complex containing pulled down P-eIF2α with eIF2γ::V5 was incubated with total cell extracts (containing PPP1) from Δ*cpc-3* cells, and the eIF2 complex pulled down with eIF2γ$^{\Delta 2\text{-}62}$ ::V5 was incubated with total cell extracts from *eIF2γ*$^{\Delta 2\text{-}62}$; Δ*cpc-3* cells (**Figure 10B**). Extracts from Δ*cpc-3* cells led to an ~50% reduction of P-eIF2α levels after 120 mins, consistent with dephosphorylation of P-eIF2α by PPP1, and the data shown in **Figure 6C.** However, extracts from *eIF2γ*$^{\Delta 2\text{-}62}$; Δ*cpc-3* cells that lack the N-terminus of eIF2γ showed

significantly reduced dephosphorylation of P-eIF2α levels (**Figure 10B**). These results, together with the lack of dephosphorylation of P-eIF2α in mutant PPP1 extracts (**Figure 6C**), support the idea that the N-terminus of eIF2γ recruits PPP1 to dephosphorylate eIF2α in *N. crassa*.

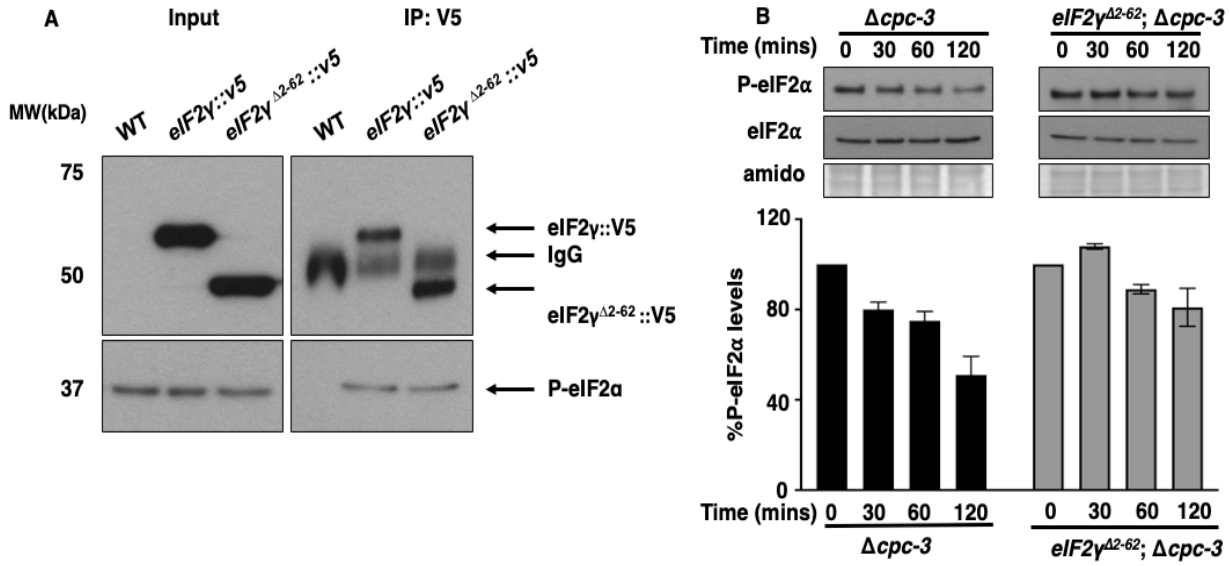

Figure 10. Deletion of the amino terminal 60 amino acids of *N. crassa* eIF2γ impacts the P-eIF2α *in vitro* dephosphorylation rate. (A) Anti-V5 antibody was used to pull down protein from cell extracts of WT, *eIF2γ::v5* and *eIF2γ*$^{\Delta 2\text{-}62}$*::v5* strains. Western blots of input and IP samples were performed using the indicated antibodies. (B) *In* vitro dephosphorylation assay using cell extracts from Δ*cpc-3* and *eIF2γ*$^{\Delta 2\text{-}62}$; Δ*cpc-3* cells incubated with pulled down P-eIF2α from *eIF2γ::v5* and *eIF2γ*$^{\Delta 2\text{-}62}$*::v5* cells respectively for 0, 30, 60 and 120 mins. P-eIF2α and total eIF2α levels were examined by western blot. The graph below shows the average signal of P-eIF2α normalized to total protein for each time point and normalized to the value at time 0 (mean ± SEM, n=3).

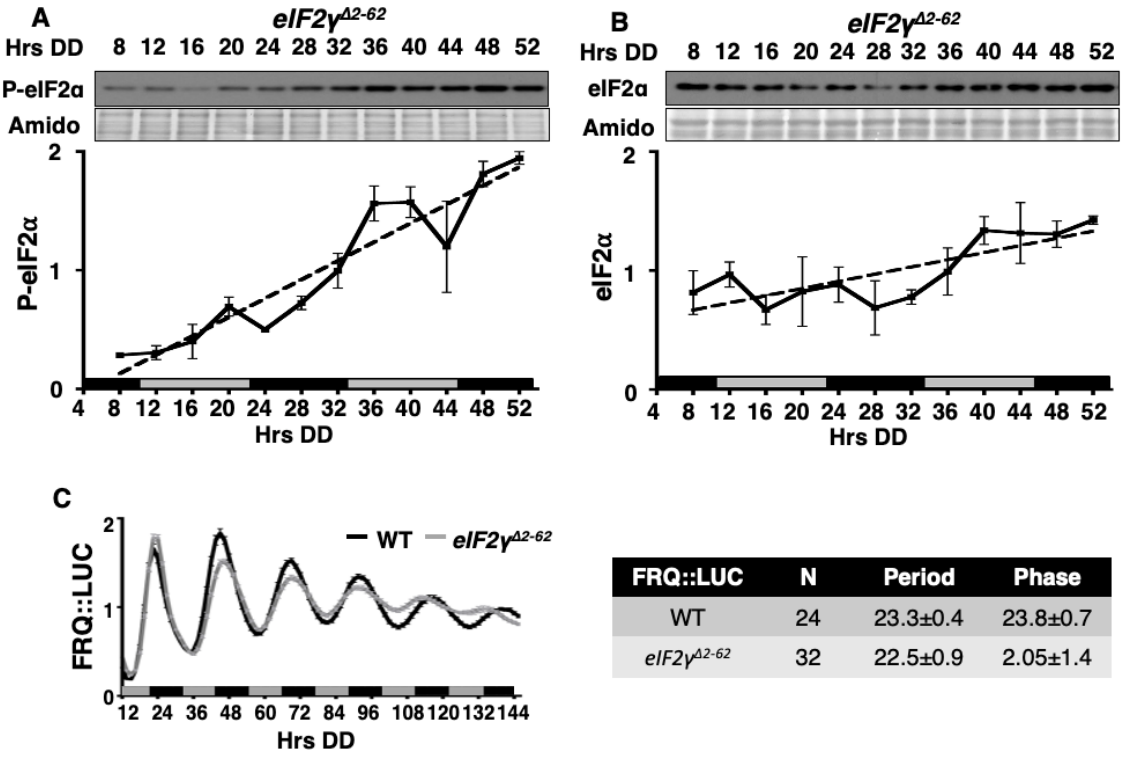

FRQ::LUC	N	Period	Phase
WT	24	23.3±0.4	23.8±0.7
eIF2γ$^{\Delta 2\text{-}62}$	32	22.5±0.9	2.05±1.4

Figure 11. Deletion of the amino terminal 60 amino acids of *N. crassa* eIF2γ dampens eIF2α phosphorylation rhythmicity. Western blots of protein from *eIF2γ*$^{\Delta 2\text{-}62}$ cells grown in a circadian time course, harvested at the indicated times in DD (Hrs DD), and probed with anti-P-eIF2α (A) or anti-total eIF2α (B) antibody. Plots of the data (mean ± SEM, n=5) below display the average P-eIF2α (A) or eIF2α (B) signal normalized to total protein (solid line). Both P-eIF2α and total eIF2α in *eIF2γ*$^{\Delta 2\text{-}62}$ cells were arrhythmic determined by F-tests of fit to a line (dotted lines). Amido black-stained protein was used as a protein loading control. (C) Luciferase activity from a FRQ::LUC translational fusion expressed in WT (black line) and *eIF2γ*$^{\Delta 2\text{-}62}$ (grey line) cells cultured in DD and monitored every 90 min for 6 days (Hrs DD). The average bioluminescence signal is plotted (mean ± SEM). Period and phase (mean ± SEM) are shown below.

Deletion of the N-terminus of eIF2γ alters eIF2α phosphorylation rhythmicity

To determine if deletion of the N-terminal extension of eIF2γ is essential for circadian clock control of P-eIF2α, the levels of P-eIF2α were examined over a circadian time course in *eIF2γ*$^{\Delta 2\text{-}62}$ cells. The levels of P-eIF2α increased over time and were arrhythmic in *eIF2γ*$^{\Delta 2\text{-}62}$ cells (**Figures 11A)**. Total eIF2α levels in *eIF2γ*$^{\Delta 2\text{-}62}$ cells were arrhythmic **(Figure 11B)**. Unlike the short period FRQ-LUC rhythm observed in *ppp1*^{RIP} cells (**Figure 8E),** the period of FRQ-LUC reporter

rhythms was not significantly altered in *eIF2γ*$^{\Delta 2\text{-}62}$ cells compared to WT cells **(Figure 11C).** Therefore, it is likely that a different regulator is used to target PPP1 to dephosphorylate FRQ. Taken together, these data support a role for the N-terminus of eIF2γ in recruiting PPP1 to P-eIF2α and driving circadian clock control of P-eIF2α levels.

Rhythmic phosphorylation of eIF2α requires rhythmic PPP1 levels

PPP1 phosphatase and the N-terminus of eIF2γ are necessary for circadian rhythms of P-eIF2α levels, but not for core clock function. Thus, rhythmic control of eIF2α activity may be through clock control of the levels and/or activities of PPP1 phosphatase and/or eIF2γ. Prior mass spectrometry proteomic studies suggested that PPP1 protein, but not eIF2γ, could be rhythmic [55]. To determine if the circadian clock controls the levels of PPP1 phosphatase and/or eIF2γ, PPP1::luciferase (PPP1::LUC) and eIF2γ::V5 C-terminal translational fusion constructs were generated. No change in P-eIF2α levels was observed cells containing the V5-tagged version of eIF2γ::V5 compared to WT cells, indicating the tag does not alter the function of eIF2γ (**Figure 12D**). PPP1::LUC protein accumulated rhythmically in WT cells, but not in control clock mutant Δ*frq* cells, (**Figure 12A**), demonstrating that PPP1 protein levels are clock-controlled. Consistent with PPP1 functioning as an eIF2α phosphatase, the early evening peak (with phase CT 14) in PPP1::LUC levels correlated with the trough of P-eIF2α levels (**see Figure 8A)**. Alternatively, eIF2γ::V5 levels did not cycle in WT cells (**Figure 12B**). In addition, PPP1::LUC rhythmicity was not altered in Δ*cpc*-3 cells that are unable to phosphorylate eIF2α [66] (**Figure 12C**), indicating that PPP1 protein level rhythms arise from mechanisms that are independent of rhythmic eIF2a activity. Together, these data suggested the possibility that the nighttime peak in PPP1 levels may be critical for P-eIF2α rhythms.

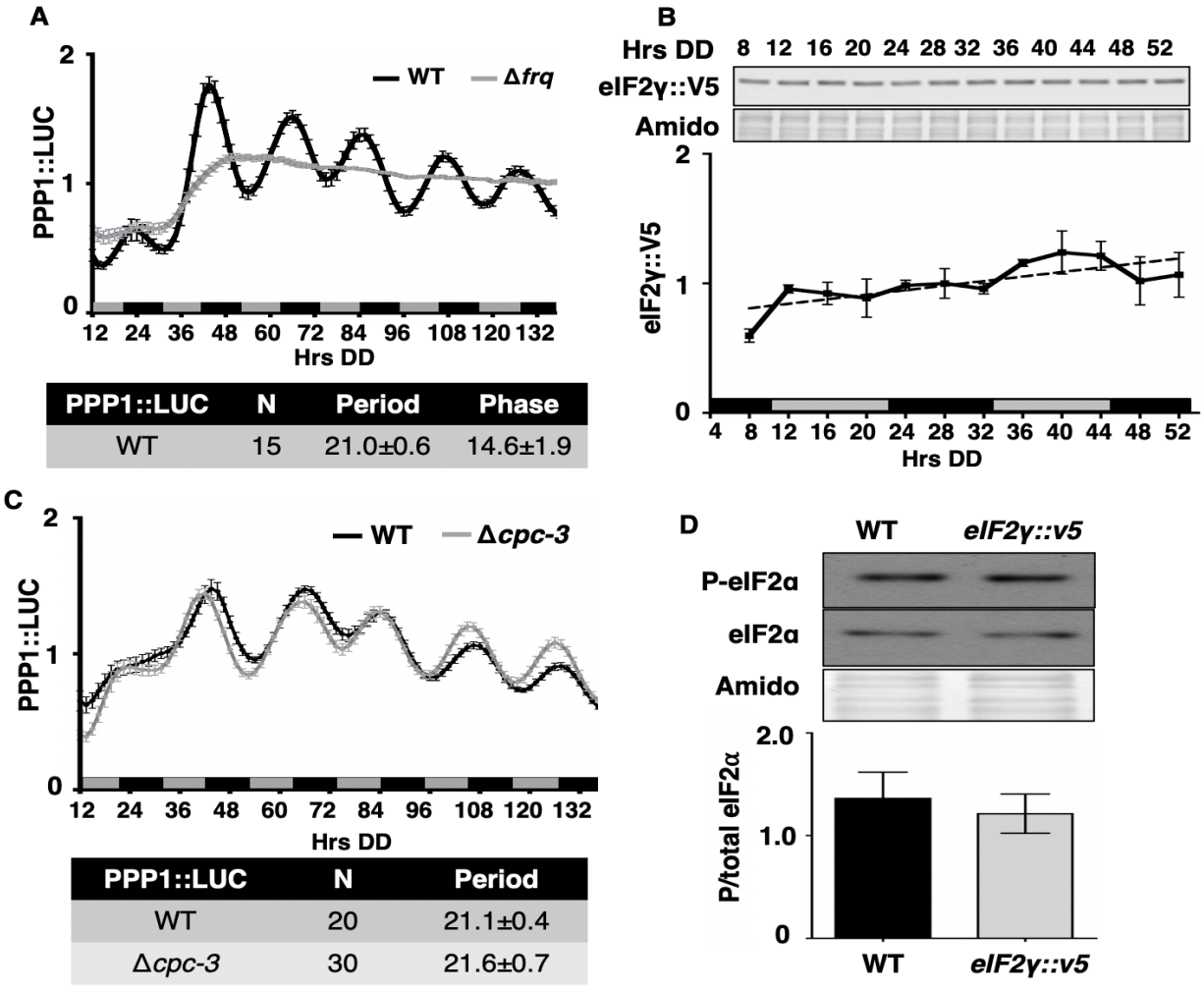

PPP1::LUC	N	Period	Phase
WT	15	21.0±0.6	14.6±1.9

PPP1::LUC	N	Period
WT	20	21.1±0.4
Δ*cpc-3*	30	21.6±0.7

Figure 12. The circadian clock controls PPP1 phosphatase levels, but not eIF2γ levels. (A) Luciferase activity from PPP1::LUC translational fusions in WT (black line) and Δ*frq* (grey line) cells cultured in DD and monitored every 90 min for 6 days (Hrs DD). The average bioluminescence signal is plotted (mean ± SEM). Period and phase (mean ± SEM) are shown below. (B) Western blot protein from *eIF2γ::v5* cells grown over a circadian time course, harvested at the indicated times (Hrs DD), and probed with anti-V5 antibody. Amino black stained protein was used as a loading control. The average normalized signal is plotted below (mean ± SEM) (solid black line). *eIF2γ::V5* levels were arrhythmic as indicated by fit of the data to a line (dotted line).

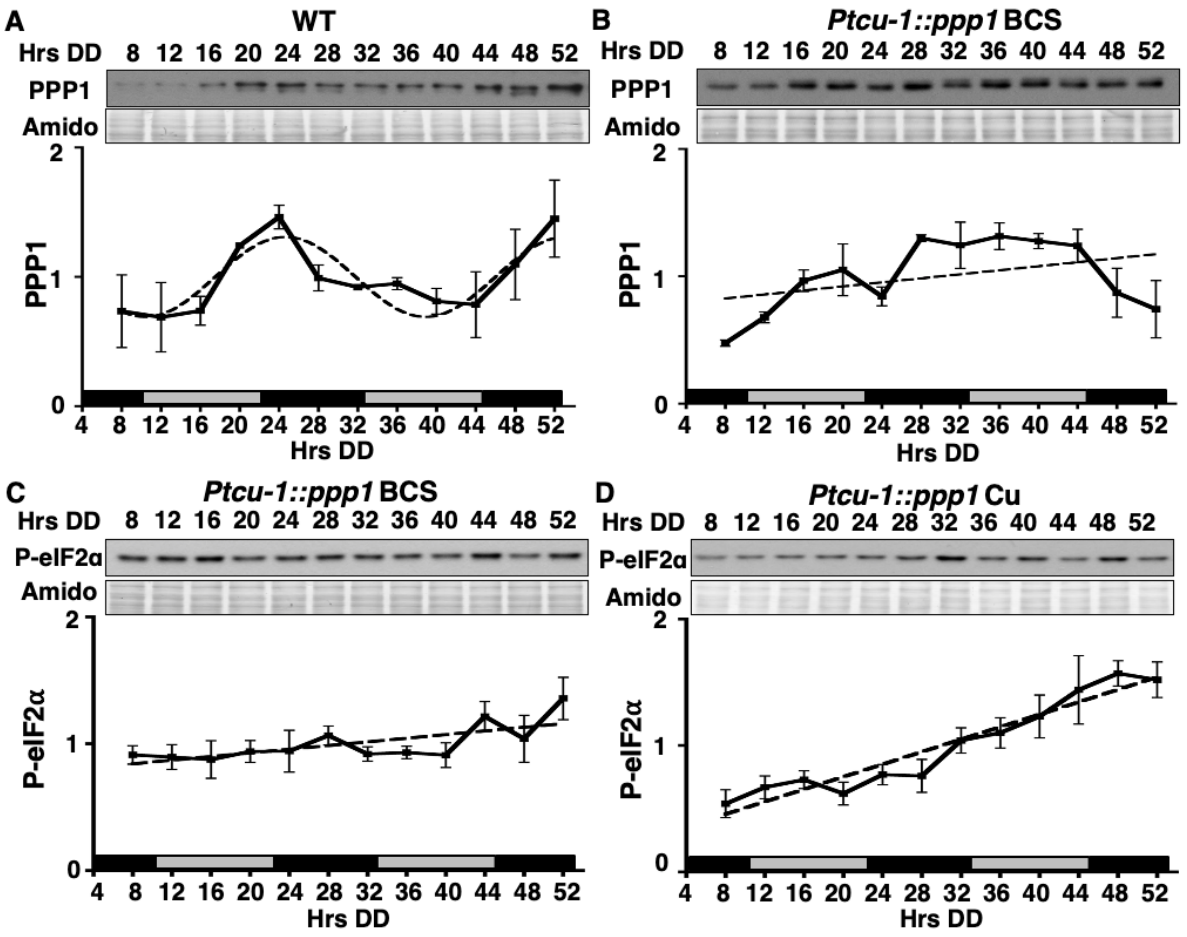

Figure 13. Clock control of PPP1 is necessary for rhythmic P-eIF2α levels. Western blots of protein extracted WT (A) or P*tcu1::ppp1* cells cultured with 50 μM of BCS (B,C) or 250 μM copper sulfate (D) over a circadian time course, harvested at the indicated times in DD (Hrs DD), and probed with anti-PPP1 (A, B) or anti-P-eIF2α (C, D) antibodies. The normalized protein levels are plotted below the blots (mean ± SEM, n=3) (solid black line). PPP1 levels in WT cells (A) were rhythmic based on fit to a sine wave (dotted line, $p<0.001$), whereas PPP1 and P-eIF2α in B-D were arrhythmic as indicated by fit to a line (dotted line).

To determine if rhythmic accumulation of PPP1 is necessary for rhythms in P-eIF2α levels, protein from strains containing P*tcu-1::ppp1* **(Figure 4B)** grown in a circadian time course were isolated and examined by western blot using anti-PPP1 antibody. Consistent with PPP1::LUC assays, PPP1 protein levels were rhythmic, peaking in the subjective early evening (DD24) in WT cells (**Figure 13A**). In P*tcu1-ppp1* cells grown in the presence of the activating chelator BCS, PPP1 levels were

high at all times of the day (**Figure 13B**), and P-eIF2α levels were low and arrhythmic (**Figure 13C**). In P*tcu1-ppp1* cells grown in the presence of the repressive copper ion (Cu), PPP1 protein levels were low at all times of the day **(Figure 4B),** and P-eIF2α levels were high and arrhythmic (**Figure 13D**). Thus, non-rhythmic PPP1 expression at either low- or high- levels abolished P-eIF2α rhythms. These data demonstrated that the rhythmic accumulation of PPP1 protein is necessary for circadian rhythms in P-eIF2α levels.

Discussion

In *N. crassa* and mice, circadian clock regulation of eIF2α phosphorylation controls rhythmic mRNA translation and protein accumulation [64, 66]. In *N. crassa* the eIF2α kinase, CPC-3, is necessary for the accumulation of P-eIF2α levels and a constitutively active allele causes arrhythmicity of P-eIF2α [66]. Here, we show that protein phosphatase PPP1, which peaks in levels during the subjective night, is also necessary for circadian rhythms in P-eIF2α levels. These data support a model whereby the circadian clock dynamically regulates both the phosphorylation, through the day-stimulated CPC-3 kinase, and dephosphorylation, by the night-peaking PPP1 phosphatase, of eIF2α (**Figure 14**). The peak in activity of eIF2α at night, together with increased nighttime activity of translation elongation factor eEF-2 [58], provide a mechanism to explain increased rhythmic protein production at night in *N. crassa* [55].

While PPP1 is necessary for rhythmic eIF2α activity, it is not sufficient to drive rhythms in P-eIF2α levels in strains with constitutively active CPC-3 (CPC-3^C). In *cpc-3^C* cells, P-eIF2α levels are high and arrhythmic [66], despite normal levels of PPP1 (**Figure 12C**). This may be due the levels or activity of PPP1 not being sufficient to dephosphorylate the constantly high levels of P-

eIF2α present in this mutant. While we showed that P-eIF2α levels are directly related to PPP1 levels in a strain with wild type CPC-3 activity **(Figure 4C),** after two hours *in vitro* only up to 50% of P-eIF2α was dephosphorylated by PPP1 indicating that the de-phosphorylation step may be kinetically unfavorable **(Figure 6C).** These data are consistent with the slow *in vitro* dephosphorylation rate of eIF2α observed in yeast extracts [94]**.** A second possibility for why PPP1 rhythms are not sufficient to drive P-eIF2α rhythms in the *cpc-3*^{C} mutant is that PPP1 may also regulate CPC-3 activity. This idea is supported by the presence of phosphatases in *S. cerevisiae* known to target both P-eIF2α and P-GCN2. The 2A-related phosphatase SIT4, which responds to the Target of Rapamycin (TOR) pathway [78, 79] and dephosphorylates eIF2α [102], also controls

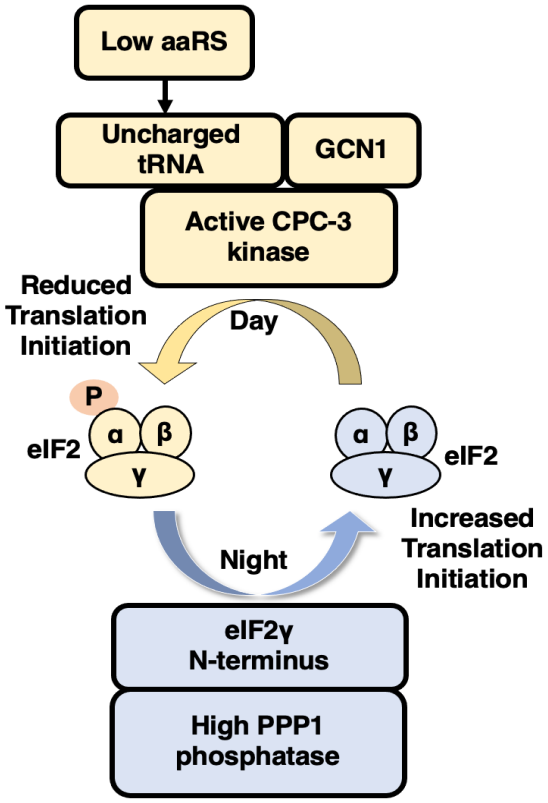

Figure 14. Model of the mechanisms of clock coordination of both the day-active eIF2α kinase CPC-3 and the night-active phosphatase PPP1 controlling rhythmic eIF2α activity and translation initiation.

Ser577 phosphorylation and activity of GCN2. In addition, phosphatase Ppz1 impacts GCN2-dependent phosphorylation of eIF2α by an unknown mechanism [103, 104]. Thus, in addition to direct dephosphorylation of eIF2α, these data support a role for phosphatases controlling the activity of the eIF2α kinases. Experiments are currently underway to identify potentially rhythmic phosphorylation sites on CPC-3 that may be dephosphorylated by PPP1.

Kinases typically target specific substrates; however, phosphatases generally have a wide substrate range [94]. In addition to dephosphorylation of eIF2α, *S. cerevisiae* GLC7, the catalytic subunit of PP1, dephosphorylates substrates that function in glycogen metabolism, glucose regulation, and cell division [85]. Furthermore, PP1 requires one or more noncatalytic regulatory subunits to target it to different cellular compartments and for substrate specificity. More than 180 PP1 regulatory subunits have been identified in mammalian cells [105], and 17 regulatory subunits were discovered in *S. cerevisiae* [106]. Most, but not all, PP1 regulatory subunits contain a conserved RVxF motif, which is typically flanked by basic residues at the N-terminus, and by acidic residues at the C-terminus [107]. Regulatory subunits that recruit PP1 to eIF2α in mammalian cells, GADD34 and CReP, contain an RVxF motif [92, 93]. In the PP1 regulatory subunit eIF2γ in *S. cerevisiae*, the RVxF motif is present in an N-terminal domain that extends beyond homology to mammalian eIF2γ [94] and deletion of the N terminus of eIF2γ does not affect yeast cell growth, indicating that the eIF2 complex is functional in translation [108]. Although *N. crassa* eIF2γ lacks the conserved RVxF motif **(Figure 9B)**, we show that the N-terminus of eIF2γ is important for P-eIF2α levels (**Figure 9C**), *in vitro* dephosphorylation **(Figure 10B),** and rhythmicity **(Figure 11)**. Because the levels of eIF2γ are not clock-controlled (**Figure 12B**), we suggest that the interaction between the eIF2γ and eIF2α in the eIF2 complex provides a platform for eIF2γ to deliver PPP1

at night, when it is at peak levels under control of the clock (**Figure 12A**). Furthermore, our data supports the possibility that interactions between PPP1 and eIF2, including eIF2γ and eIF2α subunits, as well as CPC-3, may be localized to the ribosome (**Figure 7),** although additional experiments are needed to confirm this possibility.

Disruption of P-eIF2α rhythms, either by deletion or mutation of CPC-3 kinase in *N. crassa*, impacts the rhythmic translation of *alg-11*, but not FRQ [66] or PPP1 (**Figure 12C**) protein rhythms, or overt developmental rhythms [66]. These data support that under constant environmental conditions, circadian translational regulation by the rhythmic activity of eIF2α is gene-specific, as opposed to a global translational response [66]. In $ppp1^{RIP}$cells, the period of FRQ::LUC accumulation rhythms is shorter compared to WT cells [95] **(Figure 8E)**. However, the short period FRQ::LUC rhythm in $ppp1^{RIP}$ is not due to loss of P-eIF2α rhythms in the mutant because disruption of P-eIF2α rhythms in $eIF2\gamma^{\Delta 2\text{-}62}$ cells did not significantly alter the period of FRQ::LUC rhythmicity (**Figure 11C**).

eIF2α phosphorylation regulates protein production to enable the organism to quickly respond to environmental stresses, including amino acid starvation. The circadian clock provides an additional layer of regulation of eIF2α activity to control the rhythmic translation of specific target genes. While the mechanisms underlying this specificity are not known, these data support the idea that temporal control of eIF2α activity provides organisms, from fungi to mammals, the ability to respond and adapt to internal and environmental stimuli [109]. Because mRNA translation requires significant cellular energy, clock control of translation may provide a mechanism to coordinate

energy metabolism with translation to partition translation to the times of day when energy levels are high.

Methods and Materials

N. crassa strains and growth conditions: *N. crassa* vegetative growth conditions, transformation and crossing protocols were as described previously [96]. Strains with the *hph* cassette were maintained on Vogel's minimal media containing 0.2 g/L of hygromycin B (#80055-286, VWR, Radner, PA). Strains with the *bar* cassette were maintained on Vogel's minimal media without NH_4NO_3 and with 0.5% proline and 0.2 g/L BASTA (Liberty 280 SL Herbicide, Bayer, NC). Germinated conidia were cultured and harvested as previously described [110-112]. Briefly, $1X10^5$ conidia were inoculated in 250mL Vogel's minimal media with 2% glucose. Conidia were germinated in LL 30℃ for 4 h with orbital shaking (100rpm), then transferred to DD 25℃ and cultured for 28 h (DD28). Samples were harvested using vacuum filtration, snap frozen in liquid nitrogen and processed for analysis or stored in -80℃.

N. crassa wild type (WT) FGSC #4200 (mat a, 74-OR23-IV) or FGSC #2489 (mat A, 74-OR23-IV), were obtained from the Fungal Genetics Stock Center (FGSC, Kansas State University). Δ*frq::bar* (DBP 1228) [113] and *cpc-3*^{c} (DBP 3291) [66] was previously generated. The primers used in the generation and validation strains are listed in **Table 1**. DBP3070 (*ppp1*^{RIP}) was generated by crossing *ppp1*^{RIP}, *ras-1*^{bd,} which was kindly provided by Dr. Yi Liu [95], with WT (FGSC #2489). Progenies were screened by their slow growth phenotype, and validated by PCR using *ppp1* seq F1 and R1 primers, followed by DNA sequencing using primers *ppp1* seq F. To complement *ppp1*^{RIP}, the *ppp1* gene was inserted into the *csr-1* locus by homologous

recombination using a product from 3-way PCR containing 1kb of the *csr-1* 5'flank (primers *ppp1* F1 and R1), the *ppp1* gene with the 5' and 3' UTRs (primers *ppp1* F2 and R2), and 1kb of the *csr-1* 3'flank (primers *ppp1* F3 and R3) to generate $ppp1^{RIP}$; *csr-1::ppp1* (DBP3457). The 3-way PCR product was transformed into $ppp1^{RIP}$ (DBP3070) and primary transformants were selected by cyclosporine A (30024-25MG, Sigma-Aldrich St. Louis, MO) resistance (5 μg/ml), and validated by PCR using *ppp1* F and R. For overexpression of PPP1, the *bar::*$P_{tcu\text{-}1}$*::ppp1* strain was generated by transforming a 3-way PCR product containing 1 kb of the 5' *ppp1* ORF (primers tcu1 F1 and R1), *bar::*$P_{tcu\text{-}1}$ from plasmid pDBP450 (primers tcu1 F2 and R2) [100], and 1 kb of the 3' end of *ppp1* (primers tcu1 F3 and R3) into the WT (FGSC #4200) strain. Homologous recombination was validated by PCR (primers tcu1 F4 and R4), and a *bar::*$P_{tcu\text{-}1}$*::ppp1* homokaryon (DBP3279) was obtained by microconidia filtration [114]. To generate strains deleted for the eIF2γ N-terminus (2-62 aa), the $eIF2\gamma^{\Delta 2\text{-}62}$ aa fragment was generated by 2-way PCR using primers $eIF2\gamma^{\Delta 2\text{-}62}$ F1, R1, F2 and R2. The PCR product was co-transformed with hyg^R pBP15 plasmid [115] into Δ*mus-52::bar* (FGSC#9719). Homologous recombinants were screened by PCR (primers $eIF2\gamma^{\Delta 2\text{-}62}$ F3 and R3), and selected based on the size of the PCR product. A transformant containing $eIF2\gamma^{\Delta 2\text{-}62}$ was crossed to WT (FGSC#2489) to obtain an $eIF2\gamma^{\Delta 2\text{-}62}$ homokaryon (DBP3297). To assay FRQ::LUC luciferase activity, strains $ppp1^{RIP}$ (DBP3070) and $eIF2\gamma^{\Delta 2\text{-}62}$ (DBP3297) were crossed to DBP1563 containing a FRQ::LUC translational fusion linked to *bar* [116], respectively. Progeny were screened for luciferase activity arising from *frq::luc*, sequencing of $ppp1^{RIP}$, or PCR for $eIF2\gamma^{\Delta 2\text{-}62}$, to obtain *frq::luc*, $ppp1^{RIP}$ (DBP3356) and *frq::luc*, $eIF2\gamma^{\Delta 2\text{-}62}$ (DBP3424). The PPP1::LUC translational fusion was generated by 3-way PCR of the PPP1 coding region (primers *ppp1::luc* F1 and R1), *N. crassa* codon-optimized luciferase gene [117] (primers *ppp1::luc* F2 and R2) and PPP1 3' flank (primers *ppp1::luc* F3 and R3). The

3-way PCR fragments were co-transformed with hyg^R pBP15 [115] into Δ*mus-52::bar* (FGSC#9719) and screened by luciferase activity and PCR (primers *ppp1::luc* F4 and R4) to confirm homologous insertion into the *ppp1* gene. A transformant containing *ppp1::luc* was crossed with WT (FGSC #2489) and Δ*frq::bar* (DBP1228) strains to generate a *ppp1::luc* (DBP2889) and *ppp1::luc,* Δ*frq* (DBP3001) homokaryon, respectively. *eIF2γ::v5* and $eIF2\gamma^{\Delta 2\text{-}62}$*::v5* were generated by 3-way PCR with the *eIF2γ* ORF region (primers *eIF2γ::v5* F1 and R1), *v5* gene from plasmid pDBP525 (primers *eIF2γ::v5* F2 and R2) and the 3' end of *eIF2γ* (primers *eIF2γ::v5* F3 and R3). The 3-way PCR product was co-transformed with hyg^R pBP15 [115] plasmid into Δ*mus-52::bar* (FGSC#9719) and $eIF2\gamma^{\Delta 2\text{-}62}$ (DBP3297), respectively. Homologous recombinants were screened by western blot using anti-V5 antibody, and by PCR (*eIF2γ::v5* F4 and R4) to verify homologous insertion of *v5* at *eIF2γ* and $eIF2\gamma^{\Delta 2\text{-}62}$. A transformant with *eIF2γ::v5* and $eIF2\gamma^{\Delta 2\text{-}62}$*::v5* was crossed with WT (FGSC #2489) and screened by PCR (*eIF2γ::v5* F5 and R5) to obtain an *eIF2γ::v5* (DBP3428) and $eIF2\gamma^{\Delta 2\text{-}62}$*::v5* (DBP3706) homokaryon. The $ppp1^{RIP}$*;* Δ*cpc-3* (DBP3533) strain was generated by crossing $ppp1^{RIP}$ (DBP3070) with Δ*cpc-3* (DBP1883) cells, and screened for Δ*cpc-3* by PCR as described previously [66], and $ppp1^{RIP}$ as described above. The $eIF2\gamma^{\Delta 2\text{-}62}$*;* Δ*cpc-3* (DBP3657) strain was generated by crossing $eIF2\gamma^{\Delta 2\text{-}62}$ (DBP3298) with Δ*cpc-3* (DBP1883). and screened for Δ*cpc-3* by PCR [66] and $eIF2\gamma^{\Delta 2\text{-}62}$.

Circadian time courses: Circadian time course experiments for western blots were done as previously described [96]. For constitutive expression of *bar::*$P_{tcu\text{-}1}$*::ppp1*, cells were grown in Vogel's medium containing 50 μM of the copper chelator bathocuproinedisulfonic acid (BCS, B1125; Sigma-Aldrich St. Louis, MO) or 250 μM copper sulfate (CuSO4; C7631; Sigma-Aldrich St. Louis, MO) to control the expression of the *tcu-1* promoter [100].

Protein extraction and western blotting: Protein extraction, protein concentration, and western blot analyses were performed as previously described [58]. Briefly, tissue was ground in liquid nitrogen with a mortar and pestle, and suspended in extraction buffer containing 100 mM Tris pH 7.0, 1% SDS, 10 mM NaF, 1 mM PMSF, 1 mM sodium ortho-vanadate, 1 mM β-glycerophosphate, 1X aprotinin, 1X leupeptin hemisulfate salt, and 1X pepstatin A. Protein concentration was determined by Nano Drop (Thermo Fisher Scientific, Wilmington, DE). Protein samples (100 μg) were separated on 10% SDS/PAGE gels and blotted to Immobilon-P nitrocellulose membranes (#IPVH00010, Millipore Sigma, Burlington, MA) according to standard methods.

The levels of P-eIF2α were detected using rabbit monoclonal anti-EIF2S1 (phospho S51) antibody (#ab32157, Abcam, Cambridge, UK) diluted 1:5000 in 5% Bovine Serum Albumin (BSA), 1X TBS, 0.1% Tween, and anti-rabbit IgG HRP secondary antibody (#1706515, Bio-Rad, Hercules, CA) diluted 1:10000. Total eIF2α levels were detected using rabbit polyclonal anti-EIF2S1 antibody (#47508, Abcam, Cambridge, UK) diluted 1:5000, and anti-rabbit IgG HRP secondary antibody diluted 1:10000. eIF2γ::V5 was detected using mouse monoclonal anti-V5 antibody (#R960-25, Invitrogen, Carlsbad, CA) diluted 1:5000 in 5% milk, 1XTBS, 0.1% Tween, and anti-mouse IgG HRP secondary antibody (#1706516, Bio-Rad, Hercules, CA) diluted 1:10000. PPP1 was detected using a custom rabbit polyclonal anti-PPP1 antibody (peptide EVRGSRPGKQVQLLC as antigen, Genscript, Piscataway, NJ) diluted 1:1000 in 7.5% milk, 1XTBS, 0.1% Tween, and anti-rabbit IgG HRP secondary antibody diluted 1:10000. RPL-3 protein was detected with ScRPL3 mouse monoclonal antibody (ScRPL3 mouse monoclonal supernatant was obtained from the Developmental Studies Hybridoma Bank, originally deposited

by Warner, J.R.) diluted 1:1000 in 5% milk, 1XTBS, 0.1% Tween, and anti-mouse IgG HRP secondary antibody diluted 1:10000. All proteins were visualized with Super Signal West Pico Plus Chemiluminescent Substrate (#34579, Thermo Scientific, Waltham, MA). Densitometry was performed using NIH ImageJ software [118] and normalized to protein loading using amido black-stained protein.

Expression and purification of PPP1::His6 protein in E. coli: To validate the specificity of PPP1 antibody, the *ppp1* ORF was amplified with primers PPP1::His6 F and PPP1::His6 R containing restriction sites for NdeI and NotI using *N. crassa* cDNA as template. The pET30b vector (Invitrogen) and PCR fragment were digested with NdeI and NotI restriction enzymes, and then ligated with T7 ligase (NEB). The ligated plasmids were transformed to *E. coli* DH5α cells and screened by kanamycin resistance and restriction digestion to get an IPTG inducible PPP1::His6 fusion plasmid. The plasmid was transformed into *E. coli* BL21 cells and grown in 400 ml LB at 37℃ with shaking at 250 rpm to an OD of 0.6. PPP1::His6 expression was induced by adding 1 mM IPTG 1 h before protein extraction. PPP1::His6 protein was purified with Ni-NTA column following published methods [119]. PPP1::His6 protein was visualized by Coomassie Blue stain and western blot using PPP1 antibody.

In vivo luciferase assays: Luciferase assays, which detects rhythms of bioluminescence in strains with luciferase fusions, were performed as previously described [58]. Briefly, 5µl of $1X10^5$ conidia/mL were inoculated into 96 well microtiter plates containing 150 µl of 1X Vogel's salts, 0.01% glucose, 0.03% arginine, 0.1M quinic acid, 1.5% agar, and 25 µM firefly luciferin (LUNCA-300, Gold Biotechnology, St. Louis, MO), pH 6. After inoculation, the microtiter plate

was cultured at 30ºC in constant light (LL) for a day and moved to DD 25ºC to obtain bioluminescence recordings utilizing an EnVision Xcite Multilabel Reader (PerkinElmer, Life Science, Boston, MA), with recordings taken every 90 min over at least 5 continuous days. BioDARE was used to analyze the period of recorded luciferase activity data [120]. Raw reads were normalized to the mean to graph the data.

Statistical analysis: Circadian time course data was examined using F-tests of fit of the data to a sine wave or a line as previously described [96, 113]. The student T-test was used to determine significance in changes in the levels of P-eIF2α and PPP1. Error bars in all graphs represent the SEM from at least 3 independent experiments.

In vitro dephosphorylation assay: The eIF2 complex was isolated by anti-V5 co-immunoprecipitation (co-IP) from an eIF2γ::V5 and eIF2$\gamma^{\Delta 2\text{-}62}$::V5 protein extracts. The eIF2 complex was immobilized onto magnetic Dynabeads (#10008D, Invitrogen, Carlsbad, CA) and washed with 2X phosphatase buffer (100 mM Hepes, 200 mM NaCl, 2 mM DTT, 2 mM $MnCl_2$, 0.01% Brij-35) [94]. 500µg of protein extracted from Δ*cpc-3* or *ppp1*^{RIP}; Δ*cpc-3* or *eIF2*$\gamma^{\Delta 2\text{-}62}$; Δ*cpc-3* strains, harvested at DD28, was mixed with 200µL of the immobilized eIF2-Dynabeads in 2X phosphatase buffer. Reactions were incubated at 30°C with gentle rotation, and at each time point, 48 µL of the reaction mix was transferred to a fresh tube and boiled for 5 min with 16 µL 4X SDS loading buffer (250 mM pH 6.8 Tris-Cl, 8% SDS, 0.2% bromophenol blue, 40% glycerol, 20% β-mercaptoethanol) to stop the reaction. P-eIF2α and total eIF2α levels were detected by western blot.

Sucrose Gradient Fractionation: Linear sucrose gradients (10%–50% in 10 mM HEPES-KOH, 70 mM ammonium acetate, 5 mM magnesium acetate) were prepared in ultracentrifuge tubes using a BIOCOMP gradient station (Fredericton, NB) and stored at 4°C before use. Extracts were prepared by adding polysome extraction buffer (100 mM KCl, 20 mM HEPES-KOH, 10 mM magnesium acetate, 15 mM beta-mercaptoethanol, 100 µg/mL cycloheximide) to ground tissues and centrifuging the solution to remove cellular debris and lipids. 400 µL of the extract containing 100 A [260] units/mL (1 A [260] unit corresponds to an absorbance of 1.0 at 260 nm) were added onto the sucrose gradient, and centrifuged at 41,000 rpm for 2h at 4°C. The samples were then divided into 14 fractions of approximately 1 mL each using the BIOCOMP. The absorbances at 260 nm were used as a proxy for RNA content and graphed against the fraction of the gradient. Disomes, trisomes, tetrasomes, and pentosomes fractions were pooled as the polysome fraction. Fractions representing the 40S (#4), 60S (#5), 80S (#6) ribosome, and the pooled polysome fraction, were boiled in SDS loading buffer (250 mM pH 6.8 Tris-Cl, 8% SDS, 0.2% bromophenol blue, 40% glycerol, 20% β-mercaptoethanol) and 15 µl were separated on a 10% SDS/PAGE gel for western blot.

Table 1. Primers used in Chapter II

Primer name	Used for	Primer sequence (5'->3' orientation)
ppp1 seq F1	Sequence $ppp1^{RIP}$	GCTTTGCAGAAGTGCATCTAC
ppp1 seq R1	Sequence $ppp1^{RIP}$	GACGTTTATCGGCGGCCGAAC
ppp1 seq F	Sequence $ppp1^{RIP}$	ATGGCGGACCATACCGAAGTC
ppp1 F1	$ppp1^{RIP}$ complementation	CGCTGGAGAAGCTCATTCCAC
ppp1 R1	$ppp1^{RIP}$ complementation	GAAACGCACAGGCACCTCAATGTCCATCTGATC
ppp1 F2	$ppp1^{RIP}$ complementation	CATTGAGGTGCCTGTGCGTTTCATTAGCTGC
ppp1 R2	$ppp1^{RIP}$ complementation	CTGTCTAGGCTTCGAGAACCACCCTCTATC
ppp1 F3	$ppp1^{RIP}$ complementation	GTTCTCGAAGCCTAGACAGTTTGCAGGTCATGTG
ppp1 R3	$ppp1^{RIP}$ complementation	CAACCGAGCACACCAACTAAC
ppp1 F4	$ppp1^{RIP}$ complementation	CTGCTACCGCCATACGAAGTG
ppp1 R4	$ppp1^{RIP}$ complementation	GCAAAGAAGTGCGTTACTACC
tcu1 F1	P*tcu1::ppp1*	GTAAGGTGTCACACTCACAGTC
tcu1 R1	P*tcu1::ppp1*	TTAGGTCGACGCAGCTAATGAAACGCACAGG
tcu1 F2	P*tcu1::ppp1*	CATTAGCTGCGTCGACCTAAATCTCGGTGAC
tcu1 R2	P*tcu1::ppp1*	GGTCCGCCATGGTTGGGGATGTGTGTGCGA
tcu1 F3	P*tcu1::ppp1*	ATCCCCAACCATGGCGGACCATACCGAAGTC
tcu1 R3	P*tcu1::ppp1*	GTCGACGCTCATCATAGCACC
tcu1 F4	P*tcu1::ppp1*	GCTGTTGTAATCATGCATACC
tcu1 R4	P*tcu1::ppp1*	GAATTGCTTCATCTGAGACTG
$eIF2\gamma^{\Delta 2\text{-}62}$ F1	$eIF2\gamma^{\Delta 2\text{-}62}$	GTTGCAGAGTAACGATTGTTC
$eIF2\gamma^{\Delta 2\text{-}62}$ R1	$eIF2\gamma^{\Delta 2\text{-}62}$	GACGTCGAGGTCCATGATTGTGGATGTGGGTGG
$eIF2\gamma^{\Delta 2\text{-}62}$ F2	$eIF2\gamma^{\Delta 2\text{-}62}$	CCACAATCATGGACCTCGACGTCAAGACCCTC

Table 1 Continued

Primer name	Used for	Primer sequence (5'->3' orientation)
eIF2γ$^{\Delta 2\text{-}62}$ R2	*eIF2γ*$^{\Delta 2\text{-}62}$	GAGACAATCCTGCTGAAGATG
eIF2γ$^{\Delta 2\text{-}62}$ F3	*eIF2γ*$^{\Delta 2\text{-}62}$	AGTACACAGCAACTACCAGGC
eIF2γ$^{\Delta 2\text{-}62}$ R3	*eIF2γ*$^{\Delta 2\text{-}62}$	GCTCATGAGAATATCGTGACC
ppp1::luc F1	PPP1::LUC	GGTCAATACTATGATCTCCTCC
ppp1::luc R1	PPP1::LUC	GATGTTCTTGGCGTCCTCCATTCGGCGGCCGAACCTAAAGG
ppp1::luc F2	PPP1::LUC	CCTTTAGGTTCGGCCGCCGAATGGAGGACGCCAAGAACATC
ppp1::luc R2	PPP1::LUC	GCGGGCGAAAGTATCAGACGTATCAGACGGCGATCTTGCC
ppp1::luc F3	PPP1::LUC	GGCAAGATCGCCGTCTGATACGTCTGATACTTTCGCCCGC
ppp1::luc R3	PPP1::LUC	CTCGAATACAGCATGGTGTTCG
ppp1::luc F4	PPP1::LUC	GGTAAGCAGGTGCAGCTGCTG
ppp1::luc R4	PPP1::LUC	CACTCTTGCCTCTCAGTCACC
eIF2γ::V5 F1	eIF2γ::V5	CAGCACTACGAGTCCATCCTC
eIF2γ::V5 R1	eIF2γ::V5	TCCGCCGCCTCCAGAGGTAGAAGGCTCGAGGGT
eIF2γ::V5 F2	eIF2γ::V5	GCCTTCTACCTCT GGAGGCGGCGGAGGCGGTAA
eIF2γ::V5 R2	eIF2γ::V5	CTGGTCGCTCGC CTACGTAGAATCGAGACCGAG
eIF2γ::V5 F3	eIF2γ::V5	GATTCTACGTAGGCGAGCGACCAGAAAATATCC
eIF2γ::V5 R3	eIF2γ::V5	CTATTCGATGTACAGGAGGTG
eIF2γ::V5 F4	eIF2γ::V5	CTCGGTCTCGATTCTACGTAG
eIF2γ::V5 R4	eIF2γ::V5	GTGATTGAGAATCTGGTGAAGC
eIF2γ::V5 F5	eIF2γ::V5	ACCCTCGAGCCTTCTACCTCT
eIF2γ::V5 R5	eIF2γ::V5	GATATTCATCATTAGAGCAAC
PPP1::His6 F	PPP1::His6	ACGAGTCATATGGCGGACCATACCGAAGTC
PPP1::His6 R	PPP1::His6	ATAATCGCGGCCGCTCGGCGGCCGAACTTCTG

Restriction sites in primer sequences are underlined

CHAPTER III

INVESTIGATION OF THE ROLES OF PPP1 REGULATION OF CPC-3 PHOSPHORYLATION

Introduction

Approximately 50% of rhythmic proteins in mouse liver and in *N. crassa* are produced from mRNAs that are not rhythmic [48-50, 55], suggesting circadian regulation of protein stability and/or mRNA translation. In support of clock control of mRNA translation, the expression and/or phosphorylation of some translation factors are rhythmic in eukaryotic cells [48, 56-58], including rhythms in the phosphorylation and activity of the conserved translation initiation factor eIF2α in *N. crassa* and mammals [64-66]. The mechanisms of clock control of eIF2α phosphorylation are currently best understood in *N. crassa.* Rhythmic CPC-3 activity is required for inhibitory Ser51 phosphorylation of eIF2α (P-eIF2α). Hyper-activation of CPC-3 kinase activity, achieved either by drug induced-ISR pathway activation, or by assaying a constitutively active mutant of *cpc-3* (*cpc-3*^{c}), abolished P-eIF2α rhythms [66]. However, CPC-3 is necessary, but may not be sufficient to drive rhythms in P-eIF2α accumulation. Similarly, phosphatase PPP1 is necessary, but not sufficient P-eIF2α rhythms (Chapter 2). PPP1 dephosphorylates eIF2α *in vitro*, and the clock controls PPP1 levels, with a peak in the early evening. Importantly, rhythmic PPP1 accumulation is necessary for cycling P-eIF2α levels. Our study further revealed that an N-terminal extension of eIF2γ, one of the subunits of the eIF2 complex, is required to recruit PPP1 to dephosphorylate eIF2α and maintain robust P-eIF2α rhythmicity.

Considering that both the kinase CPC-3 and the phosphatase PPP1 are required for P-eIF2α rhythms, an additional pathway for PPP1 to regulate P-eIF2α rhythms maybe through the

regulation of the phosphorylation and activity of the kinase CPC-3. We proposed a model (**Figure 15**), in which, PPP1 may activate CPC-3 during the day by removing an inhibitory phosphorylation, or inactivate CPC-3 at night by removing an activating phosphorylation. Considering that PPP1 levels peak at night, it is more likely that PPP1 inactivates CPC-3 at night by removing an activating phosphorylation. However, it is also possible that there is delayed PPP1 dephosphorylation of a CPC-3 inhibitory phosphorylation site to active the kinase during the day. In yeast, GCN2 S577 was reported as an inhibitory phosphorylation site regulated by the TOR pathway[78], and T882 and T887 were identified as activating autophosphorylation sites induced by uncharged tRNA binding [68].

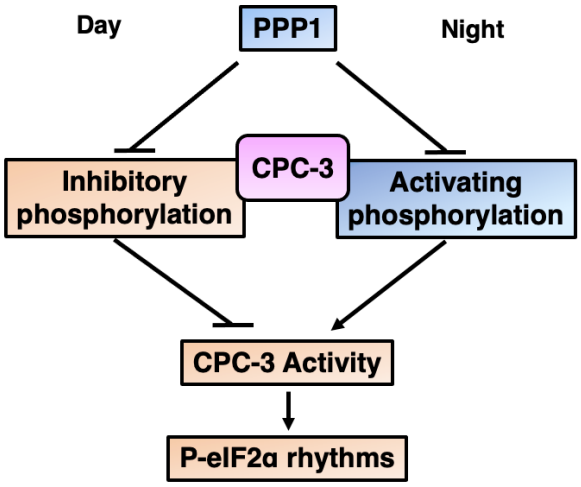

Figure 15. Proposed model for PPP1 regulation of P-eIF2α rhythmicity through regulation of CPC-3 activity through dephosphorylation of inhibitory or activating phosphorylation residues of CPC-3 protein. See the text for details.

To examine if PPP1 regulates the phosphorylation and activity of CPC-3, which in turn could affect P-eIF2α rhythms, I examined the phosphorylation levels of CPC-3 in cells with low or high PPP1 expression levels using Post Translational Modification Mass Spectrometry (PTM-MS) of

CPC-3 protein. I discovered that the phosphorylation levels of CPC-3 Serine 876 (S876) and Threonine 879 (T879) were significantly lower when PPP1 was overexpressed in cells compared with cells expressing low PPP1 levels. P-S876 activates CPC-3, but was not required for rhythmic P-eIF2α accumulation. Mutation of T879 eliminated eIF2α phosphorylation, demonstrating that T897 is essential for CPC-3 kinase activity. As a consequence, the role of T879 phosphorylation levels in rhythms of P-eIF2α accumulation could not be determined.

Results

To determine if PPP1 regulates P-eIF2α levels and rhythms through regulation of CPC-3 activity, in addition to direct dephosphorylation of eIF2α, I examined CPC-3 phosphorylation of specific amino acids in cells with low or high PPP1 levels by PTM-MS of CPC-3 protein (**Figure 16**). To perform this assay, a strain was generated to control PPP1 expression levels by copper concentration and with V5-epitope-tagged CPC-3 for immunoprecipitation (P*tcu1::ppp1; cpc-3::v5*) . Copper sulfate (Cu) repression of P*tcu1::ppp1* led to low PPP1 protein expression and high P-eIF2α levels compared to cells cultured with the BCS (**Figure 16A**). CPC-3 protein isolated by IP using anti-V5 antibody from protein extracted from P*tcu1::ppp1; cpc-3::v5* cells cultured with Cu or BCS (**Figure 16B**), and quantitative PTM-MS was used to examine the phosphorylation sites and levels of CPC-3 protein. Four phosphorylated amino acids were detected, and the phosphorylation levels of CPC-3 Serine 876 (S876) and Threonine 879 (T879) were significantly lower when PPP1 levels were high compared with cells expressing low PPP1 levels (**Figure 16C**). Furthermore, PTM-MS of CPC-3 protein in WT cells harvested at two times of the day representing the nighttime trough (DD24) and daytime peak (DD36) of P-eIF2α rhythms, showed higher levels of phosphorylated T879 (P-T879) during the day. These data support that P-T879

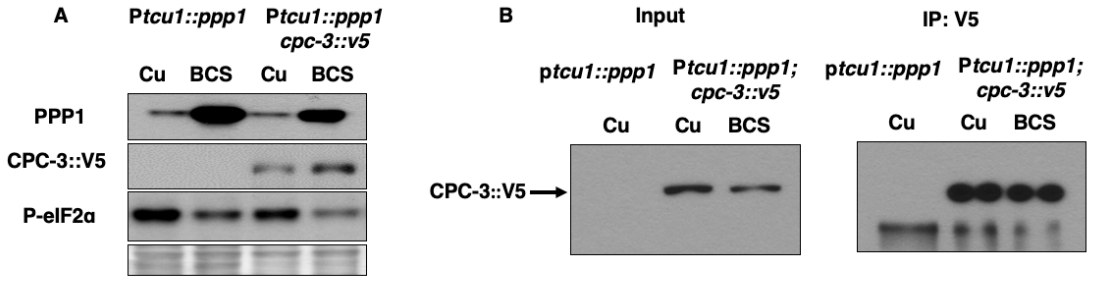

C

Peptide sequence	Abundance ratio (Cu : BCS)
SHQLS^{238}PDRAPQDPGETDETLMFDQPCK	1:1.2
GISDT^{358}DSSAPTIWTVSILTPLATK	1:1.0
S^{876}IGTAVYVAPEVR	1:0.4
STASLDASDMTRSIGT^{879}AVYVAPEVR	1:0

D

Peptide sequence	Abundance ratio (DD24 : DD36)
SHQLS^{238}PDR	1:0.5
GISDT^{358}DSSAPTIWTVSILTPLATK	1:0.9
S^{876}IGTAVYVAPEVR	1:0.9
STASLDASDMT^{874}RSIGT^{879}AVYVAPEVR	1:2.3

E

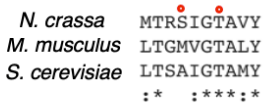

Figure 16. The phosphorylation levels of CPC-3 S876 and T879 are regulated by PPP1 protein levels. (A) Western blots of protein extracted from P*tcu1::ppp1* and P*tcu1::ppp1; cpc-3::v5* cells cultured with 50 μM of BCS or 250 μM copper sulfate in LL for 24 h, and probed with anti-PPP1, anti-V5 and anti-P-eIF2α antibodies. (B) Western blots of CPC-3::V5 protein following IP with anti-V5 antibody from the same samples in (A). Protein extracts before IP are used as input. The lower band in the IP is heavy chain of IP antibody. (C) Phospho-peptides of CPC-3::V5 identified by PTM-MS analysis of immunoprecipitants obtained from P*tcu1::ppp1; cpc-3::v5* cells cultured with 50 μM of BCS or 250 μM copper sulfate shown in (B). The ratios were calculated by comparing the relative abundance of the phospho-peptides in BCS versus Cu cultures. (D) Phospho-peptides of CPC-3::V5 identified by PTM-MS of immunoprecipitants obtained from P*tcu1::cpc-3::v5* cells cultured with 50 μM of BCS and harvested at DD24 and DD36 respectively. The ratios were calculated by comparing the relative abundance of the phospho-peptides in DD24 to DD36 cells. (E) Alignment of CPC-3/GCN2 peptide sequences in *N. crassa, M. musculus* and *S. cerevisiae*. The red stars indicate CPC-3 S876 and T879.

levels may be regulated by the clock (**Figure 16E**). Because PPP1 levels were induced in these cells using BCS, the time-of-day difference in P-T879 levels is likely not dependent on rhythmic PPP1 levels. However, the increased level of P-T879 in cells with high P-eIF2α levels compared

to low P-eIF2α levels suggested that this modification activates CPC-3 kinase, similar to the autophosphorylation and activation of GCN2 at the conserved site T887 in *S. cerevisiae* (**Figure 16D**) [68]. P-S876 may also activate CPC-3, but no time-of-day difference in levels was observed (**Figure 16D**), and the site is not conserved in *M. musculus* and *S. cerevisiae* GCN2 (**Figure 16E**). To determine if S876 and/or T879 phosphorylation is important for CPC-3 activity and P-eIF2α rhythms, I generated mutations to change the amino acids to Alanine to prevent phosphorylation (S876A and T879A) or to Glutamic Acid to mimic constitutive phosphorylation (S876E and T879E). To rule out possible redundancy in function, double mutant strains (S876A; T879A, and S876E; T879E) were also generated. To first determine if the mutations affect CPC-3 protein expression, a customized CPC-3 antibody was generated. The specificity of the anti-CPC-3 antibody was examined by probing western blots of protein extracted from Δ*cpc-3*, WT and *cpc-3*::v5 cells with anti-CPC-3 and anti-V5 antibodies (**Figure 17A**). A protein of the expected molecular weight of CPC-3 (~185 kDa) was observed using anti-V5 antibody in protein samples from *cpc-3*::v5, but not from WT cells. In WT and *cpc-3*::v5 protein extracts, a protein of similar size was detected using the CPC-3 antibody, and as expected, this band was absent in Δ*cpc-3* extracts (**Figure 17A**). These data confirmed that the anti-CPC-3 antibody detected *N. crassa* CPC-3 protein. While non-specific bands were detected using the anti-CPC-3 antibody, and the CPC-3 signal is not as strong as the anti-V5 antibody, this antibody is useful for detecting CPC-3 protein in strains that don't have V5-tagged CPC-3 (**Figure 17A**). Importantly, CPC-3 protein was expressed in all of the generated mutant strains (**Figure 17**).

All strains with CPC-3 T879 mutations (T879A, T879E, S876A;T879A and S876E; T879E) had no detectable phosphorylation of eIF2α, even under amino acid starvation conditions to induce

eIF2α phosphorylation using 3-AT treatment (**Figure 17B**). These data supported that T879 is essential for CPC-3 activity, consistent with mutant studies of GCN2 T887 in *S. cerevisiae* [68]. However, because eIF2α is not phosphorylated in T879 mutants, the role of phosphorylation of CPC-3 T879 in P-eIF2α rhythms could not be examined. In both *cpc-3*^{S876A} and *cpc-3*^{S876E} strains, P-eIF2α levels are low compared to WT, but still rhythmic (**Figure 18**). These data support that phosphorylation of S876 activates CPC-3, but that this modification is not necessary for rhythmic CPC-3 activity. P-eIF2α levels were increased in both *cpc-3*^{S876A} and *cpc-3*^{S876E} cells by 3-AT treatment, similar to WT cells, supporting that S876 phosphorylation is not required for activation of CPC-3 by uncharged tRNAs (**Figure 18A**).

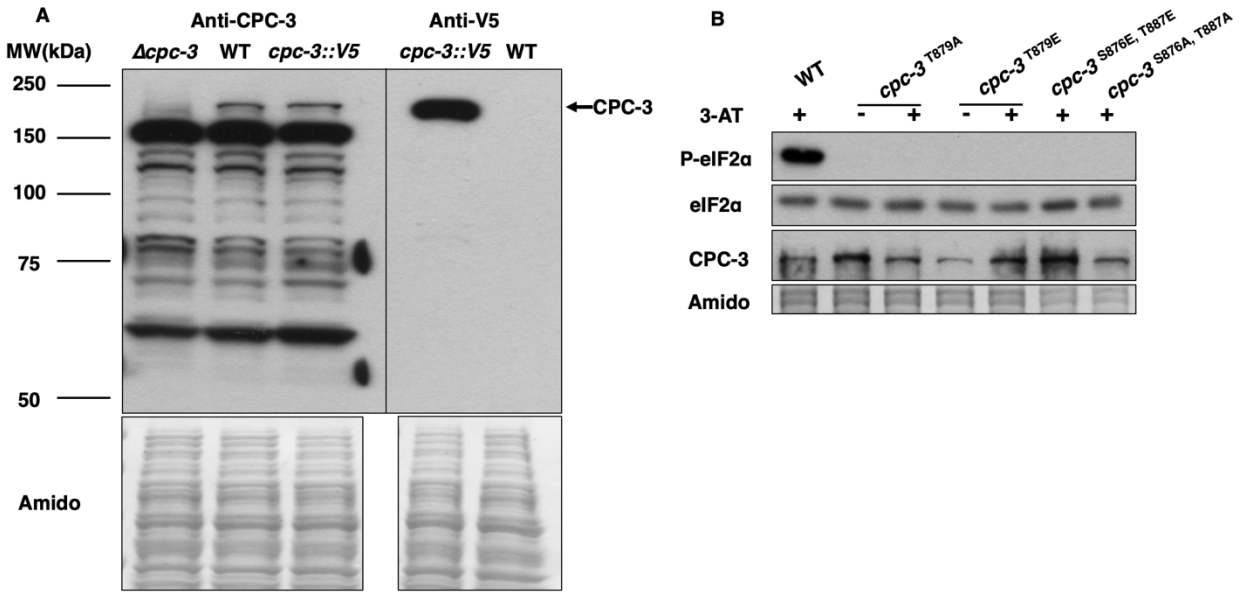

Figure 17. T879 is required for CPC-3 activity. Anti-CPC-3 antibody can detect the *N. crassa* CPC-3 protein. Protein extracted from indicated *N. crassa* cells were blotted with anti-CPC-3 (left) or anti-V5 (right) antibody. (B) Western blots of protein from indicated strains cultured in LL and treated (+) or not (-) with 3-AT. The blots were probed with anti-P-eIF2α, total eIF2α, and CPC-3 antibodies. In A and B, membranes were stained with amido black as a protein loading control.

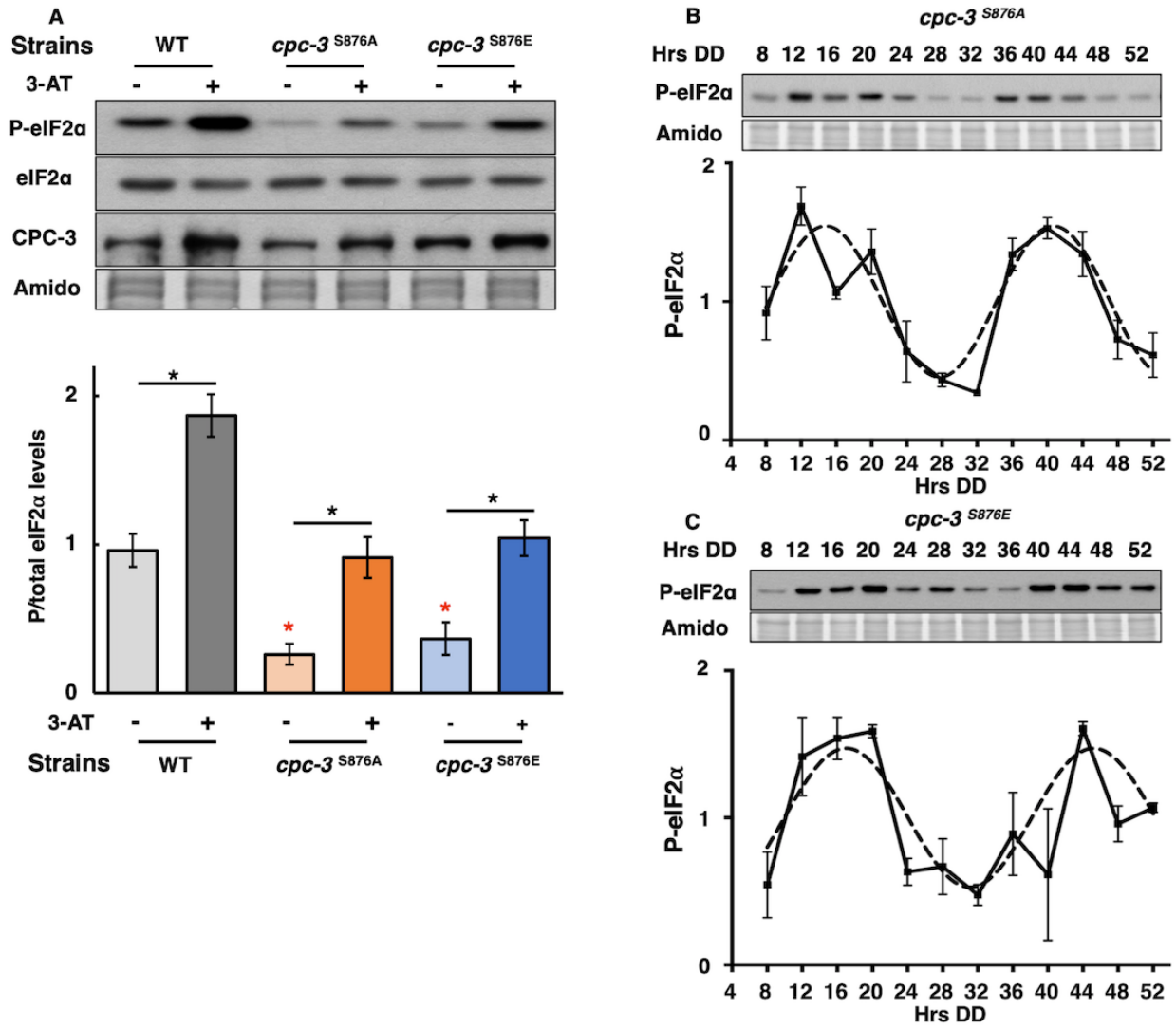

Figure 18. S876 phosphorylation activates CPC-3, but is not required for rhythmic P-eIF2α levels. (A) Western blots of protein from WT, *cpc-3*^{S876A} and *cpc-3*^{S876E} cells grown in LL and treated (+) or not (-) with 3-AT and probed with anti-P-eIF2α, anti-eIF2α and anti-CPC-3 antibodies. The P-eIF2α/total eIF2α signal is plotted below for WT and *cpc-3*^{S876A} strains (mean ± SEM, n=3; *p<0.05, student T-test, red * indicates compared with WT, no 3-AT condition). Western blot of protein isolated from *cpc-3*^{S876A} (B) and *cpc-3*^{S876E} cells (C) grown in DD and harvested at the indicated time (Hrs DD) respectively. The blots were probed with anti-P-eIF2α antibodies. The normalized P-eIF2α levels are plotted below (mean ± SEM, n=3; solid black line). P-eIF2α levels in *cpc-3*^{S876A} and *cpc-3*^{S876E} cells were rhythmic based on the best fit of the data to sine waves (dotted line, p<0.001). The membranes in A, B and C were stained with amido black as a protein loading control.

Discussion

CPC-3 kinase and PPP-1 phosphatase are required for P-eIF2α rhythms, but neither is sufficient. Deletion of CPC-3 kinase had no effect on PPP1 protein accumulation rhythms (**Figure 12C**), indicating that CPC-3 does not control PPP1 expression. These data suggested the possibility that PPP1 may activate CPC-3 during the day by removing an inhibitory phosphorylation, or inactivate CPC-3 at night by removing an activating phosphorylation. Considering that PPP1 levels peak at night, we favored the prediction that PPP1 inactivates CPC-3 at night by removing an activating phosphorylation.

PTM-MS of CPC-3 revealed that high levels of PPP1 reduced the phosphorylation of two sites, S876 and T879. Mutation of S876 to both Alanine and Glutamic Acid led to low P-eIF2 levels, supporting that P-S876 activates CPC-3 protein. However, this modification was not required for rhythmic P-eIF2α accumulation. Phosphorylation of T879 was shown to be essential for CPC-3 activation. In the homologous GCN2 site, T887 is autophosphorylated in response to binding of uncharged tRNA to GCN2, which activates GCN2 kinase [68]. The levels of uncharged tRNAs are rhythmic in *N. crassa*, peaking during the subjective day, consistent with activation of CPC-3 during the day. These data supported the idea that the clock regulates P-T879 levels, either through rhythmic binding of uncharged tRNAs during the day, and/or by rhythmic dephosphorylation by PPP1 at night. Support for rhythmic control of P-T879 is that the levels were significantly higher during the subjective day compared to subjective night from PTM-MS data. This corresponds to the peak of CPC-3 activity and P-eIF2α levels. While further experiments are needed to determine if phosphorylation of T879 is clock-controlled, and if PPP1 directly dephosphorylates CPC-3 T879 or S876, these data suggest a possible model for clock control of CPC-3 activity that can be

examined in the future (**Figure 19**). In this model, binding of uncharged tRNAs to CPC-3 during the subjective day may lead to autophosphorylation of T879, CPC-3 kinase activation, and increased P-eIF2α levels and reduced mRNA translation. PPP1, which peaks in levels during the subjective night under control of the clock, may dephosphorylate P-T879 and P-eIF2α, leading to reduced P-eIF2α levels and increased mRNA translation. This model is consistent with no detectable P-T879 in PTM-MS when PPP1 levels are overexpressed, and low P-eIF2α levels when PPP1 is induced from the copper regulatable promoter in the presence of BCS.

Surprisingly, T8979E substitutions, which were expected to mimic the phosphorylated amino acid, functioned the same as T879A. Both mutations abolished phosphorylation of eIF2α (**Figure 16B**). Similar results were reported in *S. cerevisiae* where mutation of GCN2 T882 and T887 positions to E or Asp (D) amino acids resulted in the same phenotypes as the corresponding A substitutions [68]. Thus, E or D substitutions at the autophosphorylation residues of CPC-3/GCN2 kinase were unable to substitute for the phosphorylated amino acid and activate the kinase. This may be due the amino acid substitutions altering the conformation of CPC-3/GCN-2 and rendering the kinase inactive. In addition, phosphorylation of these sites may serve as priming sites for other kinases that are needed for activation of CPC-3/GCN2.

In addition to phosphorylation of CPC-3 S876 and T879, two additional CPC-3 residues T874 and S238 were found to be phosphorylated, although they did not appear to be regulated by the levels of PPP1. CPC-3 T874 is the homologous residue of GCN2 T882 in yeast, which is a second activating autophosphorylation site in GCN2 that is induced by uncharged tRNA binding [67]. No study has reported phosphorylation of S238 of GCN2 in yeast or mammals. P-S238 levels were

higher in the subjective night (DD24) compared to the day (DD36) (**Figure 16E**), suggesting that P-S238 inhibits CPC-3 activity. Experiments are currently underway to examine the potential roles of S238 and T874 in CPC-3 rhythmic activity. Sequence coverage of CPC-3 in PTM-MS was about 65%, leaving open the possibility that other phosphorylation sites exist. For example, the region that contains the homologous amino acid of S577 in yeast was not detected in CPC-3 PTM-MS experiments.

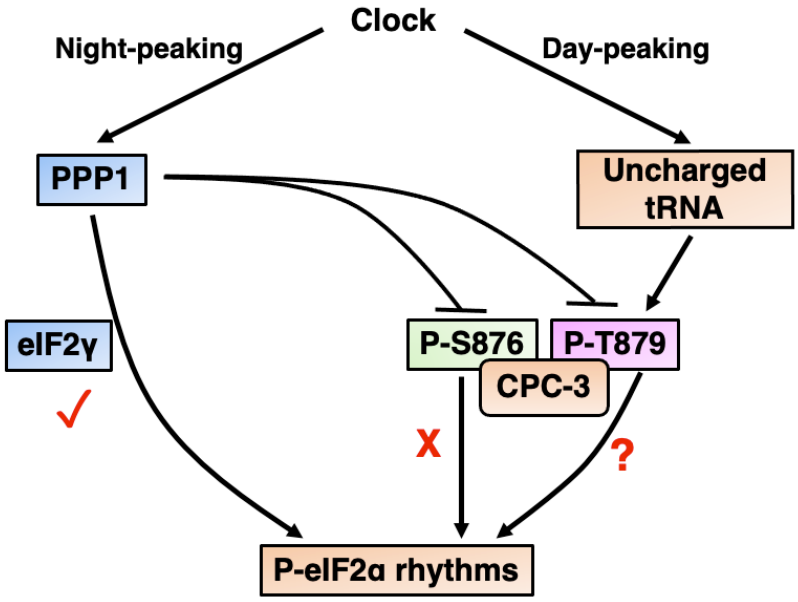

Figure 19. Potential pathways of PPP1 regulation of P-eIF2α rhythms. PPP1 dephosphorylates eIF2α by recruiting of the N-terminal extension of eIF2γ. Both PPP1 and N-eIF2γ are required for P-eIF2α rhythms, indicating that dephosphorylation of eIF2α by PPP1 is required for P-eIF2α rhythms (Chapter II). Overexpression of PPP1 also reduced P-S876 and P-T879 levels of CPC-3 (**Figure 15**). P-eIF2α levels were low, but rhythmic in *cpc-3*^{S876A}, indicating that phosphorylation of CPC-3 S876 is not required for P-eIF2α rhythms (**Figure 17**). P-T879 is essential for CPC-3 activity in phosphorylating eIF2α (**Figure 16B**), and is induced by uncharged tRNA, but it's role in clock-control of CPC-3 activity is unknown.

Together, this work revealed that overexpression of PPP1 reduced the phosphorylation levels of CPC-3 S876 and T879. P-S876 activates CPC-3, although is not required for rhythmic P-eIF2α accumulation and amino acid induction of P-eIF2α. P-T879 is essential for CPC-3 activity in

phosphorylating eIF2α, but it's role in clock-control of CPC-3 activity is unknown. These data provide insight into understanding how the activity of CPC-3 is regulated by circadian clock in *N. crassa*, which in turn regulates P-eIF2α rhythms. GCN2 plays an important role in rhythmic eIF2α phosphorylation in the mouse suprachiasmatic nucleus (SCN); however, the detailed mechanism of this regulation is not known [64]. In addition, the autophosphorylation sites in the kinase domain of GCN2 protein are conserved in mouse (T898 and T903 in mouse corresponding to T882 and T887 in yeast and T874 and T879 in *N. crassa*), and are required for GCN2 activity [68]. In addition to GCN2, PERK and PRK kinases, which are additional eIF2α kinases in mammals, are abundant in the SCN. As a result, P-eIF2α is still detectable in $GCN2^{-/-}$ mice [64]. Mutation of mouse GCN2 T903 would be needed to determine if the essential autophosphorylation site is required for P-eIF2α accumulation, and rhythmicity. Considering the principal role of eIF2α in regulating mRNA translation, and its reported connection with clock and disease, including neuronal degeneration in Alzheimer's disease [121, 122], retinal degeneration [123] and breast cancer [124], the detailed pathways of clock regulation of GCN2/eIF2α could provide insights into the development of new drug targets for treating these diseases.

Methods and Materials

***N. crassa* strains and growth conditions:** *N. crassa* vegetative growth conditions, transformation and crossing protocols were as described previously [96]. Strains with the *hph* cassette were maintained on Vogel's minimal media containing 0.2 g/L of hygromycin B (#80055-286, VWR, Radner, PA). Strains with the *bar* cassette were maintained on Vogel's minimal media without NH_4NO_3 and with 0.5% proline and 0.2 g/L BASTA (Liberty 280 SL Herbicide, Bayer, NC). Germinated conidia were cultured and harvested as previously described [110-112]. Briefly, for

the 3-AT treatment experiments, $1X10^5$ conidia were inoculated in 250mL Vogel's minimal media with 2% glucose. Conidia were germinated in LL 25℃ for 24 h with orbital shaking (100rpm). 3-AT (Sigma-Aldrich, St. Louis, MO) powder was dissolved in distilled water to make a 1M stock solution, and a final concentration of 9 mM 3-AT was added to the 3-AT treatment samples 1 h before harvest. Samples were harvested using vacuum filtration, snap frozen in liquid nitrogen and processed for analysis or stored in -80℃.

N. crassa wild type (WT) FGSC #4200 (mat a, 74-OR23-IV) or FGSC #2489 (mat A, 74-OR23-IV), were obtained from the Fungal Genetics Stock Center (FGSC, Kansas State University). *Bar::*$P_{tcu\text{-}1}$*::cpc-3::v5* (DBP2742) was generate previously in the lab [66]. The primers used in the generation and validation strains are listed in **Table 2**. To generate the *bar::*$P_{tcu\text{-}1}$*::ppp1; cpc-3::v5* strain, *bar::*$P_{tcu\text{-}1}$*::ppp1* (DBP3279) was crossed with *cpc-3::v5* (DBP2717) strain [66], and progeny were screened by western blot *cpc-3::*v5 with anti-V5 antibody (source) as described [66], and PCR (primers tcu1 F4 and R4) for *bar::*$P_{tcu\text{-}1}$*::ppp1* as described in Chapter II. To generate point mutations of CPC-3 protein (*cpc-*3^{S876A}, *cpc-*3^{S876E}, *cpc-*3^{T879A}, *cpc-*3^{T879E}, *cpc-*$3^{S876A;T879A}$ and *cpc-*$3^{S876E;T879E}$), PCR fragments containing the mutations and restriction digestion sites were made by 2-way PCR using a set of primers F1, R1, F2 and R2 for each mutation (**Table 2)**. Each fragment was cotransformed with the hyg^R pBP15 [115] into Δ*mus-52::bar* (FGSC#9719). The transformants were screened by PCR with the primers CPC-3 F and CPC-3 R, followed by restriction digestion with AfeI for *cpc-*3^{S876A}, KasI for *cpc-*3^{S876E} and *cpc-*3^{T879A}, Bstz17I for *cpc-*3^{T879E}, XhoI for *cpc-*$3^{S876A;T879A}$ and *cpc-*$3^{S876E;T879E}$ (New England Biolabs, Ipswich, MA). The heterokaryotic transformants were crossed to WT (FGSC #4200) to obtain the homokaryon

cpc-3^{S876A} (DBP3780), *cpc-3*^{S876E} (DBP3715), *cpc-3*^{T879A} (DBP3784), *cpc-3*^{T879E} (DBP3714), *cpc-3*$^{S876A;T879A}$ (DBP3712) and *cpc-3*$^{S876E;T879E}$ (DBP3708).

Circadian time courses: Circadian time course experiments for western blots were performed according to published methods [58, 96]. Briefly, mycelial mats in Vogel's minimal media containing 2% glucose (pH 6.0) were synchronized to the same time of day by a shift from 30°C constant light (LL) to 25°C constant dark (DD). The cultures were grown in LL for a minimum of 4 h and transferred to DD on day 1 (for collection at DD 36, 40, 44, 48, 52), day 2 (for collection at DD 12, 16, 20, 24, 28, 32), day 3 (for collection at DD 8), and harvested either at 9:00 a.m. (DD 12, 16, 20, 36, 40, 44) or 5:00 p.m. (DD 8, 24, 28, 32, 48, 52) on day 3. Harvested tissue was immediately frozen in liquid N_2.

Protein extraction and western blotting: Protein extraction, protein concentration, and western blot analyses were performed as previously described [58]. Briefly, tissue was ground in liquid nitrogen with a mortar and pestle, and suspended in extraction buffer containing 100 mM Tris pH 7.0, 1% SDS, 10 mM NaF, 1 mM PMSF, 1 mM sodium ortho-vanadate, 1 mM β-glycerophosphate, 1X aprotinin, 1X leupeptin hemisulfate salt, and 1X pepstatin A. Protein concentration was determined by Nano Drop (Thermo Fisher Scientific, Wilmington, DE). Protein samples (100 µg) were separated on 10% SDS/PAGE gels and blotted to Immobilon-P nitrocellulose membranes (#IPVH00010, Millipore Sigma, Burlington, MA) according to standard methods.

The levels of P-eIF2α were detected using rabbit monoclonal anti-EIF2S1 (phospho S51) antibody (#ab32157, Abcam, Cambridge, UK) diluted 1:5000 in 5% Bovine Serum Albumin (BSA), 1X TBS, 0.1% Tween, and anti-rabbit IgG HRP secondary antibody (#1706515, Bio-Rad, Hercules, CA) diluted 1:10000. Total eIF2α levels were detected using rabbit polyclonal anti-EIF2S1 antibody (#47508, Abcam, Cambridge, UK) diluted 1:5000, and anti-rabbit IgG HRP secondary antibody diluted 1:10000. CPC-3::V5 was detected using mouse monoclonal anti-V5 antibody (#R960-25, Invitrogen, Carlsbad, CA) diluted 1:5000 in 5% milk, 1XTBS, 0.1% Tween, and anti-mouse IgG HRP secondary antibody (#1706516, Bio-Rad, Hercules, CA) diluted 1:10000. CPC-3 was detected using a custom rabbit polyclonal anti-CPC-3 antibody (peptide LSPDRAPQDPGETDC as the antigen, Genscript, Piscataway, NJ) diluted 1:1000 in 7.5% milk, 1XTBS, 0.1% Tween, and anti-rabbit IgG HRP secondary antibody diluted 1:10000. All proteins were visualized with Super Signal West Pico Plus Chemiluminescent Substrate (#34579, Thermo Scientific, Waltham, MA). Densitometry was performed using NIH ImageJ software [118] and normalized to protein loading using amido black-stained protein.

Statistical analysis: Circadian time course data was examined using F-tests of fit of the data to a sine wave or a line as previously described [96, 113]. The student T-test was used to determine significance in changes in the levels of P-eIF2α. Error bars in all graphs represent the SEM from at least 3 independent experiments.

Post-Translational Modification (PTM) Mass-Spectrometry (MS) of CPC-3::V5 protein: The CPC-3 protein was immobilized onto magnetic Dynabeads (#10008D, Invitrogen, Carlsbad, CA) by IP with anti-V5 using protein extracted from P*tcu1::ppp1; cpc-3::v5* cells cultured with 50 μM

of the copper chelator BCS or 250 μM cooper sulfate respectively and P*tcu1::cpc-3::v5* cells with 50μM and harvested at DD24 and DD36 respectively and washed with 2X phosphatase buffer (100 mM Hepes, 200 mM NaCl, 2 mM DTT, 2 mM $MnCl_2$, 0.01% Brij-35) [94]. The IP beads were boiled with 2X Laemmli loading buffer and loaded on 8% SDS PAGE gel. The gel was stained with Coomassie Blue, and the target bands were cut out of the gel and sent to UT Southwestern Proteomics Core to perform a short reverse-phase LC-MS/MS on their Orbitrap Fusion Lumos mass-spectrometry platform. Peptides and PTMs were identified using Proteome Discoverer 2.4 (Thermo Fisher Scientific, Wilmington, DE).

Table 2. Primers used in Chapter III

Primer name	**Used for**	**Primer sequence (5'->3' orientation)**
ppp1 seq F1	Sequence $ppp1^{RIP}$	GCTTTGCAGAAGTGCATCTAC
ppp1 seq R1	Sequence $ppp1^{RIP}$	GACGTTTATCGGCGGCCGAAC
ppp1 seq F	Sequence $ppp1^{RIP}$	ATGGCGGACCATACCGAAGTC
ppp1 F1	$ppp1^{RIP}$ complementation	CGCTGGAGAAGCTCATTCCAC
ppp1 R1	$ppp1^{RIP}$ complementation	GAAACGCACAGGCACCTCAATGTCCATCTGATC
ppp1 F2	$ppp1^{RIP}$ complementation	CATTGAGGTGCCTGTGCGTTTCATTAGCTGC
ppp1 R2	$ppp1^{RIP}$ complementation	CTGTCTAGGCTTCGAGAACCACCCTCTATC
ppp1 F3	$ppp1^{RIP}$ complementation	GTTCTCGAAGCCTAGACAGTTTGCAGGTCATGTG
ppp1 R3	$ppp1^{RIP}$ complementation	CAACCGAGCACACCAACTAAC
tcu1 F4	P*tcu1::ppp1*	GCTGTTGTAATCATGCATACC
tcu1 R4	P*tcu1::ppp1*	GAATTGCTTCATCTGAGACTG
S876A F1	$cpc\text{-}3^{S876A}$	CCATTGAAGAGCTTCTCGATC
S876A R1	$cpc\text{-}3^{S876A}$	GCCAATAGCGCTGGTCATGTCGCTTGCATC

Table 2 Continued

Primer name	Used for	Primer sequence (5'->3' orientation)
S876A F2	*cpc-3*^{S876A}	GACCAGCGCTATTGGCACAGCAGTTTATGTC
S876A R2	*cpc-3*^{S876A}	CGAGCTCAATACCAGAGGAG
S876E F1	*cpc-3*^{S876E}	CCATTGAAGAGCTTCTCGATC
S876E R1	*cpc-3*^{S876E}	CAATTTCTCGAGTCATGTCGCTTGCATCCAAGC
S876E F2	*cpc-3*^{S876E}	CATGACTCGAGAAATTGGCACAGCAGTTTATGTC
S876E R2	*cpc-3*^{S876E}	CGAGCTCAATACCAGAGGAG
T879A F1	*cpc-3*^{T879A}	CCATTGAAGAGCTTCTCGATC
T879A R1	*cpc-3*^{T879A}	ATAAACTGCGGCGCCAATGCTCCTGGTCATGTC
T879A F2	*cpc-3*^{T879A}	CATTGGCGCCGCAGTTTATGTCGC
T879A R2	*cpc-3*^{T879A}	CGAGCTCAATACCAGAGGAG
T879E F1	*cpc-3*^{T879E}	CCATTGAAGAGCTTCTCGATC
T879E R1	*cpc-3*^{T879E}	GACGTATACTGCTTCGCCAATGCTCCTGGTCATGC
T879E F2	*cpc-3*^{T879E}	GAGCATTGGCGAAGCAGTATACGTC
T879E R2	*cpc-3*^{T879E}	CGAGCTCAATACCAGAGGAG
S876AT879A F1	*cpc-3*$^{S876A;T879A}$	CCATTGAAGAGCTTCTCGATC
S876AT879A R1	*cpc-3*$^{S876A;T879A}$	GGCGCCAATCGCCCTGGTCATGTCGCTTG
S876AT879A F2	*cpc-3*$^{S876A;T879A}$	AGGGCGATTGGCGCCGCAGTTTATGTCGCC
S876AT879A R2	*cpc-3*$^{S876A;T879A}$	CGAGCTCAATACCAGAGGAG
S876E T879E F1	*cpc-3*$^{S876E;T879E}$	CCATTGAAGAGCTTCTCGATC
S876E T879E R1	*cpc-3*$^{S876E;T879E}$	CTTCGCCAATTTCTCGAGTCATGTCGCTTGCATCCAAG
S876E T879E F2	*cpc-3*$^{S876E;T879E}$	CTCGAGAAATTGGCGAAGCAGTTTATGGTCGCC

Table 2 Continued

Primer name	Used for	Primer sequence (5'->3' orientation)
S876E T879E R2	*cpc-3*$^{S876E;T879E}$	CGAGCTCAATACCAGAGGAG
CPC-3 F	Validation of mutations of CPC-3 S876 and T879 loci	CCAAGTTCTTCAAGTCCGACC
CPC-3 R	Validation of mutations of CPC-3 S876 and T879 loci	GTCGCAATCTCATCCAGAAC

Restriction sites in primer sequences are underlined

CHAPTER IV

CLOCK-CONTROLLED eIF2α ACTIVITY REGULATES RHYTHMIC TRANSLATION OF SPECIFIC mRNAs

Introduction

Circadian oscillators regulate the expression and activity of downstream clock-controlled genes (ccgs) through output pathways to control rhythmic biological processes for internal temporal order and to anticipate predictable environmental cycles [125]. Quantitative proteomic analysis of mouse liver samples harvested at different times of the day revealed that up to 50% of rhythmically accumulating proteins are expressed from non-cycling mRNAs [48-50]. Similarly, in *N. crassa,* up to 40% of the rhythmic proteome is expressed from arrhythmic mRNAs [55]. These data indicated that protein accumulation rhythms are driven by circadian regulation of protein degradation and/or mRNA translation. In support of clock control of mRNA translation, the expression and/or phosphorylation of several translation factors are rhythmic in eukaryotic cells [48, 56-58], including rhythms in the phosphorylation and activity of the conserved translation initiation factor eIF2α [64-66]. Understanding the extent and mechanisms of clock regulation of translation, a high energy consuming process, is crucial for a complete picture of cellular growth control.

The mechanism of clock control of mRNA translation is currently best understood in *N. crassa*. However, the extent of clock control of translation is not known in any system. In *N. crassa*, ~50% of available translation elongation factor eEF2 [58] and ~30% of eIF2α [66] are phosphorylated and inactivated during the subjective day under control of the clock. These data, along with rhythmic proteomics data indicating that 27% of the identified proteome (1273 proteins) cycle in

abundance, support the notion that not all *N. crassa* proteins accumulate with a circadian rhythm [55], and that some mRNAs may be more sensitive, and others more resistant, to increased levels of P-eEF2 and P-eIF2α levels during the day.

Based on this information, we hypothesized that rhythmic P-eIF2α regulates the translation of a specific subset of mRNAs. To test this hypothesis, and to identify the mRNAs that are rhythmically translated under control of eIF2α activity rhythms, we performed ribosome profiling (ribo-seq) from WT cells, clock mutant Δ*frq* cells, Δ*cpc*-3 cells that lack P-eIF2α, and constitutively active *cpc-3*^{c} cells that have high and arrhythmic P-eIF2α levels, and harvested at different times of the day. Ribo-seq identified actively translated mRNAs, and RNA-seq was used in parallel to determine mRNA abundance. Together, these data allow an estimation of translation efficiency (TE) for expressed genes. We found that the clock regulates the rhythmic translation of 1328 transcripts, and showed that translation of 404 of these mRNAs were arrhythmic in Δ*cpc*-3 and *cpc-3*^{c} cells. These data demonstrated that rhythmic P-eIF2α levels are necessary for rhythmic translation of specific mRNAs.

In *S. cerevisiae*, amino acid starvation activates GCN2 kinase. Active GCN2 kinase phosphorylates Ser51 of eIF2α [126]. High levels of P-eIF2α activate the translation of the transcription factor GCN4 [63], which regulates the expression of amino acid biosynthetic genes to adapt to the amino acid starvation stress [127, 128]. Phosphorylation of eIF2α Ser51 reduces the formation of the active ternary complex by binding to eIF2B, the GTP exchange factor of eIF2, thus inhibiting translation initiation of many mRNAs [59, 60]. However, the existence of four short upstream open reading frames (uORFs) in the 5'UTR of GCN4 mRNA promotes translation

initiation of GCN4, and other specific mRNAs when P-eIF2α levels are high [63]. For GCN4, when amino acid levels are high and P-eIF2α levels are low, upstream uORFs restrict progression of scanning ribosomes through the 5' leader of GCN4 mRNA reducing translation of the main ORF (mORF). Alternatively, when P-eIF2α levels are high, ribosomes scan past the uORFs and translate the mORF [129]. In *N. crassa,* translation of *cpc*-1 mRNA, the homolog of GCN4, is similarly regulated by amino acid starvation and P-eIF2α levels [130]. In this study, we found that ~13% of genes with rhythmic translation that is dependent on P-eIF2α rhythms contain uORFs. Taken together, these data support a potential role for uORFs in targeting mRNAs for translational regulation by cycling P-eIF2α levels.

Results

Time-resolved ribosome profiling data from N. crassa are of high quality

To determine the extent of clock regulation of translation *in vivo*, we performed ribo-seq, in parallel with RNA-seq on WT, Δ*frq*, Δ*cpc-3*, and *cpc-3*^{c} mycelial cultures over a circadian time course, in duplicate and with 4 h resolution (**Figure 20**). FRQ protein was rhythmic in WT, Δ*cpc-3*, and *cpc-3*^{c} cells, confirming that a functional clock was present in the cultures (**Figure 21 A, B & C**). As expected, P-eIF2α levels were rhythmic in WT cultures (**Figure 21D),** and arrhythmic in *cpc-3*^{c} cultures (**Figure 21E)**. These cells were used to generate ribo-seq and RNA-seq sequencing libraries (**Figure 28)**.

Sequence reads were aligned to the *N. crassa* genome (FungiDB Release 38) using STAR [131]. The mapped RNA-seq reads were normalized to fragments per kilobase of exon model per million mapped reads (FPKM) values using Cufflinks [132]. Because ribosome protected footprints (RPF)

are enriched in coding regions, the ribo-seq mapped reads from the coding sequences (CDS) were extracted and quantified using HTSeq-count [133]. The read counts were normalized using the median of ratios method employed in the DESeq2 analysis workflow [134]. To ensure the reproducibility of the sequencing data, correlation coefficients (R^2) were calculated between the two biological replicates for each strain at all time points using FPKM values. The R^2 values ranged from 0.8932 to 0.9938 (**Table 3**). Scatter matrices to compare two replicates of individual genes of *cpc-3*^{c} RNA-seq (**Figure 22E**) and ribo-seq (**Figure 22F**) are shown as examples.

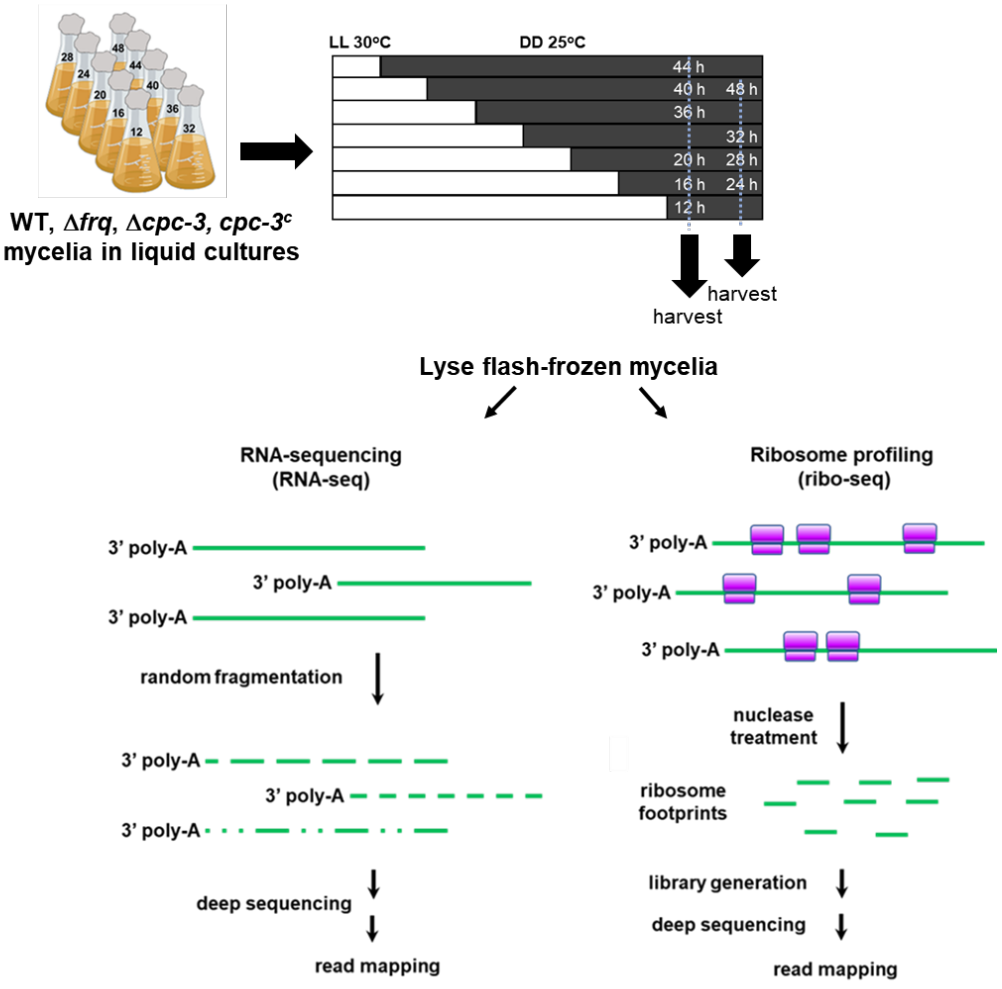

Figure 20. Sample preparation and library processing workflow for RNA-seq and ribo-seq of WT, Δ*frq*, Δ*cpc-3* and *cpc-3*^{C} strains.

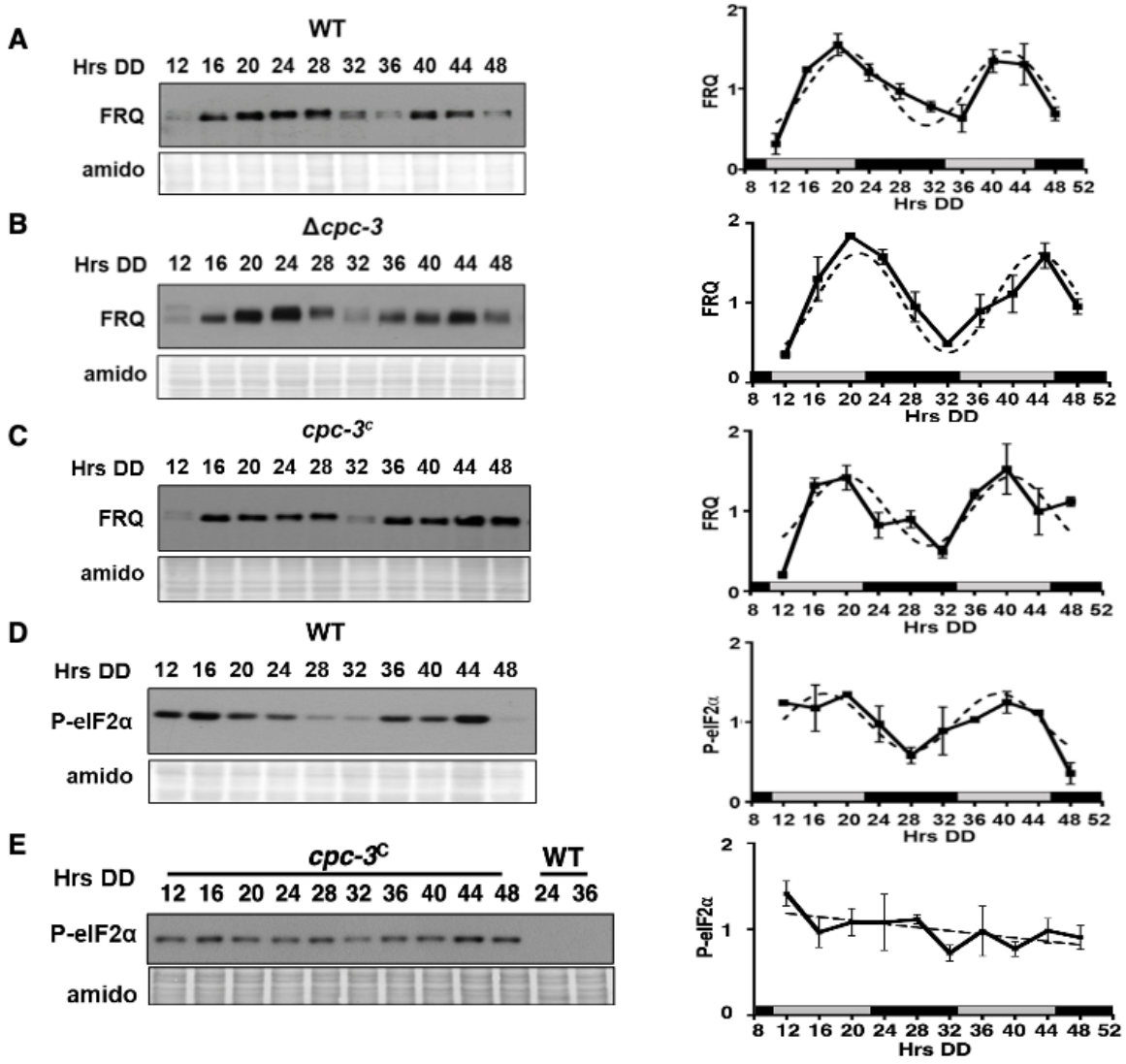

Figure 21. Validation of FRQ and P-eIF2α rhythms in sequencing samples. Representative western blots of protein extracts isolated from WT (A, D), Δ*cpc-3* (B), or *cpc-3*^{c} (C, E) strains grown in a circadian time course and probed with anti-FRQ antibody (A, B, C) or anti-P-eIF2α antibody (D, E). Amido black-stained membranes are shown as protein loading control. Plots of the data (mean ± SEM, n = 2) on the left show the average FRQ (A, B, C) or P-eIF2α (D, E) signal normalized to total protein (solid black line). Rhythmicity of FRQ and P-eIF2α was determined using F-tests of fit of the data to a sine wave (dashed black line, $p<0.001$), The black and white bars at the bottom of the plots designate subjective day (gray) and night (black).

Table 3. Correlation coefficients between ribo-seq replicates or RNA-seq replicates of WT, Δ*frq*, Δ*cpc-3*, and *cpc-3*^{c} cells across time points.

DD[1]	WT ribo-seq	WT RNA-seq	Δ*frq* ribo-seq	Δ*frq* RNA-seq	Δ*cpc-3* ribo-seq	Δ*cpc-3* RNA-seq	*cpc-3*^{c} ribo-seq	*cpc-3*^{c} RNA-seq
12	0.9360	0.9437	0.9495	0.9078	0.9057	0.9608	0.9031	0.9928
16	0.9243	0.9367	0.8965	0.9101	0.8932	0.9652	0.9388	0.9901
20	0.9364	0.9544	0.9066	0.9484	0.9466	0.9676	0.9398	0.9907
24	0.9421	0.9430	0.9361	0.9490	0.9602	0.9711	0.9499	0.9902
28	0.9209	0.9280	0.9461	0.9472	0.9613	0.9251	0.9373	0.9906
32	0.9660	0.9582	0.9661	0.9464	0.9597	0.9248	0.9443	0.9932
36	0.9292	0.9292	0.9297	0.9128	0.9482	0.9669	0.9579	0.9872
40	0.9528	0.9547	0.9380	0.9565	0.9381	0.9739	0.9348	0.9923
44	0.9436	0.9623	0.9428	0.9404	0.9520	0.9675	0.9248	0.9898
48	0.9364	0.9716	0.9594	0.9463	0.9370	0.9398	0.9363	0.9938

[1]Samples were harvested after growth in constant dark (DD) at the indicated time (h)

To confirm that the sequenced RPF were generated through protection of mRNAs by ribosomes, the footprints were examined to determine if they mapped to CDS across the genome. As expected, 90% of the average reads mapped to CDS, while 6% mapped to 5' UTRs and 4% to 3' UTRs, in WT, Δ*frq*, Δ*cpc-3* and *cpc-3*^{c} cells (**Figure 22A)**. In addition, the distribution of the read lengths, as determined using the NGS toolkit Plastid [135], were centered between 30-31 nucleotides (nt) (**Figure 22B).** This agrees with the observation that translating ribosomes protect ~28-30 nt of a transcript from nuclease digestion [136]. The physical process of ribosome movement creates triplet periodicity, or sub-codon phasing, allowing one to infer the reading frame in which a coding region is decoded when the read alignments are mapped to their P-site offsets [135]. Data with varying ribosome footprint lengths exhibit variable phasing; therefore, the most highly phased population of reads, the 31-mers, were examined to determine reading frame preference. Frame analysis revealed a strong preference for the first reading frame (phase 1) for all strains (**Figure**

22C). Taken together, using a ribo-seq protocol that was optimized for *N. crassa* resulted in footprints that 1) largely mapped to the CDS, 2) exhibited the expected size of a ribosome footprint, and 3) showed a preference for the first reading frame.

Ribosome occupancy, as a proxy for translation of the core clock genes *frq*, *wc-1*, and *wc-2,* and some clock-controlled genes (*ccgs*) were examined in WT and *cpc-3*^{c} datasets. When the averaged RNA-seq FPKMs and normalized RPF counts were plotted for *frq*, both showed rhythmic profiles. The level of *frq* mRNA peaks at DD32, while FRQ ribosome occupancy peaks ~4 h after the peak in mRNA levels (DD36) (**Figure 22 D & G**), consistent with the reported lag between its mRNA and protein accumulation [137]. The genes encoding other clock proteins, *wc-1* and *wc-2*, were previously found to have rhythmic promoter activity [45]. In our datasets, *wc-1* and *wc-2* mRNA and ribosome occupancy levels were rhythmic, peaking during early subjective night, and lagging FRQ expression by ~8 hr (**Figure 23 A & B**), consistent with previous observations [138]. Some *ccgs* including *ccg-1*, *ccg-13*, and *ccg-15* also had rhythmic mRNA and ribosome occupancy (**Figure 23 C, D & E**). We also examined a previously identified circadian output gene, *os-4*. The WCC binds rhythmically to the promoter of the MAP kinase kinase (MAPKK) of the OS-4 pathway, and drives daily rhythms in *os-4* mRNA and protein levels [96]. In our sequencing datasets, *os-4* mRNA accumulation and ribosome occupancy peaked around the same time, at DD32 (**Figure 23 F**), consistent with the reported peak times of the *os-4* mRNA and OS-4:Myc fusion protein levels [96]. Taken together, these results established that the datasets were of high quality, and that our mRNA abundance and ribosome footprint measurements can be applied to determine rhythmic translation across the *N. crassa* genome.

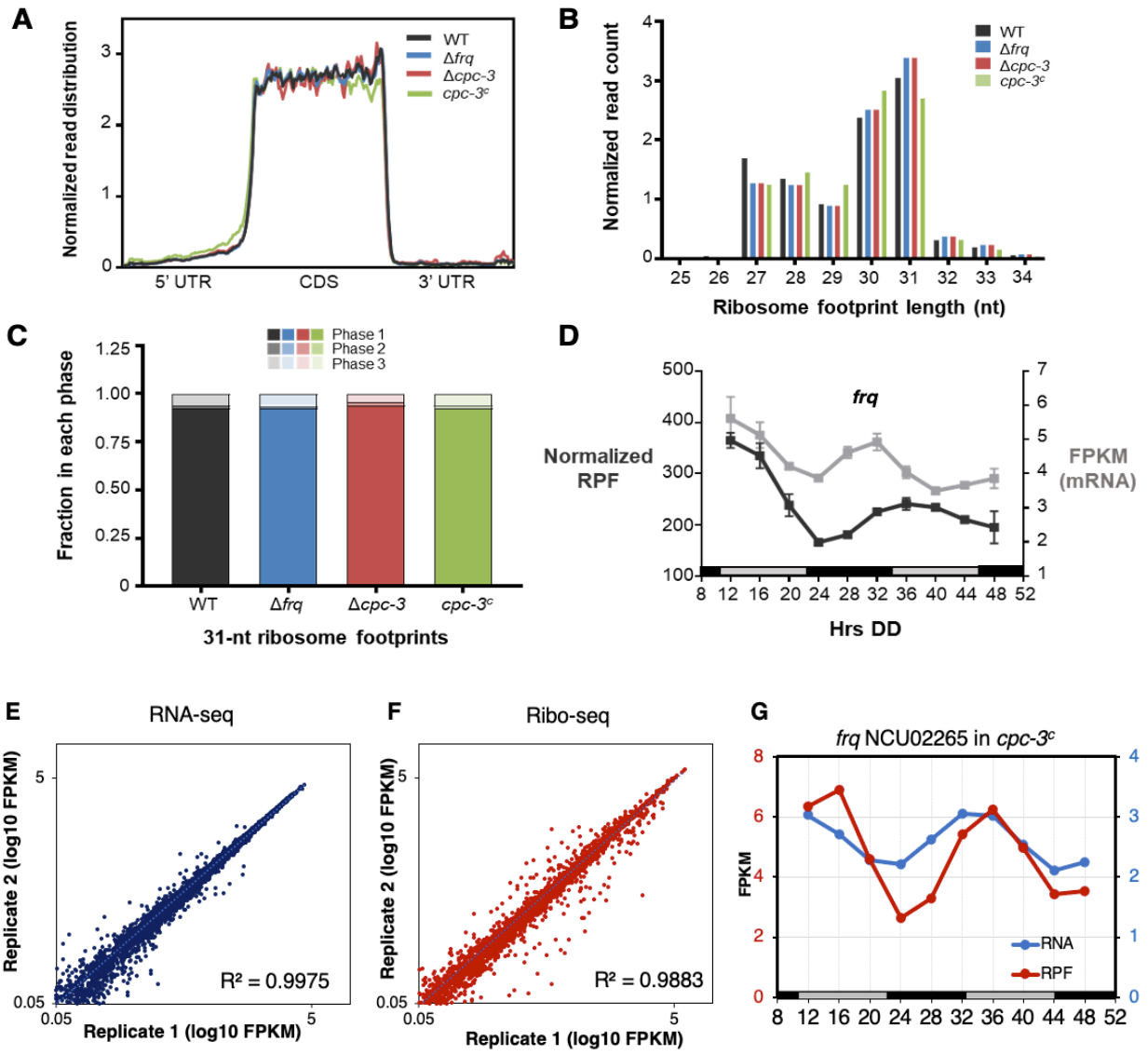

Figure 22. Ribosome profiling of *Neurospora* WT, Δ*frq*, Δ*cpc-3*, and *cpc-3*^{c} cells. (A) Fraction of total reads mapping to the coding sequence (CDS), 5'or 3' untranslated regions (5' UTR and 3'UTR) for WT (black), Δ*frq* (blue), Δ*cpc-3* (red), and *cpc-3*^{C} (green) samples. (B) Insert size distribution of RPF across all replicates and timepoints for WT (black), Δ*frq* (blue), Δ*cpc-3* (red), and *cpc-3*^{C} (green) samples. (C) Frame analysis for RPF for the most highly phased population of reads, 31-mers. The RPF are color-coded (dark, medium, light) according to the sub-codon position alignments (1, 2, 3) for WT (black), Δ*frq* (blue), Δ*cpc-3* (red), and *cpc-3*^{C} (green) samples. (D) RNA-seq FPKM data (gray, left y-axis) and normalized ribosome-protected footprint (RFP) (black, right y-axis) of *frq* from WT cells grown in DD and harvested at the indicated times (h). Scatter matrices comparing the average FPKM of the two replicates from RAN-seq (E) and ribo-seq (F) sequencing data of *cpc-3*^{c} cells. (G) RNA-seq FPKM data (blue, right y-axis) and normalized ribosome-protected footprint (RFP) (red, left y-axis) of *frq* from *cpc-3*^{c} cells grown in DD and harvested at the indicated times (h).

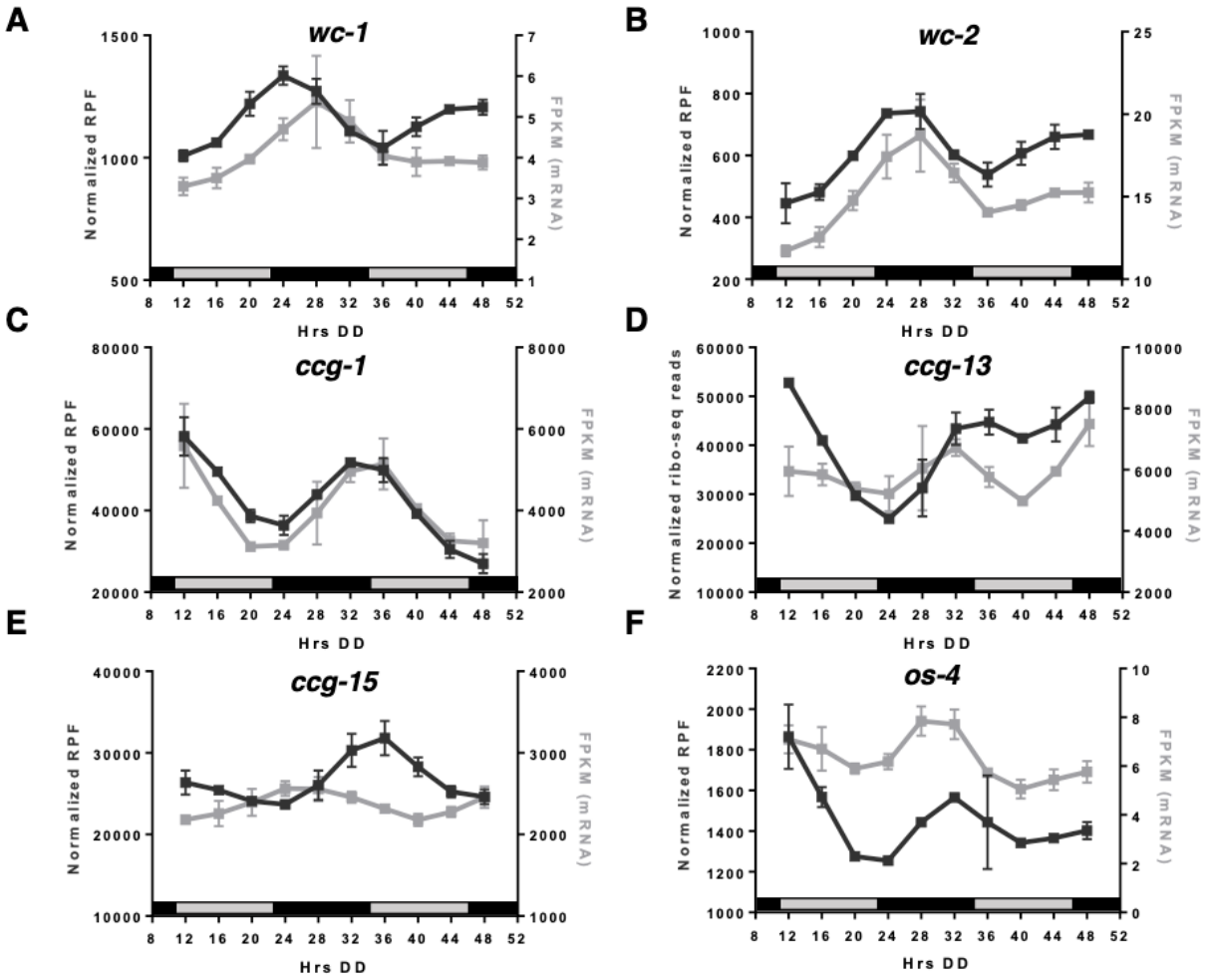

Figure 23. Core clock genes and selected *ccgs* are rhythmic. RNA-seq FPKM (grey, left y-axis) and normalized RPF reads (black, right y-axis) traces of the indicated core clock genes (A, B) and *ccgs* (C-F) in WT cells.

Clock-controlled eIF2α activity is required for rhythmic translation of specific mRNAs

Rhythms in mRNA abundance and ribosome occupancy were determined using the Extended Circadian Harmonic Oscillator application (ECHO) [139], with the following criteria for rhythmicity: a Benjamini-Hochberg (BH) adjusted p-value cutoff of <0.05 and damped, forced or harmonic oscillation types. Of the 9760 coding genes in *N.* crassa, 2086 genes (21%) had rhythmic ribosome occupancy in WT cells, and roughly half of these (N = 1328) were arrhythmic in the

clock mutant Δ*frq*, demonstrating their dependence on the clock for rhythmic translation (**Figure 24A**).

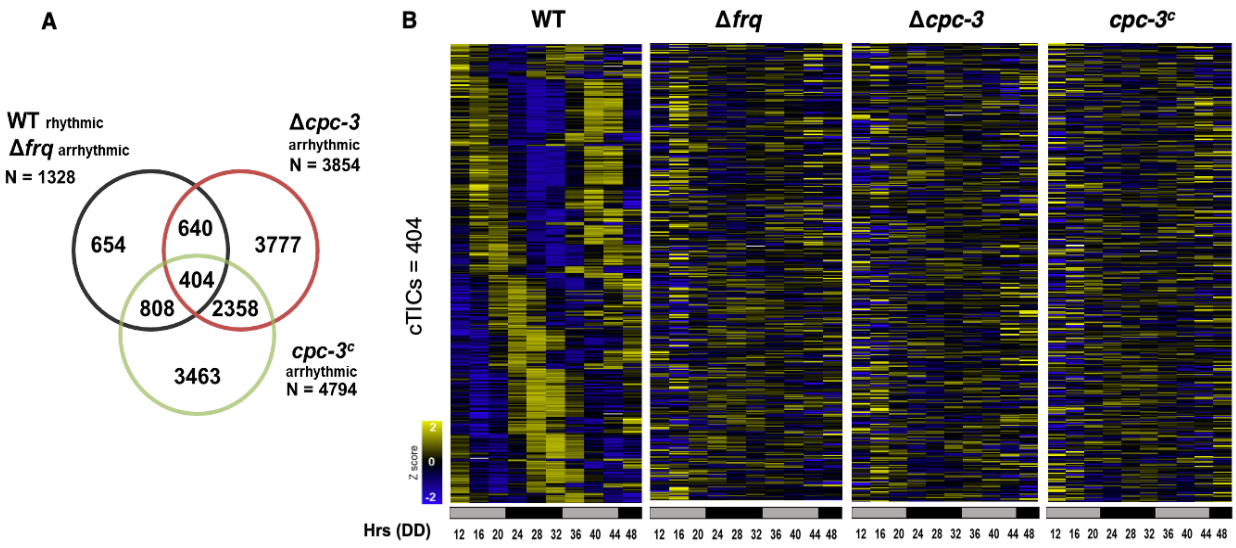

Figure 24. A subset of mRNAs requires P-eIF2α for rhythmic translation. (A) Venn diagram of the overlap between genes with rhythmic RPF counts in WT cells, and arrhythmic RPF counts in Δ*frq*, Δ*cpc-3*, and *cpc-3*^{c} cells. (B) Heat maps of the peak phase of genes with rhythmic RPF counts in WT cells, and arrhythmic RPF counts in Δ*frq*, Δ*cpc-3*, and *cpc-3*^{c} cells (N = 404) grown in DD and harvested at the indicated times (hrs). Genes are sorted by the peak phase in WT.

In the eIF2α kinase mutant Δ*cpc-3*, 48% (640 genes) of the clock-controlled translatome (1328 genes) were arrhythmic, while 61% (808 genes) were arrhythmic in the constitutive kinase mutant *cpc-3*^{c} (**Figure 24A**). To identify genes whose rhythmicity is dependent on rhythmic P-eIF2α levels, we looked at the overlapping arrhythmic genes in both Δ*cpc-3* and *cpc-3*^{c} cells. Out of the 1328 genes with clock-controlled translatome, 404 genes (30%) lost rhythmicity in both Δ*cpc-3* and *cpc*-3^{c} cells. We referred to these 404 genes as circadian translation initiation-controlled genes (cTICs) (**Figure 24A**). There were 688 genes and 520 genes that remained rhythmically translated in Δ*cpc-3* and *cpc-3*^{c} cells, respectively, suggesting that other regulatory mechanisms exist to

control translation rhythms. The relative RPF peak phases of the cTICs over a circadian time course are shown in heatmaps, where the genes are ordered by the phase of oscillation in WT cells (**Figure 24B**). Overall, these data demonstrated that clock regulation of P-eIF2α through CPC-3 results in rhythmic translation of specific mRNAs under constant conditions, rather than affecting global rhythmic translation.

Genes that depend on clock-controlled eIF2α activity are rhythmically translated from cycling or non-cycling transcripts

To determine the nature of mRNAs that are subjected to rhythmic translation through eIF2α activity, the mRNA profiles of the 404 cTICs were analyzed based on whether or not the mRNA levels cycled, and the peak phase of cycling mRNAs. This analysis led to three distinct classes: class I) genes whose mRNA and ribosome footprint levels show in-phase rhythmicity (24%), class II) genes whose mRNA and ribosome footprint levels show a phase discordance of more than 4 h (18%,), and class III) genes translated from arrhythmic mRNAs (58%) (**Figure 25A**).

Most of the class I genes peaked in translation during the subjective night (72%), whereas most class II genes peaked in translation during the subjective day (75%) (**Figure 25B**). More than half of the genes that depend on clock-controlled eIF2α activity for rhythmic translation arose from arrhythmic mRNA. This finding is consistent with the observation that about half of the oscillating proteins in the *N. crassa* identified using quantitative proteomics do not have corresponding cycling mRNAs [55]. For class III genes, 134 (57%) genes peaked in translation during the day, and 100 (43%) genes peaked in translation during the night (**Figure 25B**). As we are interested in the effect of the circadian clock on translation, we focused our subsequent analyses on class III

cTICs, as genes in this category appear to undergo distinct post-transcriptional control mechanisms to generate rhythms in translation from arrhythmic mRNAs. Go analysis of the 234 class III cTICs showed that they are enriched in pathways related to mRNA processing, translation initiation, protein modification and some metabolic processes (**Table 4**).

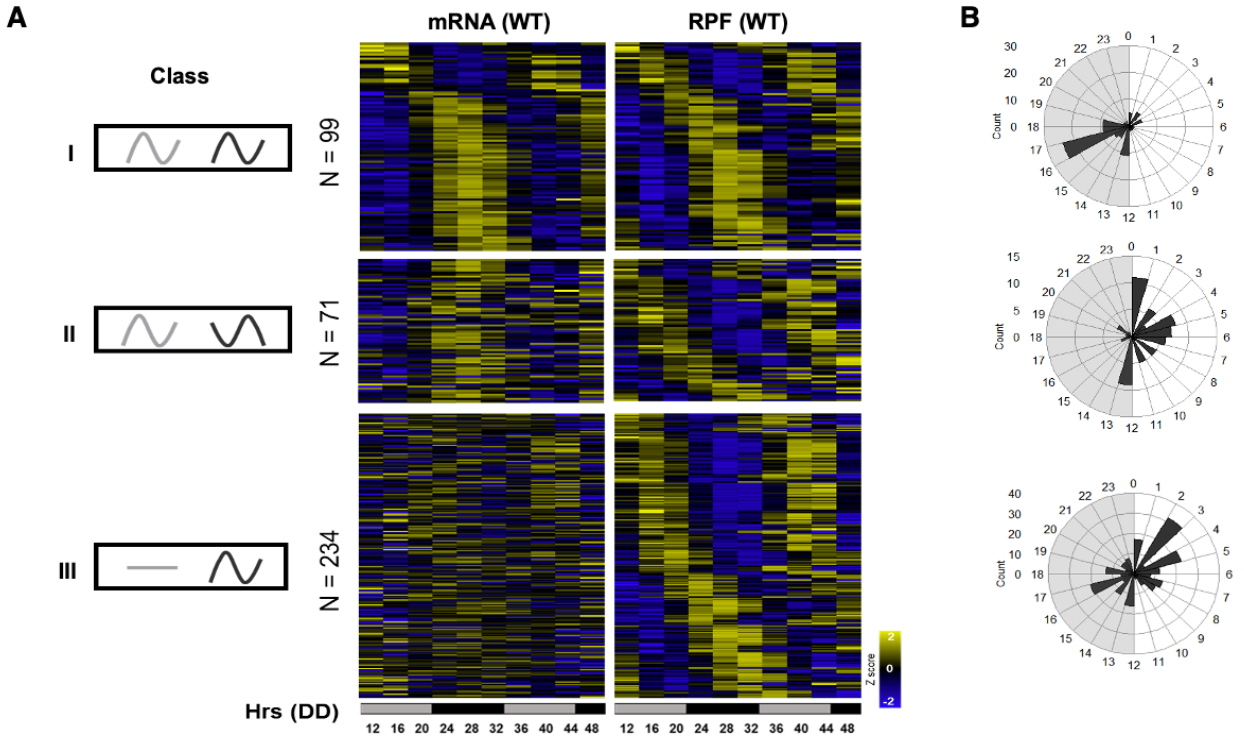

Figure 25. Proteins that depend on clock-controlled eIF2α activity for rhythmic translation arise from cycling and non-cycling transcripts. (A) Heat maps of the peak phase of genes with rhythmic RPF counts in WT cells (right panel) and their corresponding mRNA expression (FPKM) profiles (left panel). The 404 cTICs are sorted by the peak phase of WT RPF count for each class, and are divided into three classes: (I) in-phase rhythmic RPF and mRNA, (II) rhythmic RPF and mRNA with phase changes, and (III) rhythmic RPF and arrhythmic mRNAs. (B) Phase distribution based on maximal RPF counts in WT, for genes belonging to each class. The concentric circles emanate from zero at the center to increasing frequencies that and are indicated by the numeric legends. The numbers indicate circadian time (CT), with white designating subjective day (CT0-12) and gray designating subjective night (CT12-0).

Table 4. Go analysis of the 234 class III cTICs. Categories shown were considered significantly enriched with $p < 0.5$.

GO name (Biological process category)	p-value	# genes / input
7-methylguanosine mRNA capping	0.002	1 / 234
protein O-linked glycosylation	0.005	2 / 234
regulation of translational initiation	0.012	3 / 234
arabinan metabolic process	0.029	1 / 234
CVT pathway	0.029	1 / 234
demethylation	0.029	1 / 234
deoxyribonucleotide biosynthetic process	0.029	1 / 234
ER-associated ubiquitin-dependent protein catabolic process	0.029	1 / 234
glycerol-3-phosphate catabolic process	0.029	1 / 234
Golgi to plasma membrane protein transport	0.029	1 / 234
intracellular accumulation of glycerol	0.029	1 / 234
karyogamy involved in conjugation with cellular fusion	0.029	1 / 234
mannitol metabolic process	0.029	1 / 234
mitochondrion degradation	0.029	1 / 234
multicellular organismal development	0.029	1 / 234
pheromone-dependent signal transduction involved in conjugation with cellular fusion	0.029	1 / 234
posttranslational protein targeting to membrane	0.029	1 / 234
protein O-linked mannosylation	0.029	1 / 234
protein oligomerization	0.029	1 / 234
response to metal ion	0.029	1 / 234
tRNA 5'-leader removal	0.029	1 / 234
positive regulation of GTPase activity	0.037	3 / 234
response to stress	0.041	3 / 234
pentose-phosphate shunt	0.045	2 / 234
translational initiation	0.048	4 / 234

idi-4 translation is rhythmically regulated by P-eIF2α

We validated the sequencing results by examination of the expression of the class III *idi-4* (*induced during incompatibility*, NCU08055) gene. IDI-4 is a putative basic leucine zipper (b-zip) transcription factor in *N. crassa*, and microarray analyses revealed its potential role in the

regulation of carbon compound and carbohydrate metabolism [140]. In addition, the *Podospora anserina idi-4* homolog induces autophagy and cell death [141]. To validate if translation of *idi-4* mRNA is clock-controlled, rhythmicity of *idi-4* mRNA and protein levels were monitored in WT cells. As expected based on the ribosome profiling results, an IDI-4::LUC translational fusion was rhythmic in DD with a peak in the subjective night, the time of day when P-eIF2α levels are low. A transcriptional fusion of the *idi-4* promoter to luciferase, *Pidi-4::luc*, was arrhythmic **(Figure 26A)**. Consistent with translational regulation of *idi-4* by the clock and rhythmic eIF2α activity, IDI-4::LUC was arrhythmic in both Δ*frq* **(Figure 26B)** and Δ*cpc-3* **(Figure 26C)** cells. Translation efficiency (TE) plots of *idi-4* in WT and *cpc-3*^{c} cells, generated by the ratio of abundance of RPF to mRNA levels using Xtail [142], showed rhythmic translation in WT cells and arrhythmic translation in *cpc-3*^{c} cells **(Figure 26D)**. The TE values were lower in *cpc-3*^{c} cells compared to WT cells, suggesting that high levels of phosphorylation of eIF2α inhibit translation of *idi-4* mRNA, and are consistent with *idi-4* translation peaking during the subjective night when P-eIF2α levels are low in WT cells **(Figure 26D)**. Taken together, these data validated circadian translational regulation of *idi-4*, which is dependent on rhythms in the levels of P-eIF2α.

Identification of cis-elements common to mRNAs that require rhythmic P-eIF2α levels for rhythmic translation

In WT cells, P-eIF2α levels peak in the subjective day, and are low during the subjective night [66]. This implies that for eIF2α regulated genes, translation is promoted by high P-eIF2α levels in day-peaking genes, whereas translation of night-peaking genes is inhibited by high P-eIF2α levels. Thus, night-peaking genes have increased translation when P-eIF2α levels are low. Of the 234 genes with arrhythmic mRNA and rhythmic translation regulated by clock and eIF2α activity,

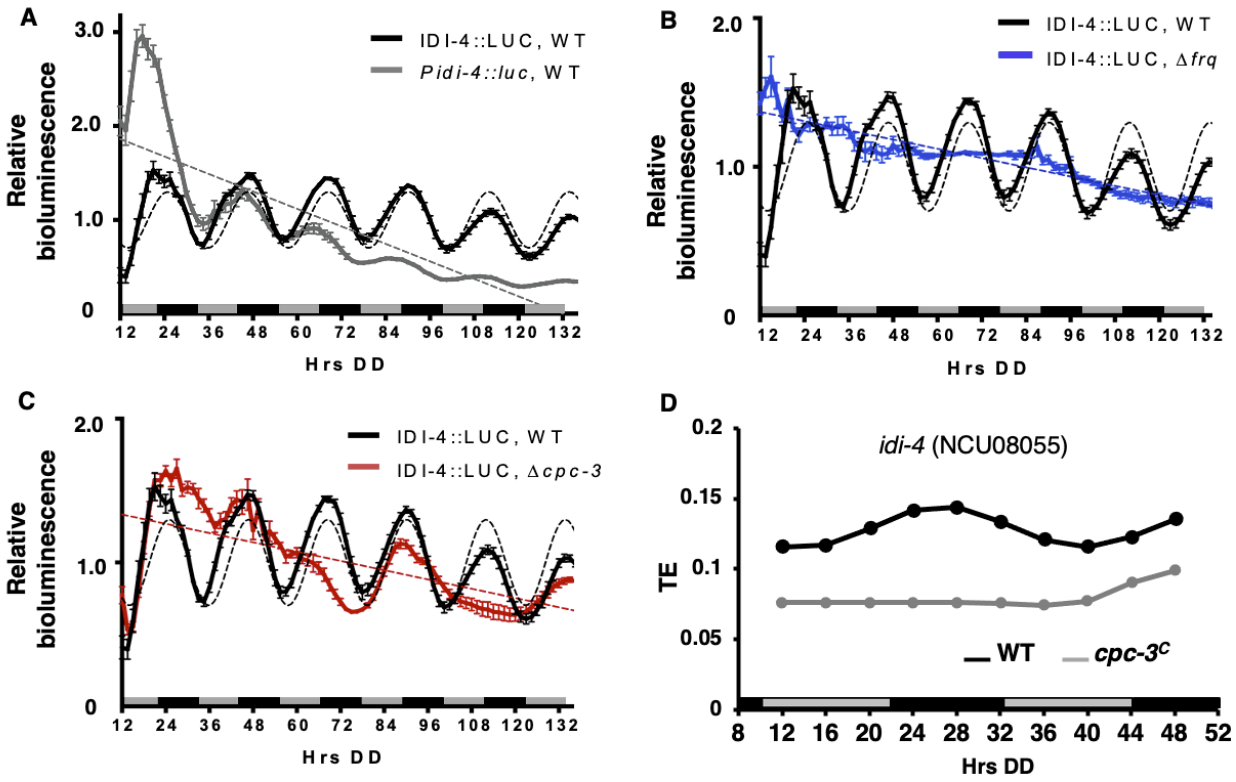

Figure 26. Rhythmic translation of *idi-4* is regulated by rhythms in the levels of P-eIF2α. Luciferase activity from *Pidi-4::luc* transcriptional (grey line) fusions in WT cells (A), IDI-4::LUC translational fusions in WT cells (black line) (A, B, C), Δ*frq* cells (Blue line) (B) and Δ*cpc-3* cells (red line) (C) cultured in DD and recorded every 90 mins. The normalized bioluminescence signal is plotted (mean ± SEM, n =12). Dotted lines show the best fit of the data to a line or sine wave ($p<0.001$) by F-test in the corresponding color. (D) Fitted TE values of *idi-4* gene in WT (black line) and *cpc-3*^{C} (grey line) cells from ribosome profiling data.

100 genes peaked during night, suggesting the phosphorylation of eIF2α inhibits their translation, and 134 genes peaked during day, suggesting that translation of these genes is promoted by P-eIF2α. To investigate what makes the translation of these genes inhibited (night-peaking) or promoted (day-peaking) by P-eIF2α, we first examined if there are cis-regulatory elements in the 5'UTR of the night peaking and day peaking genes with the MEME Suite [143]. Using the 5'UTR region (from transcription start nucleotide to the translation start nucleotide) of the transcript sequences as input, a statistically significant A-rich motif was identified in 42 out of 100 night-

peaking genes, and a C-rich motif was found in 25 out of 134 day-peaking genes (P<0.05) (**Figure 27A**). The validated night-peaking gene *idi-4* has 2 predicted regions (M1 and M2) of the A-rich motif in the 5'UTR region (P<0.01) (**Figure 27B & D**). Experiments are in progress to determine if these motifs are important for P-eIF2α regulation of rhythmic translation of *idi-4* and other day and night peaking genes by deletion or mutation of the motifs.

In addition to the potential night-acting A-rich element controlling *idi-4* mRNA translation, a major peak of the RPF reads mapped to the 5' UTR region of the *idi-4* transcript in all ribo-seq dataset, with RPF reads higher than RPF reads mapped to the annotated ORF **(Figure 27C)**. These data suggested that translation may be occurring at an upstream open reading frame (uORF) in the 5' UTR, or that the main ORF (mORF) was mis-annotated. Currently, uORF's are not annotated in the *N. crassa* genome. However, our circadian ribo-seq provided the opportunity to annotate potential uORFs across the genome [144]. We identified 879 genes (9% of the 9760 coding genes in *N. crassa*) with potential uORFs using the RiboCode program [145]. As expected, *N. crassa* genes with established uORFs were found using this method, including *cpc-1* (NCU04050), the homolog *S. cerevisiae GCN4*. We found that there are 53 genes (13%) with predicted uORFs in the 404 cTIC genes whose rhythmic translation is regulated by P-eIF2α. This is higher than the 9% of uORF-containing genes over the whole genome, suggesting the possibility that the presence of uORFs in day-peaking genes may increase translation of the main ORF when P-eIF2α levels are high under control of the clock. However, of the 404 cTICs that peak during the day, only 24 had uORFs, suggesting that this element is not the only mechanism for increased translation when P-eIF2α levels are high.

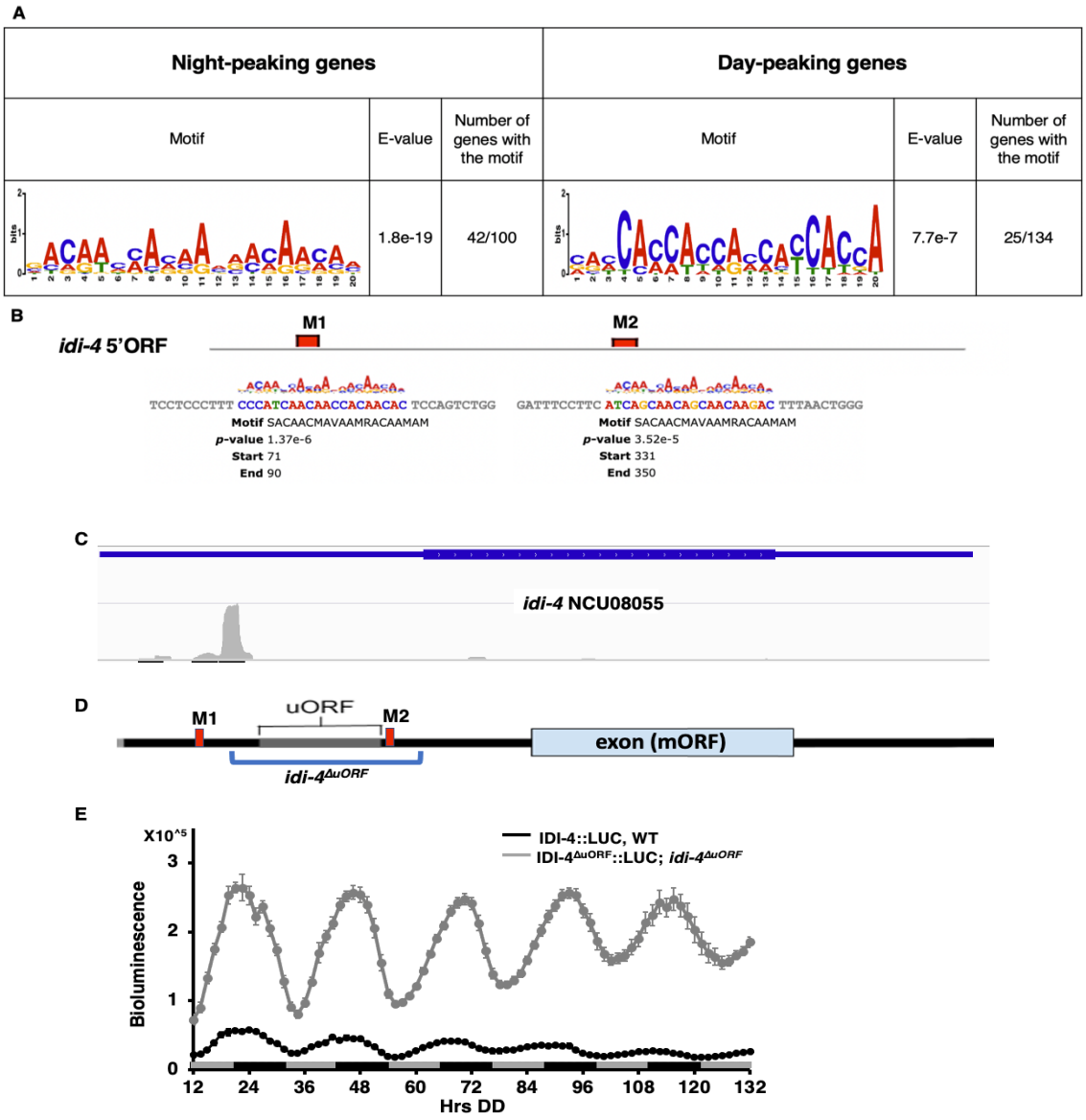

Figure 27. Motifs in the 5' UTR of transcripts regulated by rhythmic P-eIF2α. (A) MEME of the *cis*-element motifs that showed enrichment in the 5' UTR of mRNAs that are rhythmically translated and peaking during the subjective night (left) or day (right) under control of P-eIF2α. (B) Localization of the night-peaking motif in the 5'UTR of *idi-4* transcript. (C) Annotated gene structure and ribo-seq read localization in *idi-4* in the Integrative Genome Browser (IGV) indicates a potential uORF in the 5'UTR of *idi-4* transcript. The WT DD24 sample was used to represent the translation in the 5'UTR (D) Relative localization of motifs, elements and mutation design of *idi-4*. M1 and M2 indicates the night-peaking motif 1 and 2 shown in (B). The blue region marks the deletion area in the *idi-4*$^{\Delta uORF}$ mutant. (E) Luciferase activity from IDI-4::LUC translational fusions in WT cells (black line), IDI-4$^{\Delta uORF}$::LUC translational fusions in *idi-4*$^{\Delta uORF}$ cells (grey line) cultured in DD and recorded every 90 mins. The average bioluminescence signal is plotted (mean ± SEM, n =12).

To examine if the translated region in the 5'UTR of *idi-4* is an uORF, or is part of the mORF, an *idi-4*$^{\Delta uORF}$ strain was generated, in which the predicted uORF region of *idi-4* was deleted (**Figure 27D)**. One of the night-peaking motifs (M2) is next to the predicted uORF region, and M2 was also deleted in the *idi-4*$^{\Delta uORF}$ strain. An *idi-4*$^{\Delta uORF}$ translational fusion to luciferase was generated (IDI-4$^{\Delta uORF}$::LUC) and luciferase activity was examined over a circadian time course in DD to determine the impact of the predicted uORF on *idi-4* translation. If the predicted uORF is part of the mORF, we expected that deletion of the uORF would disrupt the translation of *idi-4*, and therefore, lead to no expression of IDI-4$^{\Delta uORF}$::LUC. However, IDI-4$^{\Delta uORF}$::LUC had higher luciferase activity compared to IDI-4::LUC in WT cells (**Figure 27E**), indicating that the deleted region is not part of the mORF. Instead, these data support the presence of a uORF in the 5'UTR of *idi-4* mRNA that inhibits the expression of the mORF. Moreover, while the overall levels were low, IDI-4$^{\Delta uORF}$::LUC was rhythmic, peaking at the same time of day as IDI-4::LUC in WT cells (**Figure 27E**). These data suggested that the uORF of *idi-4* is not required for P-eIF2α-dependent rhythmic translation. This may not be surprising given that *idi*-4 translation peaks during the subjective night, when P-eIF2α levels are low.

Discussion

The circadian clock in fungi and mammals controls the activity of translation initiation and elongation factors [58, 64-66]; however, the impact of this regulation on rhythmic translation was not known. In this study, we performed ribosome profiling using circadian time course samples of WT and clock mutant Δ*frq* cells to demonstrate clock control of translation. In addition, to identify genes whose rhythmic translation depends on rhythmic P-eIF2α levels, we performed ribosome profiling in cells that are unable to phosphorylate eIF2α (Δ*cpc*-3), and in cells that have high and

arrhythmic P-eIF2α levels (*cpc-3^{c}*). While we showed in the Chapter II that the phosphatase mutant *ppp1^{RIP}* strain also has high and arrhythmic P-eIF2α levels, PPP1 likely has many different substrates [94], some of which may affect translation. Because PPP1 is not as specific as the *cpc-3^{c}* mutant with regards to clock control of translation by rhythmic P-eIF2α levels, it was not included in this study. Importantly, we discovered significant overlap between the genes that are translationally controlled in the Δ*cpc-3* and *cpc-3^{c}* datasets (**Figure 24A**), supporting a role for clock control of translation by regulating P-eIF2α levels.

Rhythms in mRNA abundance and ribosome occupancy were determined using ECHO, which outperforms existing methods, including JTK cycle, in detecting rhythms, including genes with dampened oscillations, and for recovering phase information in large datasets [139]. We found that the clock regulates the translation of ~15% of the *N. crassa* genome (1328 transcripts), and 30% of these (404 cTIC transcripts) required clock-controlled P-eIF2α levels for rhythmic translation (**Figure 24**). These data suggest that other factors are involved in rhythmic translation regulation. Supporting this idea, the activity of the conserved translation elongation factor eEF2 is also under clock control in *N. crassa*, with increased eEF2 activity at night leading to an increased translation rate *in vitro* [58]. Moreover, circadian proteomic analysis in *N. crassa* revealed that many translation related proteins are rhythmic, containing ribosomal proteins and the initiation factors eIF1 (NCU01981), the delta subunit of eIF2B (NCU01468), eIF3D (NCU07380), eIF3F (NCU01021), and eIF3G (NCU08046) [55]. Several factors of the protein translation machinery were shown in this study to have rhythmic ribosome occupancy, including several ribosomal proteins and translation initiation factors including RPS5 (NCU01800), RPS30 (NCU06048), RPL14 (NCU08552), RPL19 (NCU04336), RPL24 (NCU03150), eIF2β (NCU04640), the eIF2B

alpha (NCU04344), epsilon (NCU02414) and delta (NCU01468) subunits, eIF3A (NCU00040), eIF3I (NCU03876), eIF3E (NCU02076) and the gamma subunit of eEF1B (NCU03826). Correspondingly, proteomics analysis with mouse liver samples found that the translation initiation factors EIF1, E1F4A2, EF4G1 and EIF5 had rhythmic protein abundance [48], and the phosphorylation levels of eIF4E cycled in mouse SCN [56]. Furthermore, ribosome biogenesis genes (*e.g.* RPL5, RPL23, PRL32 and PRLP0) were regulated by clock at both the mRNA and protein level [57]. These rhythmic translation factors, together with rhythmic P-eIF2α, likely contribute to rhythmic translation of output genes by the clock. However, unlike from our studies of clock control of eIF2α activity, the impact of clock control of these other factors on translation are not yet known.

Of the 404 cTICs, 234 genes had arrhythmic mRNA levels, indicating that they are controlled specifically at the translational level by the rhythmic accumulation of P-eIF2α. Go analysis showed that these cTICs are enriched in pathways related to mRNA processing, translation initiation, protein modification and some metabolic processes (**Table 4**). Of these 234 cTICs, 134 (57%) peaked in translation during the day, and 100 (43%) genes peaked in translation during the night (**Figure 25B**). P-eIF2α levels peak during the subjective day [66]; therefore, we predicted that cTICs that peak in translation during the day are more resistant to high P-eIF2α levels, while cTICs that peak in translation during the night are more sensitive to P-eIF2α. Consequently, for day-peaking cTICs, we predicted that translation efficiency would be increased in cells that have high constitutive levels of P-eIF2α, such as *cpc-3*^{c} cells, compared to WT. In contrast, we predicted that night-peaking cTICS would have lower translation in *cpc-3*^{c} cells compared with WT cells. Comparing the TE of the ORF region of cTICs in *cpc-3*^{c} versus WT cells, showed that 75% of

cTICs fit these predictions for both day-peaking and night-peaking cTICs, including *idi-4* (**Figure 26**).

The cTIC *idi-4* encodes a putative b-zip transcription factor with a potential role in the regulation of carbon compound and carbohydrate metabolism [140]. Consistent with the sequencing data, *idi-4* mRNA levels are arrhythmic, and ribosome occupancy is rhythmic in WT, but not in Δ*cpc-3* cells (**Figure 26**). Moreover, we found that the TE of *idi-4* is rhythmic in WT and arrhythmic, with a low TE in *cpc-3^{c}* cells (**Figure 26D**), suggesting that high phosphorylation levels of eIF2α inhibit the translation of *idi-4*. These data are consistent with the peak of *idi-4* translation during the subjective night (DD28) when P-eIF2α levels are low in WT cells **(Figure 26D)**.

Not only is phosphorylation of eIF2α controlled by the clock under constant environmental conditions, but it can also be induced by stresses, including amino acid starvation [146]. Under amino acid starvation conditions, the translation rate of most genes is inhibited, whereas genes that encode proteins required for adaption to stress conditions are translated [147-149]. The *cpc-3^{c}* mutation leads to consistently high P-eIF2α levels, similar to the levels observed following amino acid starvation [66]. Thus, we would expect gene expression patterns in *cpc-3^{c}* cells to be similar to cells undergoing stress. This idea still needs to be tested. It is also of interest to determine if the inhibition of *idi-4* translation by P-eIF2α is similarly controlled during amino acid starvation. The *idi-4* homolog in *P. anserina* was shown to induce autophagy and cell death [141], suggesting a potential role for IDI-4 in regulation of cell fate at specific times of the day, and under stress conditions. These data raise the possibility that a novel stress response pathway exists, which is

under control of the circadian clock to coordinate stress responses with daily environmental stress for enhanced survival and fitness.

How certain mRNAs are selected for translation regulation by cycling P-eIF2α levels is not known. Of the 404 cTICs, whose translation rhythmicity is regulated by P-eIF2α (**Figure 24**) there are 53 genes (13%) with predicted uORFs. This is slightly higher than the percentage of uORFs across the entire genome that were predicted from our riboseq studies. In addition to the presence of uORFs in the cTICs, specific sequence motifs were identified in the day-peaking and night-peaking cTICs (**Figure 27A**). If, and how, these motifs are involved in P-eIF2α regulation of translation needs further experiments. Conserved motifs have been shown to target mRNAs for regulation by specific translation factors. For example, the Translation Initiator Short 5'UTR motifs (TISU) (SAASATGGCGGC) were reported to target mRNAs to be regulated by the translation initiation factor eIF1 [150]. Also, a 5' terminal oligopyrimidine (5' TOP) motif, consisting of 5-15 pyrimidines in the 5'UTR, was enriched in genes encoding components of the translational machinery, and in genes that are responsive to mTOR signaling [151].

Other possible features of cTIC mRNAs that may be involved in their rhythmic translation include sequences that target them to the Processing-bodies (P-body), which are cytoplasmic ribonucleoprotein granules that function in controlling the fate of mRNAs [152]. Translational repressed mRNAs can either be degraded in P-bodies, or can be recycled from P-bodies to translating polysomes [153-155]. Interestingly, P-body dynamics are clock-controlled in mammalian cells through regulation of an RNA binding protein LSM1 [156]. Dr. Kathrina Castillo

in our lab is testing the idea that rhythmic P-eIF2α accumulation leads to rhythms in the formation of P-bodies and/or the pathways targeting mRNAs to P-bodies to control their rhythmic translation.

Our study has led to novel insights into temporal regulation of translation by circadian clock through the rhythmic accumulation of P-eIF2α. This posttranslational mechanism appears to be conserved; the mammalian clock controls rhythms in the levels of P-eIF2α in the SCN [64, 65]. Thus, our studies in *N. crassa* will likely provide critical information on the mechanisms of the clock regulation of mRNA translation in higher eukaryotes. Understanding the clock regulation of translation, together with circadian transcription regulation, will provide an in depth understanding of clock regulation of circadian output genes important in an organisms physical and mental health.

Methods and Materials

N. crassa strains and growth conditions: Vegetative growth conditions and crossing protocols were as previously described [110]. All strains containing the *hph* construct were maintained on Vogel's minimal media [110], supplemented with 200 μg/mL of hygromycin B. Strains containing the *bar* cassette were maintained on Vogel's minimal media lacking NH_4NO_3 and supplemented with 0.5% proline and 200 μg/mL of Basta.

N. crassa wild type (WT) FGSC #4200 (mat a, 74-OR23-IV) or FGSC #2489 (mat A, 74-OR23-IV), were obtained from the Fungal Genetics Stock Center (FGSC, Kansas State University). Δ*frq::bar* (DBP 1228) [113] and *cpc-3*^{c} (DBP 3291) [66] was previously generated. The primers used to generate and validate strains are listed in **Table 5**. Translational fusions to luciferase (LUC) were generated by 3-way PCR (primers idi-4 F1 and R1, and idi-4 F2 and R2) using the *N. crassa*

codon-optimized luciferase gene from pRMP57 (primers idi-4 F3 and R3) [61, 117], and co-transformed with hyg^R pBP15 [115] into WT (FGSC 4200). Hygromycin-resistant transformants were screened for luciferase activity and homologous insertion into the *idi-4* gene (primers idi-4 F4 and R4). IDI-4::LUC transformants were crossed with Δ*frq::bar* (DBP 1228) and Δ*cpc-3::hyg* (DBP 2789) to generate IDI-4::LUC, Δ*frq::bar* (DBP 3436) and Δ*cpc-3::hyg* (DBP 3763) homokaryons. To generate the P*idi-4::luc* transcriptional fusion, a 1.3 kb promoter region of *idi-4* was amplified with primers idi-4 F5 and idi-4 R5 containing *Not*I and *Spe*I restriction sites. The PCR product was digested with *Not*I and *Spe*I, and cloned into plasmid pRMP57 [61, 117] containing the codon-optimized luciferase gene [61]. The resulting plasmid was linearized by digestion with *Pci*I, and co-transformed with hyg^R pBP15 [115] into WT (FGSC 4200) cells. Hygromycin-resistant transformants were screened for luciferase activity. To generate a luciferase translational fusion of *idi-4* containing a deletion of the uORF region, the $idi\text{-}4^{\Delta uORF}$ fragment was generated by 2-way PCR using primers $idi\text{-}4^{\Delta uORF}$ F1, R1, F2 and R2. The PCR product was co-transformed with pBARGEM7-2 plasmid carrying the BASTA resistance gene (pDBP425) into IDI-4::LUC (DBP3234) conidia. An $idi\text{-}4^{\Delta uORF}$ homokaryon in IDI-4::LUC (DBP3439) homokaryon was obtained by microconidia filtration [114].

Circadian time courses: Circadian time course experiments for western blots and sequencing libraries were performed according to published methods [58, 96]. Briefly, mycelial mats in Vogel's minimal media containing 2% glucose (pH 6.0) were synchronized to the same time of day by a shift from 30°C constant light (LL) to 25°C constant dark (DD). The cultures were grown in LL for a minimum of 4 h and transferred to DD on day 1 (for collection at DD 36, 40, 44, 48), day 2 (for collection at DD 12, 16, 20, 24, 28, 32), and harvested either at 9:00 a.m. (DD 12, 16,

20, 36, 40, 44) or 5:00 p.m. (DD 24, 28, 32, 48) on day 3. Harvested tissue was immediately frozen in liquid N_2.

Protein extraction and western blotting: Protein extraction, protein concentration quantification, and western blot analyses were performed as previously described [58]. Briefly, tissue was ground in liquid nitrogen with a mortar and pestle, and suspended in extraction buffer containing 100 mM Tris pH 7.0, 1% SDS, 10 mM NaF, 1 mM PMSF, 1 mM sodium ortho-vanadate, 1 mM β-glycerophosphate, 1X aprotinin, 1X leupeptin hemisulfate salt, and 1X pepstatin A. Protein concentration was determined by NanoDrop (Thermo Fisher Scientific, Wilmington, DE). Protein samples (100 μg) were separated on 10% SDS/PAGE gels and blotted to Immobilon-P nitrocellulose membranes (#IPVH00010, MilliporeSigma, Burlington, MA) according to standard methods.

The levels of P-eIF2α were detected using rabbit monoclonal Anti-EIF2S1 (phospho S51) antibody (#ab32157, Abcam, Cambridge, UK) diluted 1:5000 in 5% Bovine Serum Albumin (BSA), 1X TBS, 0.1% Tween, and anti-rabbit IgG HRP secondary antibody (#1706515, Bio-Rad, Hercules, CA) diluted 1:10000. Total eIF2α levels were detected using rabbit polyclonal anti-EIF2S1 antibody (#47508, Abcam, Cambridge, UK) diluted 1:5000, and anti-rabbit IgG HRP secondary antibody diluted 1:10000. FRQ protein was detected using mouse monoclonal anti-FRQ antibody (from clone 3G11-1B10-E2, developed in M. Brunner's lab) in 7.5% non-fat milk at 1:200 concentration and anti-mouse IgG-HRP (#1706516, Bio-Rad, Hercules, CA) secondary antibody diluted 1:10000.

Ribosome profiling: Ribosome profiling was carried out as previously described [144], but with important modifications. Briefly, about 1 g of mycelia samples were ground in a SPEX CertiPrep 6850 Freezer/Mill® (#6850, SPEX Sample Prep, Metuchen, NJ) with lysis buffer beads using a 10 min pre-cooling cycle, followed by three 2 min grinding cycles, with 1min re-cooling between each cycle. Ground samples were transferred to pre-chilled 50 mL polycarbonate centrifuge tubes and thaw on ice or in a fridge for approximately 30 min, and then centrifuged at 4°C for 15 min at 16,000 rpm using a JA-20 rotor. Approximately ~1 mL of supernatant was transferred into a pre-chilled 15 mL conical tube and quantified by measuring the A260 of the extract using a Varian Cary® 50 UV-Vis Spectrophotometer (Agilent Technologies, Santa Clara, CA). Fifty A260 units of extract were brought to a final volume of 300 µL with lysis buffer, which consisted of 20 mM Tris-Cl (pH 7.5), 150 mM NaCl, 5 mM $MgCl_2$, 1 mM DTT, 1% Triton X-100, 25 U/mL Turbo DNase (#AM2238, Thermo Fisher Scientific Inc., Waltham, MA), and 100 µg/mL cycloheximide; and treated with 1.875 µL of RNase I (#AM2294, Thermo Fisher Scientific Inc., Waltham, MA) for 45 min at RT with gentle mixing. The extract was transferred to a ice-chilled 3.5 mL, 13 X 51 mm polycarbonate ultracentrifuge tube, with 0.9 mL of a 1 M polysome sucrose cushion underlay added, and ribosomes were pelleted by centrifugation at 70,000 rpm at 4°C for 4 h. All subsequent steps up to step 46 in the published method were followed as described [144]. An rRNA depletion step was not performed, but instead after heat-inactivation of CircLigase (#CL4111K, Illumina (Epicentre), Madison, WI), 2.0 µL of GlycoBlue™ (#AM9515, Thermo Fisher Scientific Inc., Waltham, MA), 6.0 µL 5 M NaCl, 74 µL of DEPC water, and 150 µL of isopropanol were added to each tube and precipitated overnight at -80°C. The DNA was pelleted by centrifugation for 30 min at 20,000 g at 4°C and washed with 70% ethanol then air-dry for 10 min. The pellet was then resuspended in 5.0 µL of 10 mM Tris (pH 8.0). cDNA was synthesized using SuperScript™ III

Reverse Transcriptase (#18080044, Thermo Fisher, Waltham, MA), followed by barcode addition by PCR amplification using Phusion Hot Start High-Fidelity DNA Polymerase (#F540L, Thermo Fisher, Waltham, MA) as described [144]. Sequencing libraries were quantified and checked for quality on a 2100 Bioanalyzer using a DNA high sensitivity chip (Agilent, Santa Clara, CA) per the manufacturer's instructions. Sequencing was carried out on an Illumina HiSeq 3000 (Illumina, Inc., San Diego, CA).

RNA-seq: 0.1~0.2 g of frozen mycelia was homogenized using a bead beater for 1 min with 1 g of 180°C autoclaved zirconium beads, 550 µl of extraction buffer (100 mM Tris-HCl pH 7.5, 100 mM LiCl, 20 mM DTT), 800 µl of phenol: chloroform (pH 4.4), and 80 ul of 10% SDS in a 2-ml screw cap tube. The homogenate was mixed by end-to-end rotation at room temperature for 4 m and centrifuged at 16,000 ×*g* for 1 m at 4°C. The aqueous phase was extracted with 800 µl of phenol: chloroform (pH 4.4) and 800 µl of chloroform. Total RNA was precipitated in 65 µl of 3 M NaOAc and 1 ml of ethanol at –80°C for 30 m, followed by a 30-m 16,000 ×*g* centrifugation at 4°C. The pellet was washed twice with 70% ethanol, air dried briefly, and dissolved in 200 µl of DEPC-treated water. Total RNA was quantified using the Quant-iT^{TM} RiboGreen RNA assay kit (# R11490, Thermo Fisher, Waltham, MA), and diluted to 0.8 µg/µl for subsequent steps. Total RNA (100 µg) was purified using preequilibrated Oligo d(T)$_{25}$ Magnetic Beads (#S1419S, New England Biolabs, Ipswich, MA). The RNA was eluted from the magnetic beads in 50 µl of the elution buffer by 2-m incubation at 50°C as per the manufacturer. The eluted RNA was subsequently treated with Turbo DNA-*free*^{TM} kit (#AM1907, Ambion, Austin, TX), and Terminator^{TM} 5′-Phosphate-Dependent Exonuclease (#TER51020, Illumina (Epicentre), Madison, WI) as instructed by the manufacturer's protocols. The RNA was ethanol precipitated and

dissolved in 20 ul of DEPC-treated water, and quantified using the Quant-iT^{TM} RiboGreen RNA assay kit (# R11490, Thermo Fisher, Waltham, MA). Purified mRNA (8 ng) was used as the input to generate RNA-seq libraries using the SENSE Total RNA-seq Library Preparation Kit (#009, Lexogen, Vienna, Austria). Sequencing was carried out on an Illumina HiSeq 3000.

***Data analysis**:* Raw sequencing reads were processed based on a lab developed pipeline (**Figure 28**). Ribosome profiling (ribo-seq) reads were trimmed using Cutadapt [157] to remove the 3′ adapter of the reads (adapter sequence – CTGTAGGCACCATCAAT). Before alignment, ribo-seq and RNA-seq datasets were analyzed using FastQC [158] to check read length and quality. Adapter-trimmed ribo-seq reads were size-filtered to the 28-34 nt range using Trimmomatic [159]. Ribo-seq and RNA-seq reads were then aligned to the *N. crassa* genome FungiDB Release 38 using STAR [131], and were normalized to fragments per kilobase of exon model per million mapped reads (FPKM) values using Cufflinks [132]. To calculate the ribo-seq read coverage over the 5' UTR, 3' UTR, or CDS regions, the geneBody_coverage2.py program from the RSeQC package was used [160]. Ribosome footprint features such as read length distribution and sub-codon phasing were determined using NGS toolkit Plastid [135]. Differential translation efficiency (TE) analysis was performed using Xtail [142], and the TE values for DD16, DD20, DD24, DD28, DD32, DD36, DD40, DD44, and DD48 were calculated for two replicates, in relation to DD12. The TE and RNA-seq (FPKMs) time series were subjected to the Extended Circadian Harmonic Oscillation (ECHO) and JTK_CYCLE analyses built within the R-powered ECHO version 3.2 application [139, 161]. The TE time series was analyzed using the following ECHO settings: single replicate, smoothing function enabled, unexpressed genes excluded from the analysis at the default 70% threshold. The RNA-seq time series was analyzed using the following ECHO settings: two

unpaired replicates, smoothing function enabled, unexpressed genes excluded from the analysis at the default 70% threshold, and OE/RE cutoff of 1.25. Genes were considered rhythmic if they had Benjamini-Hochberg p-values <0.05, and oscillation types harmonic, damped or forced. Determination of the enriched functional categories (FunCat) was done using FungiFun version 2.2.8 [162], with a value of $p<0.05$ as a cutoff for significantly enriched terms. MEME 5.1.1 analysis [143] was used for *de novo* identification of enriched motifs in candidate genes. Ribo-seq and RNA-seq BAM files were visualized using the genome browser Integrative Genome Viewer (IGV) version 2.8.2 [163].

Sequence feature analysis: The distributions of sequence lengths were determined separately for the 5' UTR, CDS, and 3' UTR using sequence length information from FungiDB Release 46 [164]. Given that the two sample sets in comparison have unequal variances and unequal sample sizes, the Welch unequal variances *t*-test was adopted for statistical comparisons. The predicted uORFs in the *N. crassa* genome were determined using the computational algorithm RiboCode to identify genome-wide translated ORFs, including novel upstream ORFs using ribosome-profiling data [145].

Luciferase assays: $1X10^5$ conidia were inoculated into 96 well microtiter plates containing 150 µl of 1X Vogel's salts, 0.01% glucose, 0.03% arginine, 0.1 M quinic acid, 1.5% agar, and 25 µM firefly luciferin, pH 6. After inoculation of conidia ($1X10^5$ conidia), the microtiter plate was incubated at 30°C in LL for 24 h and transferred to DD 25°C to obtain bioluminescence recordings using EnVision Xcite Multilabel Reader, with recordings taken every 90 min for 6 days. Raw reads were normalized to the mean to graph the data.

Statistical analysis: Rhythmic data from western blots and luciferase assays was fit to a sine wave or a line as previously described [96]. Nonlinear regression to fit the rhythmic data to a sine wave (fitting period, phase, and amplitude) and a line (fitting slope and intercept), as well as Akaike's information criteria tests to compare the fit of each data set to the 2 equations, were carried out using the Prism software package. The p values reflect the probability that, for instance, the sine wave fits the data better than a straight line. Error bars in all graphs represent the SEM from independent experiments.

Table 5. Primers used in Chapter IV

Primer name	**Used for**	**Primer sequence (5'->3' orientation)**
idi-4 F1	IDI-4::LUC	GCCAAGGTGACAGTGGACGT
idi-4 R1	IDI-4::LUC	TGGCGTCCTCCCGCCCCTGCTTAGCCATGG
idi-4 F2	IDI-4::LUC	AGCAGGGGCGGGAGGACGCCAAGAACATCAA
idi-4 R2	IDI-4::LUC	CTCAGGTACGTTAATCAGACGGCGATCTTG
idi-4 F3	IDI-4::LUC	GTCTGATTAACGTACCTGAGAGATCTGTAT
idi-4 R3	IDI-4::LUC	ACCAATCTCGCTAATCTCA
idi-4 F4	Validation of endogenous integration of IDI-4::LUC	AAGACTATGCGGCCCAAATC
idi-4 R4	Validation of endogenous integration of IDI-4::LUC	GTTTCAGGACCGCCAAACCC
idi-4 F5	*Pidi-4::luc*	ATCGGCGGCCGCGACGTCTATTTCTTTGCCTCC
idi-4 R5	*Pidi-4::luc*	CGATACTAGTGGGCGGTTGTGGTGGTGCCG
idi-4$^{\Delta uORF}$ F1	IDI-4$^{\Delta uORF}$::LUC	ACTTGTTAAGCTACCAGCCC
idi-4$^{\Delta uORF}$ R1	IDI-4$^{\Delta uORF}$::LUC	GAGCAGTGTCAGGCCGGGAGAAGATTGTCT
idi-4$^{\Delta uORF}$ F2	IDI-4$^{\Delta uORF}$::LUC	CTCCCGGCCTGACACTGCTCCAACTTCAAC
idi-4$^{\Delta uORF}$ R2	IDI-4$^{\Delta uORF}$::LUC	TGGCAAGCATCTCCCTCAACA

Restriction sites in primer sequences are underlined

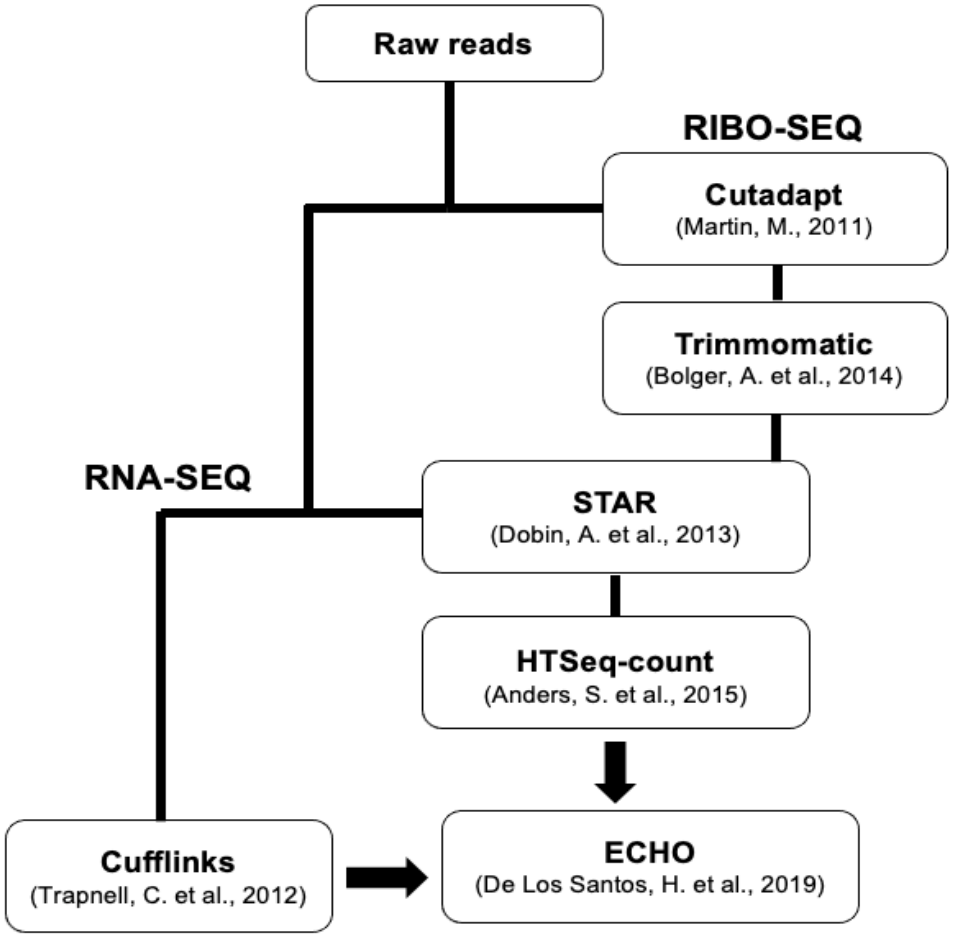

Figure 28. Read processing pipeline for the ribo-seq and RNA-seq datasets.

CHAPTER V

SUMMARY AND FUTURE DIRECTIONS

Summary

The research conducted in this study provides key insight into the mechanisms and extent of circadian clock control of protein production through the regulation of the activity of translation initiation factor eIF2α in *N. crassa*. There were three major outcomes of this research which led to the model shown in **Figure 29**. I first demonstrated that mutation of *N. crassa* PPP1 phosphatase leads to high and arrhythmic P-eIF2α levels, while maintaining core circadian oscillator function. Furthermore, I showed that PPP1 levels are clock-controlled, peaking in the early evening, and that rhythmic PPP1 levels are necessary for rhythmic P-eIF2α accumulation. Phosphatases require regulatory proteins to target them to their specific substrates. I discovered that eIF2γ, a component of the eIF2 complex, functions to recruit PPP1 to dephosphorylate eIF2α at night. Thus, in addition to the activity of CPC-3 kinase, circadian clock regulation of eIF2α activity requires dephosphorylation by PPP1 phosphatase at night.

Second, I examined potential regulation between the eIF2α kinase CPC-3 and the phosphatase PPP1. Importantly, deletion of CPC-3 had no effect on PPP1 protein rhythms, indicating that CPC-3 does not participate in clock control of PPP1 levels. PTM-MS indicated that high PPP1 levels reduced the levels of P-S876 and P-T879 of CPC-3. The functions of the phosphorylation of these two amino acids were examined by mutating the sites to the non-phosphorylatable amino acid A, and to the phosphomimic G. I found that while P-S876 activates CPC-3 kinase activity, it is not required for rhythmic accumulation of P-eIF2α. P-T879 was shown to be essential for CPC-3 activation, consistent the requirement of P-T887 in GCN2 [68]. However, its requirement for P-

eIF2α could not be tested given that P-eIF2α cannot be detected in strains with T879 mutations. It is also not known if PPP1 directly dephosphorylates P-S876 and/or P-T879 of CPC-3, or if regulation is indirect.

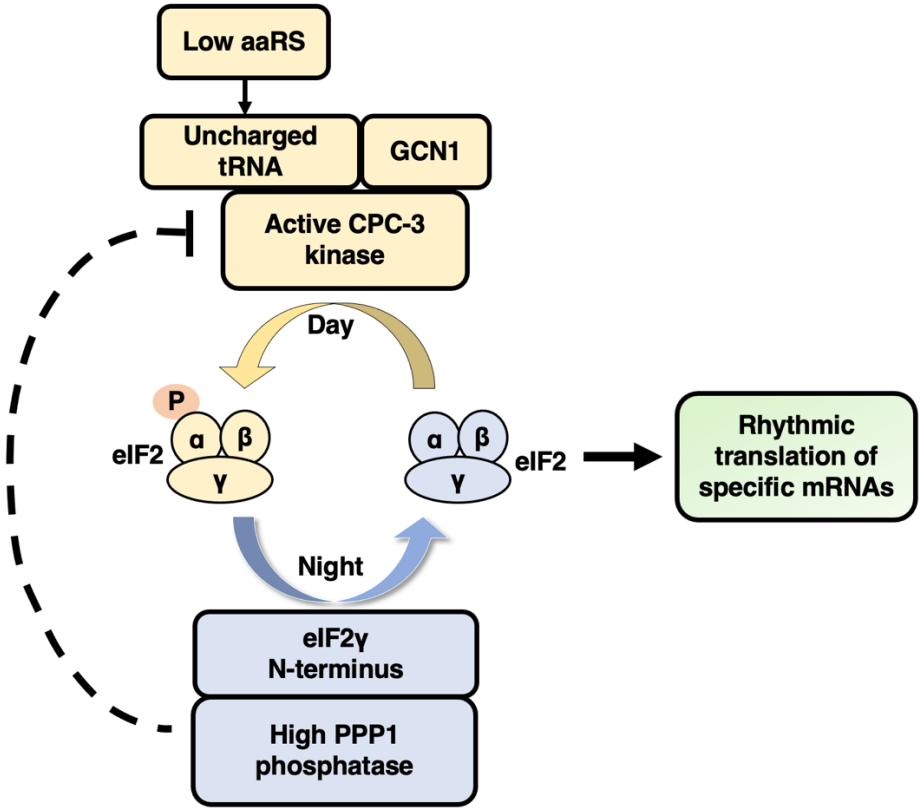

Figure 29. Model of the mechanisms of clock coordination of both the eIF2α kinase and the phosphatase to regulates day-night cycling of eIF2α activity and translation of specific mRNAs.

Lastly, I collaborated with Dr. Kathrina Castillo to examine the impact of rhythmic eIF2α activity on mRNA translation using ribosome profiling in parallel with RNA-seq in wild type and mutant strains that alter rhythmic P-eIF2α levels. We discovered that the *N. crassa* clock regulates the translation of 1328 mRNAs, of which 404 were translated arrhythmically in strains that lacked CPC-3 (Δ*cpc-3*) or had a constitutively active CPC-3 (*cpc-3*^{c}). The utility of our approach was validated by independently showing that the rhythmic translation of *idi-4* requires rhythmic P-

eIF2α levels. Taken together, these data revealed that rhythmic eIF2α activity targets specific mRNAs for rhythmic translation, rather than affecting the translation of all mRNAs.

Future directions

1. Do ribosomes function as a scaffold to recruit regulators of eIF2α to control rhythmic activation? In *S. cerevisiae*, GCN2 kinase activity requires association with ribosomes. Uncharged tRNAs are transferred from ribosomes to GCN2 by GCN1 and GCN20 to activate GCN2 [74-77, 101]. Ebi Preh in our lab discovered that CPC-3 similarly interacts with ribosomes in *N. crassa*. I also found that PPP1 associates with ribosomes in *N. crassa* (**Chapter II**), suggesting the possibility that eIF2γ recruits PPP1 to ribosomes, which may facilitate direct access to its substrate P-eIF2α. To test this hypothesis, we will examine if deleting the N-terminus extension of eIF2γ (*eIF2γ*$^{\Delta 2\text{-}62}$), which impacts the dephosphorylation of eIF2α *in vitro*, affects the association of PPP1 with ribosomes. If PPP1 no longer interacts with ribosomes in this strain, this would support the idea that eIF2γ recruits PPP1 to the ribosomes to dephosphorylate eIF2α. Furthermore, clock control of activity of CPC-3, eIF2γ and PPP1 may be facilitated by their rhythmic interaction with ribosomes, leading to rhythmic P-eIF2α levels. To test this hypothesis, we are examining if the interaction of these factors with ribosomes are rhythmic.

2. Does the rhythmic binding of uncharged tRNA to CPC-3 control its autokinase activity and phosphorylation of T879? Overexpression of PPP1 reduced the levels of CPC-3 P-S876 and P-T879, which activates CPC-3 kinase activity (**Chapter III**). The phosphorylation of T879 is essential for CPC-3 activity; however, since no P-eIF2α is detected in T879 mutants, we don't know if it is required for P-eIF2α rhythms. In yeast cells, the corresponding residue T887 of GCN2

is autophosphorylated to activate GCN2 in response to uncharged tRNA binding [68]. Previous studies in our lab showed that the levels of uncharged $tRNA^{Val}$ were rhythmic in WT cells, but were arrhythmic in the valyl-tRNA synthetase (ValRS) mutant *un-3*^{ts}. P-eIF2α rhythms were abolished in *un-3*^{ts} cells [66]. Taken together, these data support the idea that P-T879 levels in *N. crassa* may be circadian control through rhythmic binding of uncharged tRNA to CPC-3. Our quantitative PTM-MS data of samples harvested in the subjective night (DD24) and day (DD36) detected higher P-T879 levels at DD36 compared to DD24, supporting the idea that phosphorylation of T879 is clock-controlled. Thus, a possible mechanism to control rhythmic P-eIF2a levels is through rhythms in uncharged tRNA binding to CPC-3, leading to rhythmic P-T879 autophosphorylation and rhythmic CPC-3 activity. To test this model, we will first determine if P-T879 is under the clock control by generating an antibody that specifically recognizes P-T879, and examining if phosphorylation of T879 is rhythmic in WT cells and arrhythmic in Δ*frq* cells. Next, we could examine rhythms of P-T879 in *un-3*^{ts} mutant cells, which have arrhythmic uncharged $tRNA^{Val}$ and P-eIF2α levels. If the rhythms of P-T879 are lost in *un-3*^{ts} mutant cells, these data would support the proposed model that uncharged tRNA binding to CPC-3 controls rhythms in P-T879, which in turn, leads to rhythms in CPC-3 activity and P-eIF2α levels.

Rhythms in uncharged tRNA levels may be caused by rhythms in amino acid levels, tRNA abundance, and/or the process of charging tRNA with amino acid. While rhythms of 10 amino acids levels were detected in mouse SCN [165], free amino acid levels were shown to be arrhythmic in *N. crassa* under our standard growth conditions [66], suggesting that the mechanisms of clock regulation of uncharged tRNA rhythms may differ between *N. crassa* and mammals. To test if the expression of tRNAs is rhythmic, we can use RT-qPCR for each tRNA to test their levels

over a time course. To investigate other clock-controlled tRNA synthetases, in addition to ValRS, Kathrina Castillo and Emily Chapa in our lab are utilizing circadian RNA-seq, proteomic and/or ribosome profiling datasets to look for tRNA synthetases with clock-controlled mRNA and/or protein levels. Experiments are in progress to validate the expression rhythms of three candidates, Aspartyl-tRNA synthetase (NCU00915), phenylalanyl-tRNA synthetase (NCU01512) and glutaminyl-tRNA synthetase (NCU07926). Once we validate the rhythms in these tRNA synthetases, we will then examine if the corresponding uncharged tRNAs are rhythmic. Subsequently, if any of the other tRNAs have a circadian rhythm in charged versus uncharged tRNA levels, we will eliminate the rhythms of tRNA synthetases by controlling their expression levels, or by adding inhibitors, and then examine possible effects on rhythms in uncharged tRNAs and P-eIF2α levels. Moreover, there could be a shared regulatory mechanism to coordinate the rhythmic expression of the tRNA synthetases, such as through a clock-controlled transcription factor regulating the expression of multiple tRNA synthetases. Candidate clock-controlled transcription factors have been identified that bind to the promoters of several different tRNA synthetases, and these will be examined for their role in controlling tRNA synthetase mRNA rhythms.

3. Are specific sequence motifs and uORFs responsible for eIF2α-dependent rhythmic translation? Using ribosome profiling and RNA-seq, we discovered that rhythmic P-eIF2α levels control rhythmic translation of a specific subset of mRNAs, which we called cTICs, and these mRNAs are enriched in pathways related to mRNA processing, translation initiation, protein modification and some metabolic processes (**Chapter IV**). To understand why the cTIC transcripts are targeted for regulating by cycling P-eIF2α, we explored potential common *cis*-elements in these transcripts.

We discovered that specific sequence motifs and uORFs are enriched in cTICs, and are currently examining the potential function of these elements in rhythmic translation. Moreover, based on the similarity of an enriched sequence motif found in cTICs that targets mRNAs to processing bodies (P-bodies) [166], Dr. Kathrina Castillo is testing the idea that rhythmic P-eIF2α accumulation leads to rhythms in the formation of P-bodies and/or the pathways targeting mRNAs to P-bodies to control their rhythmic translation. Experiments are also in progress to test if deletion of P-body component encoding genes *lsm1* (NCU01601)*, lsm2* (NCU01930)*,* and *edc3* (NCU00427) impacts the rhythmic translation of *idi-4* mRNA.

4. Does clock control of P-eIF2α provide a mechanism to anticipate daily environmental stress? In addition to control by the circadian clock, phosphorylation of eIF2α is induced by acute stress, including amino acid deprivation [71, 167, 168], glucose starvation [169] and oxidative stress [170, 171]. As a result, most mRNAs are blocked for translation initiation, whereas mRNAs that encode proteins that help to overcome the stress are preferentially translated. Studies in mouse liver revealed that the formation of stress granules is clock-controlled and regulated by the ratio of P-eIF2α/total eIF2α [65]. Stress granules are membrane-less cytoplasmic structures, composed of primarily mRNAs with stalled initiation complexes, which appear in the cytosol when an organism is under stress. [172-176]. RNAs that are stalled for translation are stored in stress granules until the stress is removed and general translation resumes. Thus, clock control of P-eIF2α is predicted to provide a mechanism to anticipate daily environmental stress to enhance an organism's survival. To test this idea, *N. crassa* cells would be exposed to stress at different times of the day and assayed for significant differences in growth rate and/or survival. For example, hydrogen peroxide could be added to liquid cultures for an hour at different times in the circadian cycle to induce oxidative

stress, and then removed by washing the cultures, followed by assaying growth phenotypes. To determine if any growth defects are dependent on cycling P-eIF2α, the same experiments would be carried out in Δ*cpc-3*, *cpc-3*^{c} and *ppp1*^{RIP} cells that lack rhythms in P-eIF2α accumulation. In addition, our existing ribosome profiling data in *cpc-3*^{c} cells could be mined to identify genes involved in stress responses that have altered ribosome occupancy levels compared to WT cells. This is because in *cpc-3*^{c} cells, the levels P-eIF2α levels are at a level comparable to the levels observed following acute stress. These data may reveal new mechanisms for how cells respond to environmental and cellular stresses. Importantly, the inability of cells to respond to stress contributes to diseases, such as cancer and neurodegenerative diseases [177, 178]. These same diseases are also associated with a defective clock, supporting a critical role for the clock in anticipating daily stress to promote healthy living. Understanding the mechanistic links between the circadian clock and stress responses would likely support the development of time-of-day-specific therapy (chronotherapy) approaches to help reduce stress-associated disease.

5. Do rhythms in PPP1 levels control more than P-eIF2α levels? PPP1 is essential in *N. crassa*, indicating it plays a critical role in regulating various cellular functions. The catalytic subunit of the PPP1/GLC7 phosphatase combines with different regulatory subunits to form protein phosphatase 1 holoenzymes, which are predicted to hydrolyze the majority of Ser/Thr-linked phosphate ester bonds in eukaryotic cells [105, 179]. Consistent with this idea, substrates of GLC7 in yeast are involved in important cellular processes, including histone modification [180] [181], mitosis [182-185], meiosis [186], glycogen degradation and synthesis [187, 188], mRNA processing [189, 190], and actin dynamics [191, 192]. Considering that PPP1 levels are rhythmic in *N. crassa* cells, it is likely that this drives rhythms in the phosphorylation levels of key substrates

that control these biological processes. To uncover the different targets of PPP1, quantitative PTM-MS could be used to detect phosphorylated peptides in WT versus *ppp1*^{RIP} from cells harvested at the peak and trough of PPP1 levels. The expectation is that there will be target proteins with rhythmic phosphorylation levels in WT that are reduced or abolished rhythms in *ppp1*^{RIP} samples. These data may reveal rhythmic protein phosphorylation in key signaling proteins that are rhythmic through clock regulation of PPP1, and provide a better understanding of the mechanisms of clock control of molecular and cellular activity.

6. Summary: Accumulating evidence supports that rhythms in mRNA levels are not a strong predictor of protein rhythms and activity; however, circadian clock control of mRNA translation is poorly understood in any system. Our study has led to novel insights into temporal regulation of translation by the circadian clock through the rhythmic accumulation of P-eIF2α. This posttranslational mechanism appears to be conserved, as the mammalian clock also controls rhythms in the levels of P-eIF2α in the SCN [64, 65]. Thus, our studies in *N. crassa* will likely provide critical information on the mechanisms of the clock regulation of mRNA translation in higher eukaryotes. Phosphorylation of eIF2α is a key regulation step in translation rate, and mis-regulation of eIF2α activity is associated with many types of disease, including neuronal degeneration in Alzheimer's disease [121, 122], retinal degeneration [123] and breast cancer [124]. Research to uncover the basic mechanisms of clock regulation of translation, such as my studies on clock control of the conserved translation initiation factor eIF2α in *N. crassa*, together with circadian transcription regulation, will provide an in depth understanding of clock regulation of rhythmic gene expression, critical to an organisms physical and mental health.

REFERENCES

1. Panda, S., J.B. Hogenesch, and S.A. Kay, *Circadian rhythms from flies to human.* Nature, 2002. **417**(6886): p. 329-35.

2. Kondo, T., et al., *Circadian clock mutants of cyanobacteria.* Science, 1994. **266**(5188): p. 1233-6.

3. Dunlap, J.C. and J.J. Loros, *The neurospora circadian system.* J Biol Rhythms, 2004. **19**(5): p. 414-24.

4. Pittendrigh, C.S., V.G.Bruce, N.S.Rosensweig, M.L.Rubin, *Growth Patterns in Neurospora: A Biological Clock in Neurospora.* Nature, 1959. **184**: p. 169-170.

5. Czeisler, C.A., et al., *Stability, precision, and near-24-hour period of the human circadian pacemaker.* Science, 1999. **284**(5423): p. 2177-2181.

6. Bell-Pedersen, D., et al., *Circadian rhythms from multiple oscillators: lessons from diverse organisms.* Nat Rev Genet, 2005. **6**(7): p. 544-56.

7. Dunlap, J.C., *Molecular bases for circadian clocks.* Cell, 1999. **96**(2): p. 271-90.

8. Hall, J.C., *Genetics of biological rhythms in drosophila.* Adv Genet, 1998. **38**: p. 135-84.

9. Young, M.W., *The molecular control of circadian behavioral rhythms and their entrainment in Drosophila.* Annu Rev Biochem, 1998. **67**: p. 135-52.

10. Partch, C.L., C.B. Green, and J.S. Takahashi, *Molecular architecture of the mammalian circadian clock.* Trends Cell Biol, 2014. **24**(2): p. 90-9.

11. Nohales, M.A. and S.A. Kay, *Molecular mechanisms at the core of the plant circadian oscillator.* Nature Structural & Molecular Biology, 2016. **23**(12): p. 1061-1069.

12. Beadle, G.W. and E.L. Tatum, *Genetic Control of Biochemical Reactions in Neurospora.* Proc Natl Acad Sci U S A, 1941. **27**(11): p. 499-506.

13. Borkovich, K.A., et al., *Lessons from the genome sequence of Neurospora crassa: tracing the path from genomic blueprint to multicellular organism.* Microbiol Mol Biol Rev, 2004. **68**(1): p. 1-108.

14. Galagan, J.E., et al., *The genome sequence of the filamentous fungus Neurospora crassa.* Nature, 2003. **422**(6934): p. 859-68.

15. Colot, H.V., et al., *A high-throughput gene knockout procedure for Neurospora reveals functions for multiple transcription factors.* Proc Natl Acad Sci U S A, 2006. **103**(27): p. 10352-10357.

16. Beadle, G.W. and V.L. Coonradt, *Heterocaryosis in Neurospora Crassa.* Genetics, 1944. **29**(3): p. 291-308.

17. Harris, S.D., *Septum formation in Aspergillus nidulans.* Curr Opin Microbiol, 2001. **4**(6): p. 736-9.

18. Springer, M.L. and C. Yanofsky, *A morphological and genetic analysis of conidiophore development in Neurospora crassa.* Genes Dev, 1989. **3**(4): p. 559-71.

19. Nelson, M.A., *Mating systems in ascomycetes: a romp in the sac.* Trends Genet, 1996. **12**(2): p. 69-74.

20. Bistis, G.N., *Chemotropic Interactions between Trichogynes and Conidia of Opposite Mating-Type in Neurospora crassa.* Mycologia, 1981. **73**(5): p. 959-975.

21. Bobrowicz, P., et al., *The Neurospora crassa pheromone precursor genes are regulated by the mating type locus and the circadian clock.* Mol Microbiol, 2002. **45**(3): p. 795-804.

22. Raju, N.B., *Genetic control of the sexual cycle in Neurospora.* Mycological Research, 1992. **96**(4): p. 241-262.

23. Feldman, J.F. and M.N. Hoyle, *Isolation of circadian clock mutants of Neurospora crassa.* Genetics, 1973. **75**(4): p. 605-13.

24. Feldman, J.F. and M.N. Hoyle, *A Direct Comparison between Circadian and Noncircadian Rhythms in Neurospora crassa.* Plant Physiol, 1974. **53**(6): p. 928-30.

25. Crosthwaite, S.K., J.C. Dunlap, and J.J. Loros, *Neurospora wc-1 and wc-2: transcription, photoresponses, and the origins of circadian rhythmicity.* Science, 1997. **276**(5313): p. 763-9.

26. Lee, K., J.C. Dunlap, and J.J. Loros, *Roles for WHITE COLLAR-1 in circadian and general photoperception in Neurospora crassa.* Genetics, 2003. **163**(1): p. 103-14.

27. Smith, K.M., et al., *Transcription factors in light and circadian clock signaling networks revealed by genomewide mapping of direct targets for neurospora white collar complex.* Eukaryot Cell, 2010. **9**(10): p. 1549-56.

28. Cheng, P., et al., *Regulation of the Neurospora circadian clock by an RNA helicase.* Genes Dev, 2005. **19**(2): p. 234-41.

29. Froehlich, A.C., J.J. Loros, and J.C. Dunlap, *Rhythmic binding of a WHITE COLLAR-containing complex to the frequency promoter is inhibited by FREQUENCY.* Proc Natl Acad Sci U S A, 2003. **100**(10): p. 5914-9.

30. Huang, G., et al., *Protein kinase A and casein kinases mediate sequential phosphorylation events in the circadian negative feedback loop.* Genes Dev, 2007. **21**(24): p. 3283-95.

31. Cha, J., et al., *Control of WHITE COLLAR localization by phosphorylation is a critical step in the circadian negative feedback process.* Embo j, 2008. **27**(24): p. 3246-55.

32. Ballario, P., et al., *White collar-1, a central regulator of blue light responses in Neurospora, is a zinc finger protein.* EMBO J, 1996. **15**(7): p. 1650-7.

33. Linden, H., P. Ballario, and G. Macino, *Blue light regulation in Neurospora crassa.* Fungal Genet Biol, 1997. **22**(3): p. 141-50.

34. Cheng, P., et al., *WHITE COLLAR-1, a multifunctional neurospora protein involved in the circadian feedback loops, light sensing, and transcription repression of wc-2.* J Biol Chem, 2003. **278**(6): p. 3801-8.

35. Russo, V.E., *Blue light induces circadian rhythms in the bd mutant of Neurospora: double mutants bd,wc-1 and bd,wc-2 are blind.* J Photochem Photobiol B, 1988. **2**(1): p. 59-65.

36. Roenneberg, T. and M. Merrow, *The Circadian Clock and Human Health.* Curr Biol, 2016. **26**(10): p. R432-43.

37. Zhang, R., et al., *A circadian gene expression atlas in mammals: implications for biology and medicine.* Proc Natl Acad Sci U S A, 2014. **111**(45): p. 16219-24.

38. Larson, A.M., et al., *Acetaminophen-induced acute liver failure: results of a United States multicenter, prospective study.* Hepatology, 2005. **42**(6): p. 1364-72.

39. Hinson, J.A., D.W. Roberts, and L.P. James, *Mechanisms of acetaminophen-induced liver necrosis.* Handb Exp Pharmacol, 2010(196): p. 369-405.

40. Johnson, B.P., et al., *Hepatocyte circadian clock controls acetaminophen bioactivation through NADPH-cytochrome P450 oxidoreductase.* Proc Natl Acad Sci U S A, 2014. **111**(52): p. 18757-62.

41. Koike, N., et al., *Transcriptional architecture and chromatin landscape of the core circadian clock in mammals.* Science, 2012. **338**(6105): p. 349-54.

42. Menet, J.S., et al., *Nascent-Seq reveals novel features of mouse circadian transcriptional regulation.* Elife, 2012. **1**: p. e00011.

43. Duffield, G.E., *DNA microarray analyses of circadian timing: the genomic basis of biological time.* J Neuroendocrinol, 2003. **15**(10): p. 991-1002.

44. Nagel, D.H. and S.A. Kay, *Complexity in the wiring and regulation of plant circadian networks.* Curr Biol, 2012. **22**(16): p. R648-57.

45. Hurley, J.M., et al., *Analysis of clock-regulated genes in Neurospora reveals widespread posttranscriptional control of metabolic potential.* Proc Natl Acad Sci U S A, 2014. **111**(48): p. 16995-7002.

46. Vitalini, M.W., et al., *The rhythms of life: circadian output pathways in Neurospora.* J Biol Rhythms, 2006. **21**(6): p. 432-44.

47. Vollmers, C., et al., *Circadian oscillations of protein-coding and regulatory RNAs in a highly dynamic mammalian liver epigenome.* Cell Metab, 2012. **16**(6): p. 833-45.

48. Robles, M.S., J. Cox, and M. Mann, *In-vivo quantitative proteomics reveals a key contribution of post-transcriptional mechanisms to the circadian regulation of liver metabolism.* PLoS Genet, 2014. **10**(1): p. e1004047.

49. Mauvoisin, D., et al., *Circadian clock-dependent and -independent rhythmic proteomes implement distinct diurnal functions in mouse liver.* Proc Natl Acad Sci U S A, 2014. **111**(1): p. 167-72.

50. Reddy, A.B., et al., *Circadian orchestration of the hepatic proteome.* Curr Biol, 2006. **16**(11): p. 1107-15.

51. Fustin, J.M., et al., *RNA-methylation-dependent RNA processing controls the speed of the circadian clock.* Cell, 2013. **155**(4): p. 793-806.

52. Belanger, V., N. Picard, and N. Cermakian, *The circadian regulation of Presenilin-2 gene expression.* Chronobiol Int, 2006. **23**(4): p. 747-66.

53. Baggs, J.E. and C.B. Green, *Nocturnin, a deadenylase in Xenopus laevis retina: a mechanism for posttranscriptional control of circadian-related mRNA.* Curr Biol, 2003. **13**(3): p. 189-98.

54. Lipton, J.O., et al., *The Circadian Protein BMAL1 Regulates Translation in Response to S6K1-Mediated Phosphorylation.* Cell, 2015. **161**(5): p. 1138-1151.

55. Hurley, J.M., et al., *Circadian Proteomic Analysis Uncovers Mechanisms of Post-Transcriptional Regulation in Metabolic Pathways.* Cell Syst, 2018. **7**(6): p. 613-626 e5.

56. Cao, R., et al., *Light-regulated translational control of circadian behavior by eIF4E phosphorylation.* Nat Neurosci, 2015. **18**(6): p. 855-62.

57. Jouffe, C., et al., *The circadian clock coordinates ribosome biogenesis.* PLoS Biol, 2013. **11**(1): p. e1001455.

58. Caster, S.Z., et al., *Circadian clock regulation of mRNA translation through eukaryotic elongation factor eEF-2.* Proc Natl Acad Sci U S A, 2016. **113**(34): p. 9605-10.

59. Hinnebusch, A.G. and J.R. Lorsch, *The mechanism of eukaryotic translation initiation: new insights and challenges.* Cold Spring Harb Perspect Biol, 2012. **4**(10).

60. Sonenberg, N. and A.G. Hinnebusch, *Regulation of translation initiation in eukaryotes: mechanisms and biological targets.* Cell, 2009. **136**(4): p. 731-45.

61. Wei, J., et al., *The stringency of start codon selection in the filamentous fungus Neurospora crassa.* J Biol Chem, 2013. **288**(13): p. 9549-62.

62. Hinnebusch, A.G., *Structural Insights into the Mechanism of Scanning and Start Codon Recognition in Eukaryotic Translation Initiation.* Trends in Biochemical Sciences, 2017. **42**(8): p. 589-611.

63. Dever, T.E., et al., *Phosphorylation of initiation factor 2 alpha by protein kinase GCN2 mediates gene-specific translational control of GCN4 in yeast.* Cell, 1992. **68**(3): p. 585-96.

64. Pathak, S.S., et al., *The eIF2alpha Kinase GCN2 Modulates Period and Rhythmicity of the Circadian Clock by Translational Control of Atf4.* Neuron, 2019. **104**(4): p. 724-735 e6.

65. Wang, R., et al., *Circadian control of stress granules by oscillating EIF2alpha.* Cell Death Dis, 2019. **10**(3): p. 215.

66. Karki, S., et al., *Circadian clock control of eIF2alpha phosphorylation is necessary for rhythmic translation initiation.* Proc Natl Acad Sci U S A, 2020.

67. Dong, J., et al., *Uncharged tRNA activates GCN2 by displacing the protein kinase moiety from a bipartite tRNA-binding domain.* Mol Cell, 2000. **6**(2): p. 269-79.

68. Romano, P.R., et al., *Autophosphorylation in the activation loop is required for full kinase activity in vivo of human and yeast eukaryotic initiation factor 2alpha kinases PKR and GCN2.* Mol Cell Biol, 1998. **18**(4): p. 2282-97.

69. Qiu, H., et al., *Mutations that bypass tRNA binding activate the intrinsically defective kinase domain in GCN2.* Genes Dev, 2002. **16**(10): p. 1271-80.

70. Dong J, Q.H., Garcia-Barrio M, Anderson J, Hinnebusch AG, *Uncharged tRNA Activates GCN2 by Displacing the Protein Kinase Moiety from a Bipartite tRNA-Binding Domain.* Molecular cell, 2000. **6**(2): p. 269-79.

71. Wek SA, Z.S., Wek RC, *The histidyl-tRNA synthetase-related sequence in the eIF-2 alpha protein kinase GCN2 interacts with tRNA and is required for activation in response to starvation for different amino acids.* Mol Cell Biol, 1995. **15**(8): p. 4497-506.

72. Narasimhan, J., K.A. Staschke, and R.C. Wek, *Dimerization is required for activation of eIF2 kinase Gcn2 in response to diverse environmental stress conditions.* J Biol Chem, 2004. **279**(22): p. 22820-32.

73. Padyana, A.K., et al., *Structural basis for autoinhibition and mutational activation of eukaryotic initiation factor 2alpha protein kinase GCN2.* J Biol Chem, 2005. **280**(32): p. 29289-99.

74. Garcia-Barrio, M., et al., *Association of GCN1-GCN20 regulatory complex with the N-terminus of eIF2alpha kinase GCN2 is required for GCN2 activation.* EMBO J, 2000. **19**(8): p. 1887-99.

75. Marton, M.J., D. Crouch, and A.G. Hinnebusch, *GCN1, a translational activator of GCN4 in Saccharomyces cerevisiae, is required for phosphorylation of eukaryotic translation initiation factor 2 by protein kinase GCN2.* Mol Cell Biol, 1993. **13**(6): p. 3541-56.

76. Sattlegger, E. and A.G. Hinnebusch, *Separate domains in GCN1 for binding protein kinase GCN2 and ribosomes are required for GCN2 activation in amino acid-starved cells.* Embo j, 2000. **19**(23): p. 6622-33.

77. Vazquez de Aldana CR1, M.M., Hinnebusch AG., *GCN20, a novel ATP binding cassette protein, and GCN1 reside in a complex that mediates activation of the eIF-2 alpha kinase GCN2 in amino acid-starved cells.* EMBO J, 1995. **14**(13): p. 3184-99.

78. Garcia-Barrio, M., et al., *Serine 577 is phosphorylated and negatively affects the tRNA binding and eIF2alpha kinase activities of GCN2.* J Biol Chem, 2002. **277**(34): p. 30675-83.

79. Cherkasova, V.A. and A.G. Hinnebusch, *Translational control by TOR and TAP42 through dephosphorylation of eIF2alpha kinase GCN2.* Genes Dev, 2003. **17**(7): p. 859-72.

80. Pao, L.I., et al., *Nonreceptor protein-tyrosine phosphatases in immune cell signaling.* Annu Rev Immunol, 2007. **25**: p. 473-523.

81. Shi, Y., *Serine/threonine phosphatases: mechanism through structure.* Cell, 2009. **139**(3): p. 468-84.

82. Sanvoisin, J. and D. Gani, *Protein phosphatase 1 catalyses the direct hydrolytic cleavage of phosphate monoester in a ternary complex mechanism.* Bioorg Med Chem Lett, 2001. **11**(4): p. 471-4.

83. Williams, N.H., *Models for biological phosphoryl transfer.* Biochim Biophys Acta, 2004. **1697**(1-2): p. 279-87.

84. McConnell, J.L. and B.E. Wadzinski, *Targeting protein serine/threonine phosphatases for drug development.* Mol Pharmacol, 2009. **75**(6): p. 1249-61.

85. Stark, M.J., *Yeast protein serine/threonine phosphatases: multiple roles and diverse regulation.* Yeast, 1996. **12**(16): p. 1647-75.

86. Breitkreutz, A., et al., *A global protein kinase and phosphatase interaction network in yeast.* Science, 2010. **328**(5981): p. 1043-6.

87. Park, G., et al., *Global analysis of serine-threonine protein kinase genes in Neurospora crassa.* Eukaryot Cell, 2011. **10**(11): p. 1553-64.

88. Ghosh, A., et al., *Global analysis of serine/threonine and tyrosine protein phosphatase catalytic subunit genes in Neurospora crassa reveals interplay between phosphatases and the p38 mitogen-activated protein kinase.* G3 (Bethesda), 2014. **4**(2): p. 349-65.

89. Wek, R.C., et al., *Truncated protein phosphatase GLC7 restores translational activation of GCN4 expression in yeast mutants defective for the eIF-2 alpha kinase GCN2.* Mol Cell Biol, 1992. **12**(12): p. 5700-10.

90. Connor, J.H., et al., *Growth arrest and DNA damage-inducible protein GADD34 assembles a novel signaling complex containing protein phosphatase 1 and inhibitor 1.* Mol Cell Biol, 2001. **21**(20): p. 6841-50.

91. Cohen, P.T., *Protein phosphatase 1--targeted in many directions.* J Cell Sci, 2002. **115**(Pt 2): p. 241-56.

92. Harding, H.P., et al., *Ppp1r15 gene knockout reveals an essential role for translation initiation factor 2 alpha (eIF2alpha) dephosphorylation in mammalian development.* Proc Natl Acad Sci U S A, 2009. **106**(6): p. 1832-7.

93. Brush, M.H., D.C. Weiser, and S. Shenolikar, *Growth arrest and DNA damage-inducible protein GADD34 targets protein phosphatase 1 alpha to the endoplasmic reticulum and promotes dephosphorylation of the alpha subunit of eukaryotic translation initiation factor 2.* Mol Cell Biol, 2003. **23**(4): p. 1292-303.

94. Rojas, M., A.C. Gingras, and T.E. Dever, *Protein phosphatase PP1/GLC7 interaction domain in yeast eIF2gamma bypasses targeting subunit requirement for eIF2alpha dephosphorylation.* Proc Natl Acad Sci U S A, 2014. **111**(14): p. E1344-53.

95. Yang, Y., et al., *Distinct roles for PP1 and PP2A in the Neurospora circadian clock.* Genes Dev, 2004. **18**(3): p. 255-60.

96. Lamb, T.M., et al., *Direct transcriptional control of a p38 MAPK pathway by the circadian clock in Neurospora crassa.* PLoS One, 2011. **6**(11): p. e27149.

97. Goldsmith, C.S., et al., *Inhibition of p38 MAPK activity leads to cell type-specific effects on the molecular circadian clock and time-dependent reduction of glioma cell invasiveness.* BMC Cancer, 2018. **18**(1): p. 43.

98. Hogenesch, J.B., *It's all in a day's work: Regulation of DNA excision repair by the circadian clock.* Proc Natl Acad Sci U S A, 2009. **106**(8): p. 2481-2.

99. Damulewicz, M., et al., *Daily Regulation of Phototransduction, Circadian Clock, DNA Repair, and Immune Gene Expression by Heme Oxygenase in the Retina of Drosophila.* Genes (Basel), 2018. **10**(1).

100. Lamb, T.M., J. Vickery, and D. Bell-Pedersen, *Regulation of gene expression in Neurospora crassa with a copper responsive promoter.* G3 (Bethesda), 2013. **3**(12): p. 2273-80.

101. Ramirez, M., R.C. Wek, and A.G. Hinnebusch, *Ribosome association of GCN2 protein kinase, a translational activator of the GCN4 gene of Saccharomyces cerevisiae.* Mol Cell Biol, 1991. **11**(6): p. 3027-36.

102. Cherkasova, V., H. Qiu, and A.G. Hinnebusch, *Snf1 promotes phosphorylation of the alpha subunit of eukaryotic translation initiation factor 2 by activating Gcn2 and inhibiting phosphatases Glc7 and Sit4.* Mol Cell Biol, 2010. **30**(12): p. 2862-73.

103. Calafi, C., et al., *Overexpression of budding yeast protein phosphatase Ppz1 impairs translation.* Biochim Biophys Acta Mol Cell Res, 2020. **1867**(8): p. 118727.

104. Velazquez, D., et al., *Yeast Ppz1 protein phosphatase toxicity involves the alteration of multiple cellular targets.* Sci Rep, 2020. **10**(1): p. 15613.

105. Heroes, E., et al., *The PP1 binding code: a molecular-lego strategy that governs specificity.* FEBS J, 2013. **280**(2): p. 584-95.

106. Cannon, J.F., *Function of protein phosphatase-1, Glc7, in Saccharomyces cerevisiae.* Adv Appl Microbiol, 2010. **73**: p. 27-59.

107. Wakula, P., et al., *Degeneracy and function of the ubiquitous RVXF motif that mediates binding to protein phosphatase-1.* J Biol Chem, 2003. **278**(21): p. 18817-23.

108. Erickson, F.L., et al., *Functional analysis of homologs of translation initiation factor 2gamma in yeast.* Mol Gen Genet, 1997. **253**(6): p. 711-9.

109. Jackson, R.J., C.U. Hellen, and T.V. Pestova, *The mechanism of eukaryotic translation initiation and principles of its regulation.* Nat Rev Mol Cell Biol, 2010. **11**(2): p. 113-27.

110. Davis, R.H. and F.J. de Serres, *Genetic and microbiological research techniques for Neurospora crassa.* Methods in Enzymology, 1970. **17A**: p. 79-143.

111. Wu, C., et al., *Genome-wide characterization of light-regulated genes in Neurospora crassa.* G3 (Bethesda), 2014. **4**(9): p. 1731-45.

112. Sachs, M.S. and C. Yanofsky, *Developmental expression of genes involved in conidiation and amino acid biosynthesis in Neurospora crassa.* Dev Biol, 1991. **148**(1): p. 117-28.

113. Bennett, L.D., et al., *Circadian activation of the mitogen-activated protein kinase MAK-1 facilitates rhythms in clock-controlled genes in Neurospora crassa.* Eukaryot Cell, 2013. **12**(1): p. 59-69.

114. Ebbole, D.J., and Sachs, M.S., *A rapid and simple method for isolation of Neurospora crassa homokaryons using microconidia.*, in *Fungal Genetic Newsletter*. 1990. p. 17-18.

115. Beasley, A., et al., *A ras-1bd Mauriceville strain for mapping mutations in Oak Ridge ras-1bdstrains.* Fungal Genetics Reports, 2006. **53**.

116. Larrondo, L.F., J.J. Loros, and J.C. Dunlap, *High-resolution spatiotemporal analysis of gene expression in real time: in vivo analysis of circadian rhythms in Neurospora crassa using a FREQUENCY-luciferase translational reporter.* Fungal Genet Biol, 2012. **49**(9): p. 681-3.

117. Gooch, V.D., et al., *Fully codon-optimized luciferase uncovers novel temperature characteristics of the Neurospora clock.* Eukaryot Cell, 2008. **7**(1): p. 28-37.

118. Schneider, C.A., W.S. Rasband, and K.W. Eliceiri, *NIH Image to ImageJ: 25 years of image analysis.* Nat Methods, 2012. **9**(7): p. 671-5.

119. Liu, H. and J.H. Naismith, *A simple and efficient expression and purification system using two newly constructed vectors.* Protein Expr Purif, 2009. **63**(2): p. 102-11.

120. Zielinski, T., et al., *Strengths and limitations of period estimation methods for circadian data.* PLoS One, 2014. **9**(5): p. e96462.

121. Chang, R.C., et al., *Phosphorylation of eukaryotic initiation factor-2alpha (eIF2alpha) is associated with neuronal degeneration in Alzheimer's disease.* Neuroreport, 2002. **13**(18): p. 2429-32.

122. Ma, T., et al., *Suppression of eIF2alpha kinases alleviates Alzheimer's disease-related plasticity and memory deficits.* Nat Neurosci, 2013. **16**(9): p. 1299-305.

123. Starr, C.R. and M.S. Gorbatyuk, *Delineating the role of eIF2alpha in retinal degeneration.* Cell Death Dis, 2019. **10**(6): p. 409.

124. Guo, L., et al., *Phosphorylated eIF2alpha predicts disease-free survival in triple-negative breast cancer patients.* Sci Rep, 2017. **7**: p. 44674.

125. Sharma, V.K., *Adaptive significance of circadian clocks.* Chronobiol Int, 2003. **20**(6): p. 901-19.

126. Vazquez de Aldana, C.R., et al., *Multicopy tRNA genes functionally suppress mutations in yeast eIF-2 alpha kinase GCN2: evidence for separate pathways coupling GCN4 expression to unchanged tRNA.* Molecular and Cellular Biology, 1994. **14**(12): p. 7920.

127. Arndt, K. and G.R. Fink, *GCN4 protein, a positive transcription factor in yeast, binds general control promoters at all 5' TGACTC 3' sequences.* Proc Natl Acad Sci U S A, 1986. **83**(22): p. 8516-20.

128. Hope, I.A. and K. Struhl, *GCN4 protein, synthesized in vitro, binds HIS3 regulatory sequences: implications for general control of amino acid biosynthetic genes in yeast.* Cell, 1985. **43**(1): p. 177-88.

129. Lu, P.D., H.P. Harding, and D. Ron, *Translation reinitiation at alternative open reading frames regulates gene expression in an integrated stress response.* J Cell Biol, 2004. **167**(1): p. 27-33.

130. Ivanov, I.P., et al., *Translation Initiation from Conserved Non-AUG Codons Provides Additional Layers of Regulation and Coding Capacity.* mBio, 2017. **8**(3): p. e00844-17.

131. Dobin, A., et al., *STAR: ultrafast universal RNA-seq aligner.* Bioinformatics, 2013. **29**(1): p. 15-21.

132. Trapnell, C., et al., *Differential gene and transcript expression analysis of RNA-seq experiments with TopHat and Cufflinks.* Nat Protoc, 2012. **7**(3): p. 562-78.

133. Anders, S., P.T. Pyl, and W. Huber, *HTSeq--a Python framework to work with high-throughput sequencing data.* Bioinformatics (Oxford, England), 2015. **31**(2): p. 166-169.

134. Love, M.I., W. Huber, and S. Anders, *Moderated estimation of fold change and dispersion for RNA-seq data with DESeq2.* Genome Biology, 2014. **15**(12): p. 550.

135. Dunn, J.G. and J.S. Weissman, *Plastid: nucleotide-resolution analysis of next-generation sequencing and genomics data.* BMC Genomics, 2016. **17**(1): p. 958.

136. Brar, G.A. and J.S. Weissman, *Ribosome profiling reveals the what, when, where and how of protein synthesis.* Nat Rev Mol Cell Biol, 2015. **16**(11): p. 651-64.

137. Garceau, N.Y., et al., *Alternative initiation of translation and time-specific phosphorylation yield multiple forms of the essential clock protein FREQUENCY.* Cell, 1997. **89**(3): p. 469-76.

138. Lee, K., J.J. Loros, and J.C. Dunlap, *Interconnected feedback loops in the Neurospora circadian system.* Science, 2000. **289**(5476): p. 107-10.

139. De Los Santos, H., et al., *ECHO: an Application for Detection and Analysis of Oscillators Identifies Metabolic Regulation on Genome-Wide Circadian Output.* Bioinformatics, 2019.

140. Tian, C., J. Li, and N.L. Glass, *Exploring the bZIP transcription factor regulatory network in Neurospora crassa.* Microbiology (Reading), 2011. **157**(Pt 3): p. 747-759.

141. Dementhon, K., S.J. Saupe, and C. Clave, *Characterization of IDI-4, a bZIP transcription factor inducing autophagy and cell death in the fungus Podospora anserina.* Mol Microbiol, 2004. **53**(6): p. 1625-40.

142. Xiao, Z., et al., *Genome-wide assessment of differential translations with ribosome profiling data.* Nat Commun, 2016. **7**: p. 11194.

143. Bailey, T.L., et al., *MEME SUITE: tools for motif discovery and searching.* Nucleic Acids Res, 2009. **37**(Web Server issue): p. W202-8.

144. Ingolia, N.T., et al., *The ribosome profiling strategy for monitoring translation in vivo by deep sequencing of ribosome-protected mRNA fragments.* Nat Protoc, 2012. **7**(8): p. 1534-50.

145. Xiao, Z., et al., *De novo annotation and characterization of the translatome with ribosome profiling data.* Nucleic Acids Res, 2018. **46**(10): p. e61.

146. Clemens, M.J., *Initiation factor eIF2 alpha phosphorylation in stress responses and apoptosis.* Prog Mol Subcell Biol, 2001. **27**: p. 57-89.

147. Sattlegger, E., A.G. Hinnebusch, and I.B. Barthelmess, *cpc-3, the Neurospora crassa homologue of yeast GCN2, encodes a polypeptide with juxtaposed eIF2alpha kinase and histidyl-tRNA synthetase-related domains required for general amino acid control.* J Biol Chem, 1998. **273**(32): p. 20404-16.

148. Castilho, B.A., et al., *Keeping the eIF2 alpha kinase Gcn2 in check.* Biochim Biophys Acta, 2014. **1843**(9): p. 1948-68.

149. Wu, C.C., et al., *Ribosome Collisions Trigger General Stress Responses to Regulate Cell Fate.* Cell, 2020. **182**(2): p. 404-416 e14.

150. Haimov, O., et al., *Efficient and Accurate Translation Initiation Directed by TISU Involves RPS3 and RPS10e Binding and Differential Eukaryotic Initiation Factor 1A Regulation.* Mol Cell Biol, 2017. **37**(15).

151. Meyuhas, O., *Synthesis of the translational apparatus is regulated at the translational level.* Eur J Biochem, 2000. **267**(21): p. 6321-30.

152. Luo, Y., Z. Na, and S.A. Slavoff, *P-Bodies: Composition, Properties, and Functions.* Biochemistry, 2018. **57**(17): p. 2424-2431.

153. Eulalio, A., et al., *P-body formation is a consequence, not the cause, of RNA-mediated gene silencing.* Mol Cell Biol, 2007. **27**(11): p. 3970-81.

154. Decker, C.J., D. Teixeira, and R. Parker, *Edc3p and a glutamine/asparagine-rich domain of Lsm4p function in processing body assembly in Saccharomyces cerevisiae.* J Cell Biol, 2007. **179**(3): p. 437-49.

155. Brengues, M., D. Teixeira, and R. Parker, *Movement of eukaryotic mRNAs between polysomes and cytoplasmic processing bodies.* Science, 2005. **310**(5747): p. 486-9.

156. Jang, C., et al., *Ribosome profiling reveals an important role for translational control in circadian gene expression.* Genome Res, 2015. **25**(12): p. 1836-47.

157. Martin, M., *Cutadapt removes adapter sequences from high-throughput sequencing reads.* EMBNet, 2011. **17**(1).

158. Simon, A., *FastQC: a quality control tool for high throughput sequence data.* http://www.bioinformatics.babraham.ac.uk/projects/fastqc, 2010.

159. Bolger, A.M., M. Lohse, and B. Usadel, *Trimmomatic: a flexible trimmer for Illumina sequence data.* Bioinformatics, 2014. **30**(15): p. 2114-20.

160. Wang, L., S. Wang, and W. Li, *RSeQC: quality control of RNA-seq experiments.* Bioinformatics, 2012. **28**(16): p. 2184-5.

161. Hughes, M.E., J.B. Hogenesch, and K. Kornacker, *JTK_CYCLE: an efficient nonparametric algorithm for detecting rhythmic components in genome-scale data sets.* J Biol Rhythms, 2010. **25**(5): p. 372-80.

162. Priebe, S., et al., *FungiFun: a web-based application for functional categorization of fungal genes and proteins.* Fungal Genet Biol, 2011. **48**(4): p. 353-8.

163. Robinson, J.T., et al., *Integrative genomics viewer.* Nat Biotechnol, 2011. **29**(1): p. 24-6.

164. Stajich, J.E., et al., *FungiDB: an integrated functional genomics database for fungi.* Nucleic Acids Res, 2012. **40**(Database issue): p. D675-81.

165. Fustin, J.M., S. Karakawa, and H. Okamura, *Circadian Profiling of Amino Acids in the SCN and Cerebral Cortex by Laser Capture Microdissection-Mass Spectrometry.* J Biol Rhythms, 2017. **32**(6): p. 609-620.

166. Buske, F.A., et al., *Assigning roles to DNA regulatory motifs using comparative genomics.* Bioinformatics, 2010. **26**(7): p. 860-6.

167. Zhang, P., et al., *The GCN2 eIF2alpha kinase is required for adaptation to amino acid deprivation in mice.* Mol Cell Biol, 2002. **22**(19): p. 6681-8.

168. Wek, R.C., *eIF-2 kinases: regulators of general and gene-specific translation initiation.* Trends Biochem Sci, 1994. **19**(11): p. 491-6.

169. Yang, R., S.A. Wek, and R.C. Wek, *Glucose limitation induces GCN4 translation by activation of Gcn2 protein kinase.* Mol Cell Biol, 2000. **20**(8): p. 2706-17.

170. Chaveroux, C., et al., *Identification of GCN2 as new redox regulator for oxidative stress prevention in vivo.* Biochem Biophys Res Commun, 2011. **415**(1): p. 120-4.

171. Harding, H.P., et al., *An integrated stress response regulates amino acid metabolism and resistance to oxidative stress.* Mol Cell, 2003. **11**(3): p. 619-33.

172. Schwabedal, P.E., *Influence of stress on the amount of "Gomori-positive" granules in the outer layer of the median eminence of bilaterally adrenalectomized rats.* J Neural Transm, 1974. **35**(3): p. 217-31.

173. Ebba, F., et al., *Stress relaxation studies of granules as a function of different lubricants.* Eur J Pharm Biopharm, 2001. **52**(2): p. 211-20.

174. Anderson, P. and N. Kedersha, *Visibly stressed: the role of eIF2, TIA-1, and stress granules in protein translation.* Cell Stress Chaperones, 2002. **7**(2): p. 213-21.

175. Kedersha, N. and P. Anderson, *Stress granules: sites of mRNA triage that regulate mRNA stability and translatability.* Biochem Soc Trans, 2002. **30**(Pt 6): p. 963-9.

176. Buchan, J.R. and R. Parker, *Eukaryotic stress granules: the ins and outs of translation.* Mol Cell, 2009. **36**(6): p. 932-41.

177. Barnham, K.J., C.L. Masters, and A.I. Bush, *Neurodegenerative diseases and oxidative stress.* Nat Rev Drug Discov, 2004. **3**(3): p. 205-14.

178. Dues, D.J., et al., *Aging causes decreased resistance to multiple stresses and a failure to activate specific stress response pathways.* Aging (Albany NY), 2016. **8**(4): p. 777-95.

179. Bollen, M., et al., *The extended PP1 toolkit: designed to create specificity.* Trends Biochem Sci, 2010. **35**(8): p. 450-8.

180. Hsu, J.Y., et al., *Mitotic phosphorylation of histone H3 is governed by Ipl1/aurora kinase and Glc7/PP1 phosphatase in budding yeast and nematodes.* Cell, 2000. **102**(3): p. 279-91.

181. Bazzi, M., et al., *Dephosphorylation of gamma H2A by Glc7/protein phosphatase 1 promotes recovery from inhibition of DNA replication.* Mol Cell Biol, 2010. **30**(1): p. 131-45.

182. Akiyoshi, B., et al., *Quantitative proteomic analysis of purified yeast kinetochores identifies a PP1 regulatory subunit.* Genes Dev, 2009. **23**(24): p. 2887-99.

183. Pinsky, B.A., et al., *Glc7/protein phosphatase 1 regulatory subunits can oppose the Ipl1/aurora protein kinase by redistributing Glc7.* Mol Cell Biol, 2006. **26**(7): p. 2648-60.

184. Woodbury, E.L. and D.O. Morgan, *Cdk and APC activities limit the spindle-stabilizing function of Fin1 to anaphase.* Nat Cell Biol, 2007. **9**(1): p. 106-12.

185. Sassoon, I., et al., *Regulation of Saccharomyces cerevisiae kinetochores by the type 1 phosphatase Glc7p.* Genes Dev, 1999. **13**(5): p. 545-55.

186. Bailis, J.M. and G.S. Roeder, *Pachytene exit controlled by reversal of Mek1-dependent phosphorylation.* Cell, 2000. **101**(2): p. 211-21.

187. Ho, Y., et al., *Systematic identification of protein complexes in Saccharomyces cerevisiae by mass spectrometry.* Nature, 2002. **415**(6868): p. 180-3.

188. Anderson, C. and K. Tatchell, *Hyperactive glycogen synthase mutants of Saccharomyces cerevisiae suppress the glc7-1 protein phosphatase mutant.* J Bacteriol, 2001. **183**(3): p. 821-9.

189. Gilbert, W. and C. Guthrie, *The Glc7p nuclear phosphatase promotes mRNA export by facilitating association of Mex67p with mRNA.* Mol Cell, 2004. **13**(2): p. 201-12.

190. He, X. and C. Moore, *Regulation of yeast mRNA 3' end processing by phosphorylation.* Mol Cell, 2005. **19**(5): p. 619-29.

191. Zeng, G., et al., *Scd5p mediates phosphoregulation of actin and endocytosis by the type 1 phosphatase Glc7p in yeast.* Mol Biol Cell, 2007. **18**(12): p. 4885-98.

192. Gardiner, F.C., R. Costa, and K.R. Ayscough, *Nucleocytoplasmic trafficking is required for functioning of the adaptor protein Sla1p in endocytosis.* Traffic, 2007. **8**(4): p. 347-58.

APPENDIX A

Table A1. Genes with rhythmic ribosome occupancies dependent on P-eIF2α rhythmicity.

Locus	Symbol	Name
NCU00005		hypothetical protein
NCU00022		hypothetical protein
NCU00040	eif3a	eukaryotic translation initiation factor 3 110 kDa subunit
NCU00115	rrm-4	rRNA-processing protein FCF2
NCU00196	rho-8	rho GTPase activator, rho GTPase activator, variant 1, rho GTPase activator, variant 2
NCU00207		hypothetical protein
NCU00226		hypothetical protein
NCU00236		hypothetical protein
NCU00287		hypothetical protein
NCU00334	exr-5	exoribonuclease 5
NCU00338		aspartic proteinase
NCU00408		hypothetical protein
NCU00471		hypothetical protein
NCU00506	pkr1	ER membrane protein
NCU00570	rpo-16	DNA-directed RNA polymerase III polypeptide
NCU00609	och-1	initiation-specific alpha-1,6-mannosyltransferase
NCU00633		hypothetical protein
NCU00690	trn-1	tRNA-processing-1
NCU00701		hypothetical protein
NCU00737	pam17	presequence translocated-associated motor subunit pam-17
NCU00742	glp-1	glycerol-3-phosphate dehydrogenase
NCU00744		hypothetical protein
NCU00803		hypothetical protein
NCU00825		hypothetical protein
NCU00876		hypothetical protein
NCU00881		hypothetical protein
NCU00898		hypothetical protein
NCU00903		hypothetical protein
NCU00915		Aspartyl-tRNA synthetase
NCU00992		hypothetical protein
NCU01036		DUF907 domain-containing protein
NCU01124		hypothetical protein

Locus	Symbol	Name
NCU01201	rmt-1	trm-112
NCU01214		hypothetical protein
NCU01223		hypothetical protein
NCU01278		hypothetical protein
NCU01302		hydrolase
NCU01330		hypothetical protein
NCU01336		hypothetical protein
NCU01343		TPR repeat protein
NCU01386		hypothetical protein
NCU01408		hypothetical protein
NCU01442		hypothetical protein
NCU01466		hypothetical protein
NCU01469		hypothetical protein
NCU01545	atg-8	autophagy protein 8
NCU01546	ppy-5	porphyrin-5
NCU01580		hypothetical protein
NCU01599		hypothetical protein
NCU01632	aro-1	Pentafunctional arom polypeptide
NCU01648	gt39-2	dolichyl-phosphate-mannose-protein mannosyltransferase 2
NCU01725		hypothetical protein
NCU01740	cha-1	histone H2A.Z-specific chaperone chz-1
NCU01758		YdiU domain-containing protein
NCU01762	rbg-23	nucleolar RNAse III, nucleolar RNAse III, variant 1
NCU01763		hypothetical protein
NCU01791	ens-10	endosome-10
NCU01811		hypothetical protein
NCU01814		hypothetical protein
NCU01843	cpn-3	T-complex protein 1 subunit gamma
NCU01850		hypothetical protein
NCU01884		hypothetical protein
NCU01912	gt39-1	mannosyltransferase 1, mannosyltransferase 1, variant 1
NCU01936	polh	sister chromatid cohesion protein Eso1
NCU01992	cvc-3	coatomer subunit gamma
NCU01997		hypothetical protein
NCU02007		hypothetical protein

Locus	Symbol	Name
NCU02009		hypothetical protein
NCU02018		Short chain dehydrogenase
NCU02039		hypothetical protein
NCU02064		hypothetical protein
NCU02070	pex2	peroxisomal biogenesis factor 2
NCU02075	hsp70-2	heat shock protein 70
NCU02090	ad- 10	adenine-10
NCU02101		hypothetical protein
NCU02122		HCO3
NCU02142		hypothetical protein
NCU02162		SURF-family protein
NCU02179	ldh-3	D-lactate dehydrogenase
NCU02193	cfp	Pyruvate decarboxylase, pyruvate decarboxylase, variant 1
NCU02208	un-10	eukaryotic translation initiation factor 3
NCU02274	for	Serine hydroxymethyltransferase
NCU02282	gsl-11	aureobasidin-resistance protein
NCU02364	znf-29	zinc finger transcription factor-29
NCU02368	rbd2-2	rhomboid protein 2
NCU02370		hypothetical protein
NCU02374	rpn-9	Proteasome regulatory particle subunit
NCU02428	rbg-24	nucleolar essential protein 1, nucleolar essential protein 1, variant 1
NCU02466	apg-14	SVP1-like protein 2, SVP1-like protein 2, variant 1
NCU02480		hypothetical protein
NCU02493	pca-7	proteasome component C1
NCU02505	suc	pyruvate carboxylase
NCU02520		hypothetical protein
NCU02546	nog2	nucleolar GTP-binding protein 2
NCU02614		hypothetical protein
NCU02621	znf-30	zinc finger transcription factor-30
NCU02624	erg-11	Lanosterol 14-alpha demethylase, putative
NCU02625		hypothetical protein
NCU02633		nuclear mRNA splicing factor-associated protein
NCU02702	gki-1	glucokinase-1
NCU02727	gly-3	glycine-3

Locus	Symbol	Name
NCU02749		hypothetical protein
NCU02772		hypothetical protein
NCU02778	gh47-1	Mannosyl-oligosaccharide 1,2-alpha-mannosidase
NCU02779		hypothetical protein
NCU02849		hypothetical protein
NCU02938		hypothetical protein
NCU02948	ncw-4	non-anchored cell wall protein 4
NCU02994		hypothetical protein
NCU03043		hypothetical protein
NCU03062		formin binding protein
NCU03096		hypothetical protein
NCU03097	mic-38	nucleotide-sugar transporter
NCU03117	gua-1	inosine-5'-monophosphate dehydrogenase IMD2
NCU03118	lys-4	hypothetical protein
NCU03132		hypothetical protein
NCU03139	his-3	histidine biosynthesis trifunctional protein
NCU03158		hypothetical protein
NCU03178		hypothetical protein
NCU03205		hypothetical protein
NCU03215		hypothetical protein
NCU03233	qcr9	ubiquinol-cytochrome C reductase 9
NCU03241	fkr-4	FK506-binding protein 4
NCU03253		hypothetical protein
NCU03264		hypothetical protein
NCU03282	nic-2	3-hydroxyanthranilate 3,4-dioxygenase
NCU03285		hypothetical protein
NCU03308		hypothetical protein
NCU03313		hypothetical protein
NCU03321	rbg-59	ribosome biogenesis-59
NCU03339	gtr-1	Glutathione reductase, glutathione reductase, variant 1
NCU03345		hypothetical protein
NCU03399		hypothetical protein
NCU03400		hypothetical protein
NCU03430		hypothetical protein
NCU03471		DUF6 domain-containing protein

Locus	Symbol	Name
NCU03491		hypothetical protein
NCU03492	gsl-5	inositolphosphorylceramide-B C-26 hydroxylase
NCU03493		hypothetical protein
NCU03516	mrp-36	mitochondrial ribosomal protein subunit L32
NCU03526	ubi-9	ubiquitin-activating enzyme E1 3, ubiquitin-activating enzyme E1 3, variant 1
NCU03539	un-24	ribonucleoside-diphosphate reductase large subunit
NCU03571	stk-23	serine/threonine protein kinase
NCU03579	ala-5	alanine-5
NCU03630		hypothetical protein
NCU03678		ssh-4
NCU03691		hypothetical protein
NCU03714		hypothetical protein
NCU03717		hypothetical protein
NCU03784	aap-4	cation chloride cotransporter
NCU03787		hypothetical protein, hypothetical protein, variant 1
NCU03820		hypothetical protein
NCU03846		DRAP deaminase, DRAP deaminase, variant 1
NCU03861		hypothetical protein
NCU03884		hypothetical protein
NCU03890	ens-12	stromal membrane-associated protein
NCU03898	ens-7	endosome-7
NCU03905	nap-1	Ap1-like protein
NCU03913		hypothetical protein
NCU03938	aod-5	alternative oxidase-5
NCU03952	rbg-13	U3 small nucleolar ribonucleoprotein mpp10
NCU03953		hypothetical protein
NCU03982	grp78	glucose-regulated protein
NCU04016		hypothetical protein
NCU04024		hypothetical protein
NCU04039		hypothetical protein
NCU04050	cpc-1	cross-pathway control protein 1
NCU04059		hypothetical protein
NCU04063	nup-20	protein transporter sec-13
NCU04066		hypothetical protein

Locus	Symbol	Name
NCU04092		hypothetical protein
NCU04112		hypothetical protein
NCU04135		hypothetical protein
NCU04166	rbg-38	nucleolar GTP-binding protein 2
NCU04207		hypothetical protein
NCU04256		hypothetical protein
NCU04300		hypothetical protein
NCU04301	pex19	peroxin
NCU04344	eif2B-alpha	translation initiation factor eIF-2B alpha subunit
NCU04363		hypothetical protein
NCU04369		hypothetical protein
NCU04387	vma-7	vacuolar membrane ATPase 7
NCU04459	ada-19	SAGA complex subunit
NCU04466		cyanamide hydratase
NCU04578		hypothetical protein
NCU04583		hypothetical protein
NCU04596		hypothetical protein
NCU04606	nup-24	pre-mRNA splicing factor, pre-mRNA splicing factor, variant 1
NCU04638		hypothetical protein
NCU04640	eif2-beta	eukaryotic translation initiation factor 2 beta subunit, eukaryotic translation initiation factor 2 beta subunit, variant 1
NCU04641		hypothetical protein
NCU04646	dnp-2	DNA primase large subunit
NCU04665		hypothetical protein
NCU04732		hypothetical protein
NCU04852		hypothetical protein
NCU04910		hypothetical protein
NCU04983	erg-3	lathosterol oxidase
NCU05068		hypothetical protein
NCU05083		hypothetical protein
NCU05095		phenylalanyl-tRNA synthetase subunit alpha
NCU05129	trp-2	anthranilate synthase component I
NCU05189		hypothetical protein
NCU05225	nde-1	mitochondrial NADH dehydrogenase

Locus	Symbol	Name
NCU05234	gtp-9	guanine triphosphate binding-9
NCU05257		hypothetical protein
NCU05275	crp-79	ubiquitin fusion protein
NCU05279		hypothetical protein
NCU05294		hypothetical protein
NCU05452	msp-29	splicing factor 3b
NCU05521		hypothetical protein
NCU05526	lys-5	Homocitrate synthase, homocitrate synthase, variant 1, homocitrate synthase, variant 2
NCU05565		hypothetical protein
NCU05574		hypothetical protein
NCU05587	arp6	actin-like protein arp-6, actin-like protein arp-6, variant 1
NCU05591	abc-5	ABC transporter CDR4
NCU05641		hypothetical protein
NCU05750	rnh1	ribonuclease H-2
NCU05834		hypothetical protein
NCU05945		hypothetical protein
NCU05977		hypothetical protein
NCU05989	qcr6	ubiquinol-cytochrome C reductase 6
NCU06012		hypothetical protein
NCU06037		hypothetical protein
NCU06038		hypothetical protein
NCU06048	crp-73	40S ribosomal protein S30, 40S ribosomal protein S30, variant 1
NCU06051		hypothetical protein
NCU06055		hypothetical protein
NCU06063	fam-6	long-chain-fatty-acid-CoA ligase
NCU06069		hypothetical protein
NCU06105	adr-7	ADP-ribosylation factor-binding protein GGA1
NCU06114		hypothetical protein
NCU06156		hypothetical protein
NCU06176		TRAPP complex subunit, TRAPP complex subunit, variant 1
NCU06181		hypothetical protein
NCU06193	mmm-1	mitochondrial morphology maintaining protein MMM1
NCU06224		hypothetical protein

Locus	Symbol	Name
NCU06227		hypothetical protein
NCU06260	rnp-2	mRNA-capping enzyme subunit alpha, mRNA-capping enzyme subunit alpha, variant 1
NCU06278	rbg-37	elongation factor 2, elongation factor 2, variant 1, elongation factor 2, variant 2
NCU06282		hypothetical protein
NCU06318	msp-32	ATP-dependent RNA helicase DHX8
NCU06333	sec62-1	translocation protein Sec62
NCU06353		hypothetical protein
NCU06386	alg-5	dolichyl-phosphate beta-glucosyltransferase
NCU06425		hypothetical protein
NCU06484		hypothetical protein
NCU06549	pdx-2	pyridoxine 2
NCU06574		hypothetical protein
NCU06583		hypothetical protein
NCU06587		hypothetical protein
NCU06608		hypothetical protein
NCU06610		hypothetical protein
NCU06623		hypothetical protein
NCU06711		hypothetical protein
NCU06712	pca-6	proteasome component Pre5
NCU06717	trm-53	arsenical pump-driving ATPase
NCU06731		hypothetical protein
NCU06750		coiled-coil domain-containing protein 25
NCU06760		hypothetical protein
NCU06792		mannosylphosphate transferase
NCU06931		hypothetical protein
NCU06981	wsc-2	Cell wall integrity and stress response component 2
NCU06993		Ash2-trithorax family protein
NCU06994	msp-37	pre-mRNA-splicing factor cef-1
NCU07110		hypothetical protein
NCU07112		hypothetical protein
NCU07135		hypothetical protein
NCU07172	stk-8	serine/threonine-protein kinase prk1, serine/threonine-protein kinase prk1, variant 1

Locus	Symbol	Name
NCU07238		hypothetical protein
NCU07277		hypothetical protein
NCU07288		hypothetical protein
NCU07301		hypothetical protein, hypothetical protein, variant 1
NCU07318		hypothetical protein
NCU07360		DnaJ domain-containing protein
NCU07432		hypothetical protein
NCU07467		hypothetical protein
NCU07497		hypothetical protein
NCU07528	tpus-1	tRNA-pseudouridine synthase-1
NCU07529		hypothetical protein
NCU07559		hypothetical protein
NCU07583		hypothetical protein
NCU07654	paa-10	pre-mRNA polyadenylation factor fip-1
NCU07671		hypothetical protein
NCU07707		hypothetical protein
NCU07728		hypothetical protein
NCU07739		YTP1
NCU07742		poly(p)/ATP NAD kinase
NCU07756	tca-11	Succinate dehydrogenase cytochrome b560 subunit
NCU07769		hypothetical protein
NCU07776		hypothetical protein
NCU07778		hypothetical protein
NCU07845		hypothetical protein
NCU07849	thi-4	thiamine-4, thiamine-4, variant 1
NCU07851	cha-3	superoxide dismutase 1 copper chaperone
NCU07972		hypothetical protein
NCU07993	lcm-1	leucine carboxyl methyltransferase 1
NCU08042		hypothetical protein
NCU08055	idi-4	B-zip transcription factor, putative
NCU08057		hypothetical protein
NCU08121	rbg-48	ribosome biogenesis-48
NCU08123		hypothetical protein
NCU08148		hypothetical protein
NCU08153		hypothetical protein

Locus	Symbol	Name
NCU08159		hypothetical protein
NCU08295		RNA-binding La domain-containing protein
NCU08390		hypothetical protein
NCU08396		hypothetical protein
NCU08403		hypothetical protein
NCU08409	trp-3	Tryptophan synthetase
NCU08410	mrp-30	50S ribosomal protein L24
NCU08418		hypothetical protein
NCU08421	rbg-4	hypothetical protein
NCU08552	mrp-41	50S ribosomal protein L14
NCU08559		hypothetical protein
NCU08617		hypothetical protein
NCU08692		hypothetical protein
NCU08701		hypothetical protein
NCU08763		hypothetical protein
NCU08857		hypothetical protein
NCU08882		hypothetical protein
NCU08939		hypothetical protein
NCU08941	mic-32	calcium-binding mitochondrial carrier protein Aralar2
NCU08955		hypothetical protein
NCU08967		hypothetical protein
NCU08989	adr-2	ADP-ribosylation factor 1
NCU08995		dual specificity phosphatase, dual specificity phosphatase, variant 1
NCU09020		hypothetical protein
NCU09045		hypothetical protein
NCU09116	val-2	aromatic aminotransferase Aro8, aromatic aminotransferase Aro8, variant 1
NCU09178		hypothetical protein
NCU09187		hypothetical protein
NCU09193		hypothetical protein
NCU09204		hypothetical protein
NCU09227		kelch repeat-containing protein
NCU09247		hypothetical protein
NCU09274		hypothetical protein

Locus	Symbol	Name
NCU09309		hypothetical protein
NCU09347	fbp-1	Fructose-2,6-bisphosphatase
NCU09371	rib-7	riboflavin-7
NCU09372		hypothetical protein
NCU09375		hypothetical protein
NCU09384	msh5	hypothetical protein
NCU09386		hypothetical protein
NCU09395		hypothetical protein
NCU09422		hypothetical protein
NCU09450	rpn-2	26S proteasome regulatory subunit Rpn2
NCU09451		hypothetical protein
NCU09465		hypothetical protein
NCU09485	hsp70-6	chaperone DnaK
NCU09503		hypothetical protein
NCU09504		hypothetical protein
NCU09505		hypothetical protein
NCU09506		hypothetical protein
NCU09513		hypothetical protein
NCU09516	mus-41	DNA repair protein rad-5
NCU09540		hypothetical protein
NCU09570	gst-5	glutathione transferase
NCU09609	cen-c	centromere protein C
NCU09629		hypothetical protein
NCU09658		hypothetical protein
NCU09670		amidohydrolase
NCU09674		hypothetical protein
NCU09685		hypothetical protein
NCU09709		T-complex protein 1 subunit zeta
NCU09735		Short-chain dehydrogenase
NCU09737		hypothetical protein
NCU09741		NADPH-cytochrome P450 reductase
NCU09775		hypothetical protein
NCU09782		hypothetical protein
NCU09825	dnr-21	DNA repair-21
NCU09847		hypothetical protein

Locus	Symbol	Name
NCU09856		hypothetical protein
NCU09857		hypothetical protein
NCU09896	adsk-1	adenylyl-sulfate kinase-1
NCU10035		hypothetical protein
NCU10059		hypothetical protein
NCU10185	tipt-1	tRNA isopentenyltransferase-1
NCU10246		hypothetical protein
NCU10622	trn-6	tRNA-processing-6
NCU10760		hypothetical protein
NCU10987	mfs-14	MFS transporter Fmp42
NCU11180	lpl-5	patatin-like phospholipase domain-containing protein
NCU11186		hypothetical protein
NCU11211		hypothetical protein
NCU11259		hypothetical protein
NCU11288	dpp-7	xaa-Pro dipeptidase, xaa-Pro dipeptidase, variant 1
NCU11338		hypothetical protein
NCU11356		phenazine biosynthesis PhzC/PhzF protein
NCU11370		hypothetical protein
NCU11371		COBW domain-containing protein 1
NCU11405		hypothetical protein
NCU11409	arh-1	ATP-dependent RNA helicase chl-1
NCU11426	nuc-2	nuc-2 protein
NCU12024		hypothetical protein
NCU12040		hypothetical protein
NCU16024		ATPase subunit 8
NCU16329		hypothetical protein
NCU16346		hypothetical protein
NCU16368		hypothetical protein
NCU16793		hypothetical protein
NCU17030		heterogeneous nuclear ribonucleoprotein HRP1
NCU17041		hypothetical protein
NCU17088		hypothetical protein
NCU17123		hypothetical protein

Table A2. Genes of the 404 cTICs with predicted uORFs

Locus	Symbol	Name
NCU00005		hypothetical protein
NCU00196	rho-8	rho GTPase activator, rho GTPase activator, variant 1, rho GTPase activator, variant 2
NCU00898		hypothetical protein
NCU01124		hypothetical protein
NCU01599		hypothetical protein
NCU02039		hypothetical protein
NCU02162		SURF-family protein
NCU02193	cfp	Pyruvate decarboxylase, pyruvate decarboxylase, variant 1
NCU02364	znf-29	zinc finger transcription factor-29
NCU03132		hypothetical protein
NCU03253		hypothetical protein
NCU03282	nic-2	3-hydroxyanthranilate 3,4-dioxygenase
NCU03345		hypothetical protein
NCU03526	ubi-9	ubiquitin-activating enzyme E1 3, ubiquitin-activating enzyme E1 3, variant 1
NCU04050	cpc-1	cross-pathway control protein 1
NCU04256		hypothetical protein
NCU04369		hypothetical protein
NCU04583		hypothetical protein
NCU04596		hypothetical protein
NCU04606	nup-24	pre-mRNA splicing factor, pre-mRNA splicing factor, variant 1
NCU04665		hypothetical protein
NCU04732		hypothetical protein
NCU05526	lys-5	Homocitrate synthase, homocitrate synthase, variant 1, homocitrate synthase, variant 2
NCU05565		hypothetical protein
NCU05989	qcr6	ubiquinol-cytochrome C reductase 6
NCU06012		hypothetical protein
NCU06055		hypothetical protein
NCU06224		hypothetical protein
NCU06227		hypothetical protein
NCU06260	rnp-2	mRNA-capping enzyme subunit alpha, mRNA-capping enzyme subunit alpha, variant 1
NCU06484		hypothetical protein
NCU06610		hypothetical protein

Locus	Symbol	Name
NCU06711		hypothetical protein
NCU06981	wsc-2	Cell wall integrity and stress response component 2
NCU07110		hypothetical protein
NCU07135		hypothetical protein
NCU07301		hypothetical protein, hypothetical protein, variant 1
NCU07360		DnaJ domain-containing protein
NCU07707		hypothetical protein
NCU07742		poly(p)/ATP NAD kinase
NCU07769		hypothetical protein
NCU07778		hypothetical protein
NCU08055	idi-4	B-zip transcription factor, putative
NCU08396		hypothetical protein
NCU09375		hypothetical protein
NCU09422		hypothetical protein
NCU09504		hypothetical protein
NCU09513		hypothetical protein
NCU09629		hypothetical protein
NCU09782		hypothetical protein
NCU10035		hypothetical protein
NCU10246		hypothetical protein
NCU17123		hypothetical protein